UNIVERSITÁ DEGLI STUDI DI MILANO
FACOLTÁ DI MEDICINA E CHIRURGIA

DOTTORATO DI RICERCA IN FISIOLOGIA

SETTORE SCIENTIFICO DISCIPLINARE BIO-09

CICLO XXIV°

Tesi di Dottorato di Ricerca

HS1 regulates the trafficking and bone marrow homing of leukemic B cells

Dottorando: Dott.ssa Cristina SCIELZO
Matricola: R08211

Tutor: Dott.ssa Valeria Caiolfa
Prof. Antonio Malgaroli
Istituto di Ricerca Biologica e Tecnologica, San Raffaele, Milano

Coordinatore: Prof. Paolo Cavallari

Anno Accademico 2010-2011

CONSULTAZIONE TESI DI DOTTORATO

La sottoscritta Cristina Scielzo, n° matr. RO8211
nata a Genova il 19/03/1975

autore della tesi dal titolo:

HS1 regulates the trafficking and bone marrow homing of leukemic B cells

AUTORIZZA

la consultazione della tesi stessa, fatto divieto di riprodurre, in tutto o in parte, quanto in esso contenuto.

Data Firma

Index

1. Introduction

1.1 Normal and malignant B lymphocytes

B lymphocytes are devoted to recognize foreign antigens with a specific B cell receptor (BCR), to present it to T lymphocytes and eventually to secrete a monoclonal antibody. B cell development prior to birth takes place mostly in the fetal liver and spleen, while after birth occurs mostly in the bone marrow where it lasts all life [1]. B lymphopoiesis in the bone marrow is a dynamic process involving different B cell precursors which differentiate along a tightly regulated developmental pathway to finally give raise to mature, antigen-reactive B lymphocytes. The differential expression of proteins on the surface and inside of the cells as well as analyses of the status of rearrangements in the Immunoglobulin heavy and light chains loci has allowed a clear definition and separation of the different B lineage subpopulations of both mouse and human bone marrow. All developmental events are dependent on cell-cell interactions, different haematopoietic growth factors, and stimulation through the pre- and B-cell antigen receptors (BCR) [2].

Rearrangement of the Ig loci is actually one of the first events occurring along the B-cell differentiation pathway, originating from the Hematopoietic stem cells (HSC) and allowing for the production and the selection of a complete immunoglobulin on the cell surface of the maturing B lymphocytes.

CD19 is the prototype of B cell specific marker as it is expressed in all stages of B cell development from the progenitors to the mature B lymphocytes, decreasing on plasma cells, both in humans and mice [3]. In addition, during all stages of development within the BM, B cell precursors express CD10 which is then lost on mature B cells [4]. Progenitor B (pro-B) cells are considered to be already committed to the B-cell lineage, though they did not yet started rearranging both IgH and IgL chain loci. This compartment has not yet been characterized in man. Pro-B cells differentiate into Precursors B (pre-B) cells where the sequential steps of the Ig rearrengements occour. They can be that can be subdivided into large proliferating pre-B-I cells, large proliferating pre-B-II cells and small resting pre-B-II cells [4], based on cell cycle analysis.

After expression of a complete IgM on the cell surface and selection of immature autoreactive B cells by negative selection, newly generated functional B cells finally differentiate into mature B lymphocytes. The final developmental stage is characterized by the acquisition of IgD on the surface, with the same specificity of IgM, resulting in double positive IgM+IgD+ cells. In mouse it is well established that the maturation from immature to mature B cells takes place in the spleen [5], while in human it is yet to be determined.

Mature naïve B cells that encounter an antigen-activated become activated and are driven into primary B-cell follicles in spleen and in other secondary lymphoid organs such as lymph nodes, where they establish germinal centres (**Figure 1.1**). The naive IgM+IgD+ B cells that constitute the primary B-cell follicle are replaced by the proliferating GC B cells and displaced to the outside of the follicle, where they form a mantle zone around the GC. In the GC, a dark zone and a light zone

can be distinguished . The dark zone mainly consists of proliferating GC B cells, whereas the GC B cells in the light zone are resting. In proliferating GC B cells, the process of somatic hypermutation is activated, which leads to the introduction of mutations at a high rate into the rearranged Ig variable (V)-region genes of the B cells. Most mutations are disadvantageous for the cells and cause cells to undergo apoptosis. A few GC B cells will acquire mutations in the BCR that increase the affinity for antigen, and these cells will be positively selected. The selection process presumably takes mainly place in the light zone, where the GC B cells are in close contact with T cells and follicular dendritic cells (FDCs). A fraction of these GC B cells undergo class-switch recombination [6], leading to a change in the constant region of the Ig. Finally, GC B cells differentiate into memory B cells or plasma cells and leave the GC microenvironment.

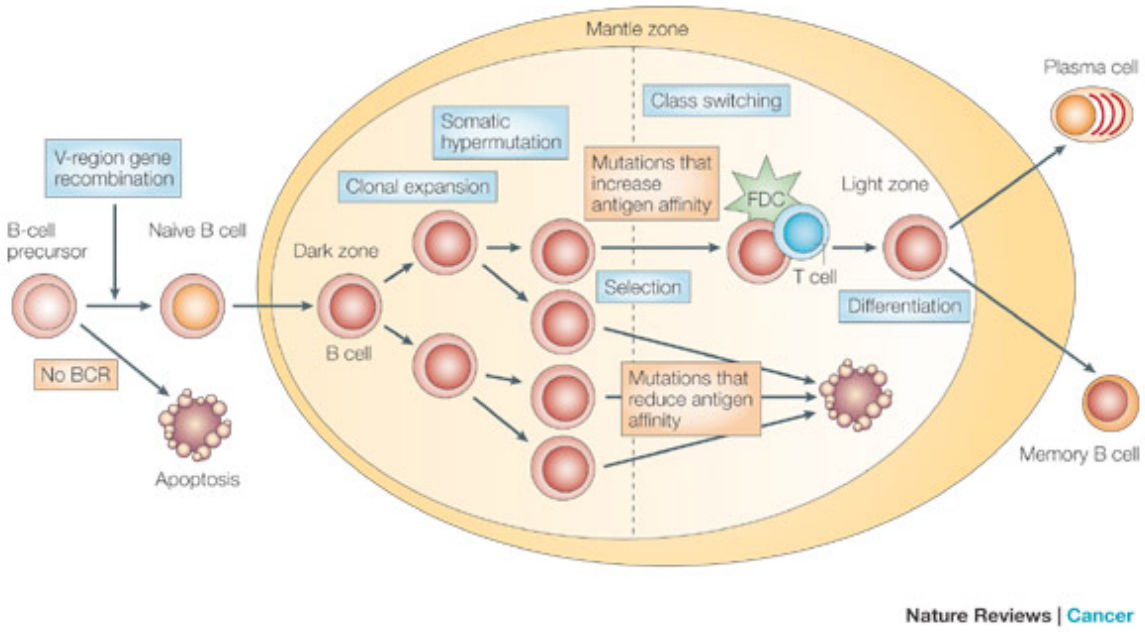

Figure 1.1. B-cell differentiation in the germinal-centre [7]

As distinct stages of B-cell development are characterized by a particular BCR structure and by the expression of specific differentiation markers, these features were used to determine the origin of the various human B-cell lymphomas. Lymphomagenesis is a multistep transformation process; a number of genetic changes, environmental and infectious factors contributing to the development and malignant progression of B cell lymphoproliferative disorders are well documented [7] (**Figure 1.2**). Reciprocal chromosomal translocations involving the immunoglobulin loci are a hallmark of many mature B cell lymphomas and lead to dysregulated expression of proto-oncogenes important for cell proliferation (i.e. c-myc in Burkitt lymphoma) or genes involved in cell cycle progression (i.e. cyclin D1 in Mantle cell lymphoma), differentiation block (i.e. bcl-6 in DLBCL) and cell survival (i.e. bcl-2 in follicular lymphoma and DLBCL). In addition, genetic alterations that

inactivate tumor suppressor genes (p53, ATM) have been frequently detected in lymphomas (i.ei Mantle cell lymphoma and Chronic Lymphocytic Leukemia). Several evidence supports the hypothesis that infectious agents may play a contributory role in the development and evolution of at least some B cell lymphoproliferative disorders by either directly inducing polyclonal B cell hyperactivation (EBV, HCV), or providing a chronic antigenic stimulus (EBV, HCV, HBV, H. pylori), or mimicking B cell antigen receptor signaling (EBV, HCV, HHV8), it still remains to be defined whether these are causative factors or they are secondary to genetic changes occurring during the process of lymphomagenesis. In addition, modulation of the B cell antigen receptor signaling emerges as a key step for controlling the growth of certain B cell lymphomas and CLL in particular (see chapter CLL number 1.6)[8].

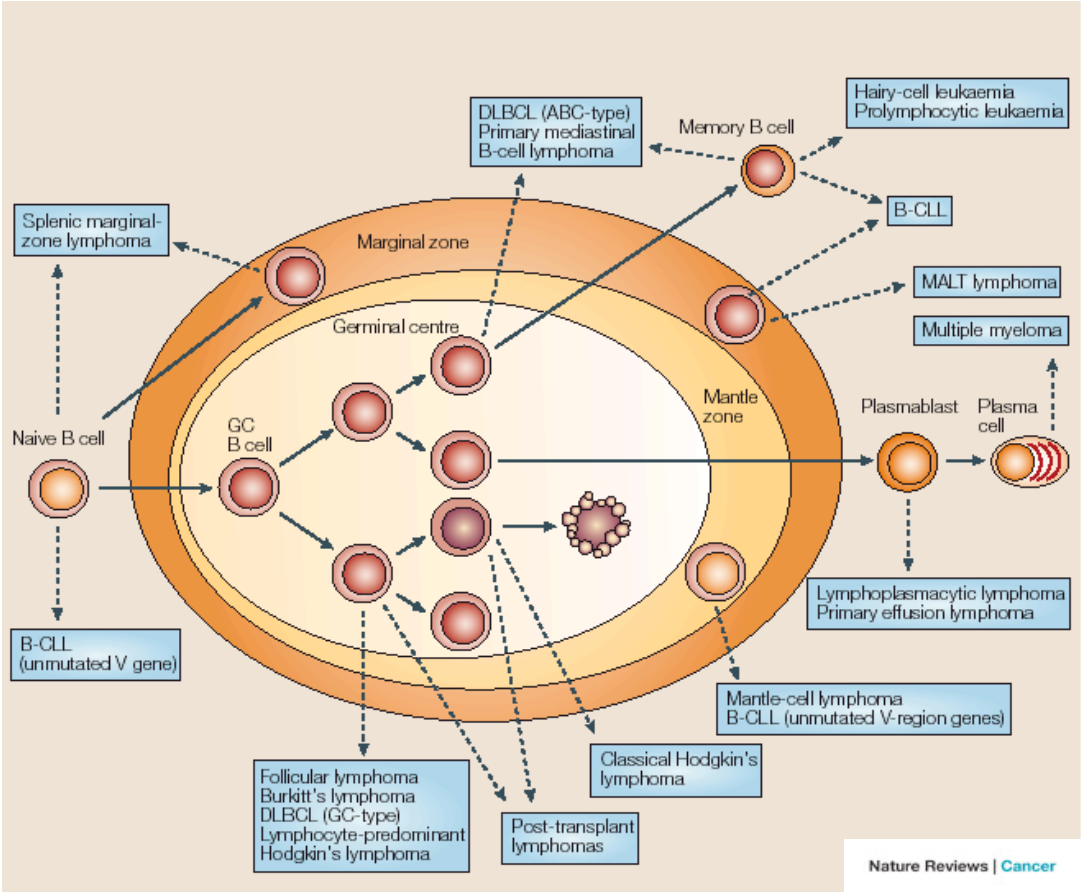

Figure 1.2. B-cell lymphomagenesis [7]

1.2 B cell receptor (BCR) signaling complex

The BCR belongs to the family of multichain immune recognition receptors (MIRR) which includes the T-cell receptor (TCR) and the receptors for the Fc portions of IgG and IgE. The BCR is a multiproteic structure composed by an antigen binding subunit (a membrane-bound form of an IgM or IgD) and a signalling subunit containing a disulfide linked heterodimer of Igα (CD79a) and Igβ (CD79b) (**Figure 1.3**). Igα and Igβ are members of the immunoglobulin superfamily and contain a single extracellular immunoglobulin like (Ig-like) domain, a single transmembrane region and a cytoplasmic tail containing an immunoreceptor tyrosine-based activation motif (ITAM) sequence responsible for signal transduction after BCR engagement [9].

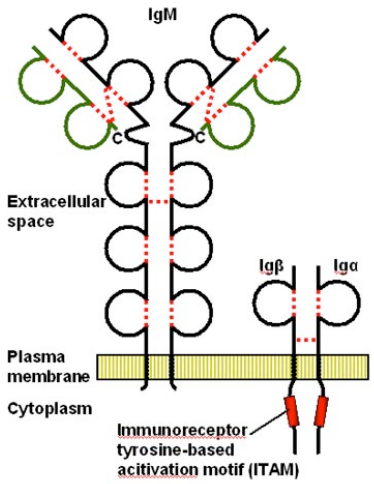

Figure 1.3. **The B-cell receptor (BCR) complex**. The BCR is composed of an antigen binding subunit (membrane-bound IgM or IgD) and two signalling subunit (Igα and Igβ) containing immunoreceptor tyrosine-based activation motifs (ITAMs) responsible for signal transduction.

B-cell activation is initiated in response to specific antigen binding to the BCR. Upon receptor engagement, intracellular Igαβ-ITAMs are tyrosine phosphorylated by Src-family kinases, such as Lyn, leading to the assembly of a multiprotein complex of intracellular signalling molecules and adaptors at the plasma membrane, known as the "signalosome" [10;11].

The fine tuning of intracellular signalling pathways allows the regulation of a variety of cellular processes including gene expression, cytoskeletal reorganization, immune synapse (IS) formation and BCR-mediated internalization of antigen complexes. After internalization, the antigen is processed and presented on major histocompatibility complex II (MHCII) molecules to recruit specific T-cell help [12].

Early after antigen binding, the cell undergoes a major cytoskeletal reorganization that is crucial for BCR microcluster formation, signalosome assembly and ultimately for the maturation of the IS.

High resolution imaging studies [13; 14] have shed light on the highly coordinated and sequential recruitment of initiating kinases, such as Lyn and Syk, intracellular signalling molecules such as Vav, phosphoinositide 3-kinase (PI3K), phospholipase C gamma2 (PLCγ2), Bruton's tyrosine kinase (Btk) and adaptors such as B-cell linker (BLNK) and CD19 after antigen binding to the BCR (**Figure 1.4**) .

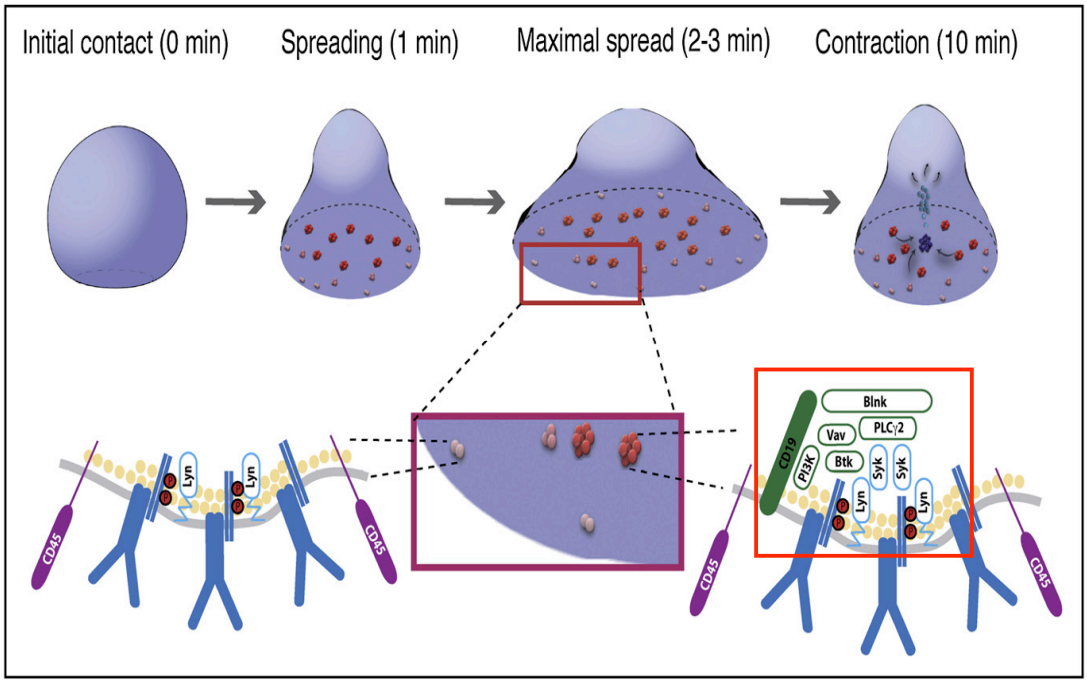

Figure 1.4. **Signalosome assembly following B-cell spreading**. After antigen encounter, B cells spread and accumulate signalling proteins (red box), such as CD19, Lyn, Syk, Bruton's tyrosine kinase (Btk), phosphoinositide 3-kinase (PI3K), Vav, phospholipase C gamma2 (PLCγ2), B-cell linker (BLNK) at the contact zone with the antigen presenting cell (APC). After spreading, a slower contraction occurs that ultimately leads to antigen internalization for later presentation to helper T cells. Adapted from [11].

Upon BCR engagment, the cell undergoes a rapid spreading response [15], through the generation of numerous lamellipodial extrusions that allow B cells to engage more antigen. BCR microclusters act as sites of assembly of numerous signalosomes and may therefore be responsible for the initiation of signalling. Within 10 minutes from initial BCR engagement, a slower contraction occurs, collecting BCR signalosomes to the center of the contact zone, termed central supramolecular activation cluster (cSMAC) (**Figure 1.5**).

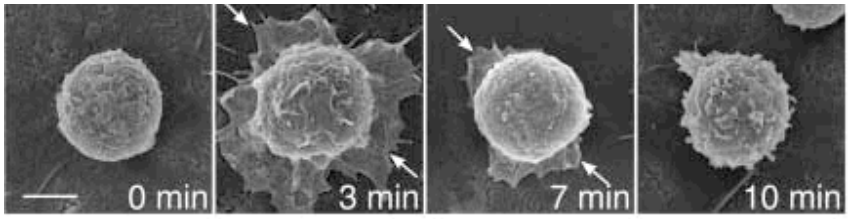

Figure 1.5. **The spreading and contraction response following B-cell receptor (BCR) engagement**. Scanning electron microscopy (SEM) images show that maximal spreading occurs within 3 minutes after antigen encounter, followed by a progressive contraction after 10 minutes. White arrows indicate the limits of the B-cell membrane. Adapted from [15].

The mature IS is characterized by a spatial segregation of immunoreceptors to the cSMAC, where signal is terminated and antigen internalized, while integrins, such as lymphocyte function-associated antigen 1 (LFA-1), are retained in the peripheral SMAC (pSMAC) and allow prolonged adhesion to the APC (**Figure 1.6**).

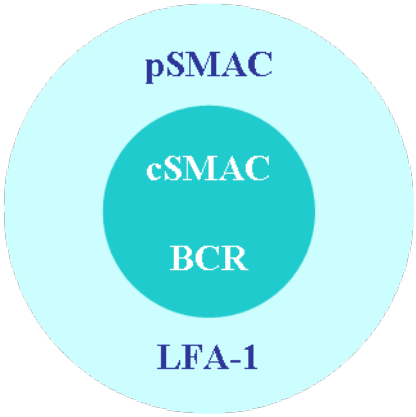

Figure 1.6. **Schematic representation of the B-cell immunological synapse (IS)**. The IS forms between the B cell and an antigen-bearing antigen presenting cell (APC) and is composed of a central supramolecular activation cluster (cSMAC), enriched in B-cell receptor (BCR) microclusters, and a peripheral supramolecular activation cluster (pSMAC), enriched in lymphocyte function-associated antigen 1 (LFA-1) molecules.

Signalosome assembly is essential for cell spreading since B cells either expressing signalling-deficient BCR, treated with Src-family kinase inhibitors [15], or deficient for any member of the signalosome, with the exception of Btk [14], fail to spread properly.

It is evident that spreading and contraction need major morphological changes to occur, that have been shown to involve the actin cytoskeleton. Indeed, spreading is abrogated in the presence of actin-polymerization inhibitors latrunculin A and cytochalasin D [15] and a rapid global actin depolymerization, followed by polarized actin polymerization [16] occur after antigen stimulation. Several players are involved in the molecular mechanisms underlying cytoskeletal

reorganization, such as the haematopoietic lineage cell-specific protein (HS1), that will be described in chapter **1.5**.

1.3 Signalosome components and BCR proximal molecules

CD19

The CD19 molecule is a B-cell specific coreceptor with two extracellular Ig-like domains and a cytoplasmic tail (**Figure 1.7**).

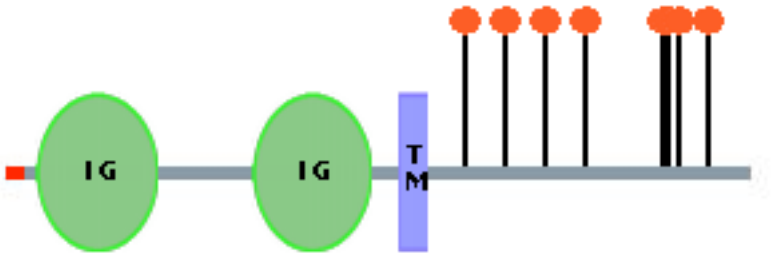

Figure 1.7. **A schematic representation of CD19 structure**. Immunoglobulin (Ig)-like domains: interaction with CD21 and CD81; Cytoplasmic tail: intracellular signalling.
Adapted from human protein reference database

CD19 is expressed on the surface of B cells early during development. In mature B cells, it associates with CD21, CD81 and leu-13 and augments intracellular signalling following CD21 binding by C3d complement-tagged antigens. After BCR crosslinking, CD19 is phosphorylated on one or more of its cytoplasmic-domain tyrosine residues and becomes able to recruit several signalosome components such as Lyn, Vav, PLCγ2 and the p85 subunit of PI3K [17]. While $CD19^{-/-}$ B cells are known to have intact BCR signalling following soluble antigen engagement [18], CD19 is essential for signalling initiation, spreading and BCR microcluster recruitment after membrane-bound antigen binding [13]. Mice lacking CD19 have impaired T-dependent antibody responses, GC formation, development of B1 cells and B-cell memory.
These evidences suggest an essential and potentially independent role for CD19 in the initiation of B-cell responses *in vivo*.

LYN

Lyn is a member of the Src kinase family and shows a conserved structure (**Figure 1.8**): an N-terminal attachment site for fatty acids, a Src homology 3 (SH3) domain, a Src homology 2 (SH2) domain and a tyrosine kinase domain. The SH3 domain allows protein-protein interaction via proline-rich peptide binding, and the SH2 domain mediates high affinity binding to phosphorylated tyrosines.

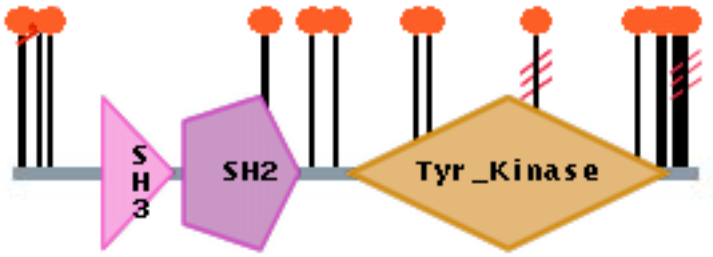

Figure 1.8. **A schematic representation of Lyn structure**. Src homology 3 (SH3) domain: protein-protein interaction via proline-rich peptide binding; Src homology 2 (SH2) domain: recruitment of phosphorylated tyrosines; Kinase: catalytic domain. N, N-terminus; C, C-terminus. Adapted from human protein reference database

The kinase activity is regulated by phosphorylation; phosphorylation of tyrosine (Y)396 within the Src catalytic domain is stimulatory, while C-terminal phosphorylation of Y507 is inhibitory [19]. Within seconds after BCR engagement [20], Lyn is activated through Y396 phosphorylation by neighboring Src kinases or by autophosphorylation. *In vitro* binding studies show that Lyn, which is palmytoilated and stably associated with the plasma membrane, can already interact with the resting BCR. Once activated, Lyn phosphorylates the Igα subunit of the BCR, the coreceptor CD19 and the kinases Syk and Btk, thus contributing to downstream signalling initiation [21]. Although showing peripheral B-cell proliferation impairment, Lyn-deficient mice show normal B-cell development in the bone marrow, suggesting that Lyn activity can probably be replaced by other Src-family kinases during development.

Besides positive contribution to BCR signalling, Lyn has also a negative regulatory function in the signalling process. Lyn has been shown to be essential for phosphorylation of CD22 and CD5 and consequent recruitment of the SH2-domain-containing protein tyrosine phosphatase 1 (SHP1), thus contributing to negative regulation of BCR signalling [22]. Multiple layers of regulation allow fine tuning of Lyn activity. The inhibitory residue Y507 is phosphorylated by Csk kinase and dephosphorylated by the membrane phosphatase CD45. Intramolecular interaction between phospho-Y507 and the SH2 domain is thought to maintain the protein in a closed conformation and inactive state that can also be competed out by external ligands, such

as CD19 [17]. Furthermore, protein degradation could contribute to the downregulation of Lyn activity, probably through proteasomal degradation [21].

SYK

Syk kinase has two N-terminal SH2 domains and a C-terminal kinase domain (**Figure 1.9**). Two tyrosine residues (Y342 and Y346) are involved in aromatic-aromatic intramolecular interactions that keep the protein in an inactive state. Binding of SH2 domains of Syk to BCR-phosphorylated ITAMs after receptor engagement disrupts this interaction, thus facilitating phosphorylation on Y519 in the activation loop [23].

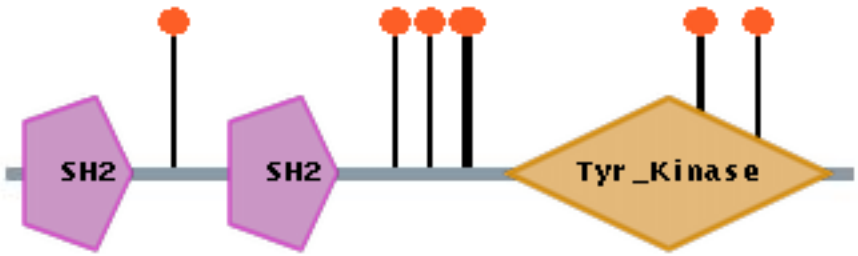

Figure 1.9. **A schematic representation of Syk structure**. Src homology 2 (SH2) domain: recruitment of phosphorylated tyrosines; Kinase: catalytic domain. N, N-terminus; C, C-terminus. Adapted from human protein reference database

Even though Syk may be associated with the BCR even in the absence of antigen stimulation through binding of SH2 domain with constitutively phosphorylated ITAMs, it is known that maximal activation of BCR signalling needs Src-kinase contribution. Indeed, the loss of Lyn dramatically inhibits Syk activation after BCR stimulation {Kurosaki, 1994 #662}. Syk activation is crucial for the phosphorylation and recruitment of early signalling molecules such as BLNK and Btk.

Syk activity is downmodulated by autophosphorylation on Y130, dephosphorylation by proximal phosphatases such as SHP1 [24] and also by proteasomal degradation. Interestingly, Lyn is thought to phosphorylate Syk on Y323 thus creating a docking site for the ubiquitin ligase Cbl.

BLNK

BLNK, also termed SH2 domain-containing leukocyte phosphoprotein of 65 kDa (SLP65), is a key adaptor molecule for the recruitment and stable signalling of signalosome components such as Btk [25] and PLCγ2 [26]. Its structure contains a tyrosine-enriched N-terminal region, a proline-rich (PR) central domain and a C-terminal SH2 domain (**Figure 1.10**).

Figure 1.10 A schematic representation of B-cell linker (BLNK) structure. Phospho-tyrosine (P-Y) sites: N-terminal region containing several tyrosine residues; proline-rich (PR) domain: protein-protein interaction via Src homology 3 (SH3)-domain binding ; Src homology 2 (SH2) domain: recruitment of phosphorylated tyrosines. N, N-terminus; C, C-terminus.
Adapted from human protein reference database

The mechanism of BLNK targeting to the plasma membrane is still unknown. Its homologue in T cells, the SH2 domain-containing leukocyte phosphoprotein of 76 kDa (SLP76) is recruited via the linker for the activation of T cells (LAT), which is constitutively in the membrane {Su, 2003 #676}. It has been proposed that the N-terminal region of BLNK is associated with the plasma membrane before BCR engagement and that, after antigen binding, the phosphorylation of Y204 on the Igα recruits BLNK via its SH2 domain. BLNK then undergoes extensive phosphorylation by Syk, and recruits PLCγ2 and Btk via their SH2 domains [21]. BLNK-deficient mice display partial impairment in B-cell development, and develop pre-B cell leukemia that resembles human acute lymphoblastic leukemia, indicating the importance of this adaptor in the modulation of B-cell responses

PLCγ2

PLCγ2 is the B-cell specific isoform of PLC, that mediates Ca^{++} signalling through the generation of inositol-1,4,5,-triphosphate (IP3) from PIP2. PLCγ2 contains a PH domain, two conserved catalytic subdomains (X and Y), separated by two SH2 domains and one SH3 domain, and an additional PH domain that is split by the SH domains (**Figure 1.11**). The most relevant activatory tyrosine residues Y753 and Y759 are located in the SH2-SH3 linker region.

Figure 1.11. **A schematic representation of phospholipase C gamma2 (PLCγ2) structure**. Pleckstrin homology (PH) domain: binding of phosphatidylinositol lipids; X and Y: catalytic subdomains; Src homology 2 (SH2) domain: recruitment of phosphorylated tyrosines; Src homology 3 (SH3): protein-protein interaction via proline-rich peptide binding. N, N-terminus; C, C-terminus. Adapted from human protein reference database.

After BCR engagement, PLCγ2 is recruited and activated through the binding of the SH2 domains to phosphorylated tyrosine residues on BLNK [26] and Btk [27]. The production of IP3 opens Ca^{++} stores in the endoplasmic reticulum (ER) via binding to IP3 receptors, allowing Ca^{++} to enter the cytoplasm. Once ER stores are sufficiently depleted, extracellular Ca^{++} enters the cell via calcium-release-activated calcium (CRAC) channels in the plasma membrane [28]. Interestingly, B-cell spreading is unaffected by triple deficiency in IP3 receptors [14], showing that intracellular calcium release is not absolutely required for this process in B cells.

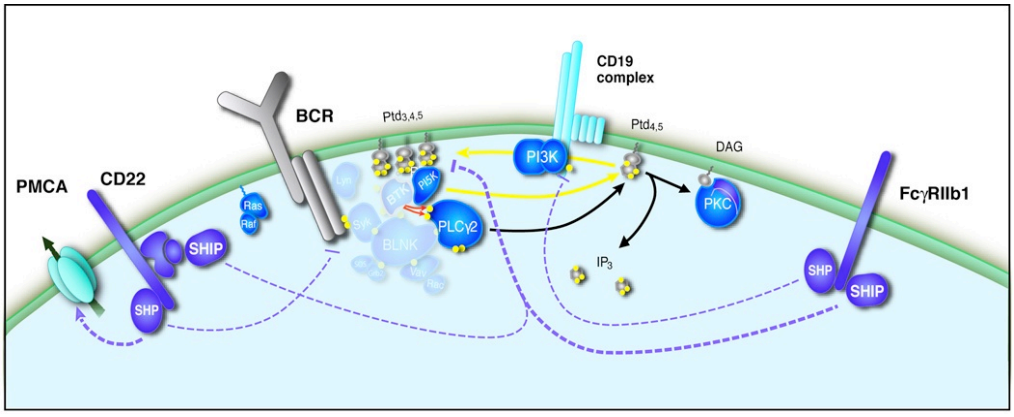

Figure 1.12. **B-cell receptor (BCR) proximal events leading to amplified phospholipase C gamma 2 (PLCγ2) activation**. Bruton's tyrosine kinase (Btk) binds phosphatidylinositol-3,4,5-trisphosphate (PtdIns(3,4,5)P3) via the plekstrin homology (PH) domain, and the interaction of Btk with PLCγ2 brings the lipase to the regions enriched with its substrate, phosphatidylinositol-4,5-diphosphate (PtdIns(4,5)P2). Btk interacts also with phosphatidylinositol-4-phosphate 5-kinase (PIP5K), which promotes the formation of additional PIP2 and phosphorylates PLCγ2, leading to its maximal activation. DAG, diacylglycerol; GRB2, growth factor receptor-bound protein 2; InsP3, inositol-1,4,5-trisphosphate; PI3K, phosphoinositide 3-kinase; PKC, protein kinase C; SOS, son of sevenless homologue. Adapted from [29].

PLCγ2 activation (**Figure 1.12**) is positively regulated by the accumulation of PIP2, that generally localizes to membrane areas enriched with its phosphorylated product PIP3. Since Btk binds PIP3 via its PH domain, the interaction of Btk with PLCγ2 brings the lipase to the regions enriched with its substrate, PIP2.

Moreover, Btk interacts also with phosphatidylinositol-4-phosphate 5-kinase (PIP5K), which promotes the formation of additional PIP2. The maximal activation of the protein is achieved after Btk-dependent phosphorylation of Y753 and Y759. Therefore a positive feedback loop of signal amplification exists between PLCγ2, Btk and PI3K.

Downmodulation of any of these elements, e.g. through activation of phosphatases such as SHP1, results in signal attenuation and limited Ca^{++} influx [29].

Along with the observation in signalosome-components deficient mice, PLCγ2$^{-/-}$ mice show a block in B-cell development and in the generation of memory B cells [30].

SHP

SHP1/2 are cytosolic tyrosine phosphatases consisting of two N-terminal SH2 domains, followed by a phosphatase domain and a C-terminal domain that contains two conserved tyrosine phosphorylation sites (Y536 and Y564 on SHP1; Y542 and Y580 on SHP2). In addition, SHP2 has a proline-rich sequence within the C-terminal domain that may interact with SH3-domain-containing proteins (**Figure 1.13**).

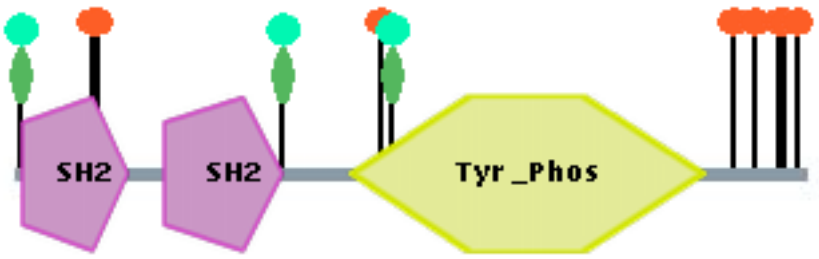

Figure 1.13. **A schematic representation of SH2-domain-containing protein tyrosine phosphatase 1/2 (SHP1/2) structure**. Src homology 2 (SH2) domain: recruitment of phosphorylated tyrosines; Phosphatase: catalytic domain; phospho-tyrosine (P-Y) sites: C-terminal domain containing conserved tyrosine phosphorylation sites. SHP2 contains an additional proline-rich sequence at the C-terminus for protein-protein interaction via Src homology 3 (SH3)-domain binding. N, N-terminus; C, C-terminus.
Adapted from human protein reference database

SHP1 binds through its SH2 domains to tyrosine phosphorylated ITIMs (immunoreceptor tyrosine-based inhibitory motifs) on BCR proximal molecules, including CD22, and dephosphorilates several BCR signalling molecules, such as Syk [24] and BLNK [31]. SHP1 and

SHP2, although showing structure similarity, have non-redundant and even opposing signalling roles. While SHP2 seems to play a positive role downstream various growth factor receptors, through direct activation of Ras [32], several findings indicate a negative regulatory role for SHP1 in BCR signalling. Besides interacting with other known inhibitory receptors such as CD22 and CD5 {Sen, 1999 #658} upon BCR crosslinking, SHP1-deficient mice have increased $CD5^+$ activated B-1 lymphocytes, with enhanced mitogen-activated protein kinase (MAPK) signalling in response to submitogenic doses of anti-BCR antibodies [32]. Additionally, antigen-specific B cells undergo rapid deletion instead of anergy when exposed to antigen and this process involves, along with SHP1, Lyn and CD22 [22]. SHP1 is also involved in the regulation of cytokine and chemokine receptor signalling, since $SHP1^{-/-}$ mice show impaired responses to stromal-cell-derived factor 1 (SDF-1).

1.4 Cytoskeleton components in lymphocyte activation

Lymphocyte architecture differs dramatically depending on whether the cell is circulating within the bloodstream, migrating through the tissues, or interacting with an APC. The transition between these states requires important signalling-dependent changes in actin-cytoskeleton dynamics. Recent studies on T cells focused on the connection between actin remodelling and signal transduction in response to different environmental cues. B-cell dynamics remain yet less characterized.

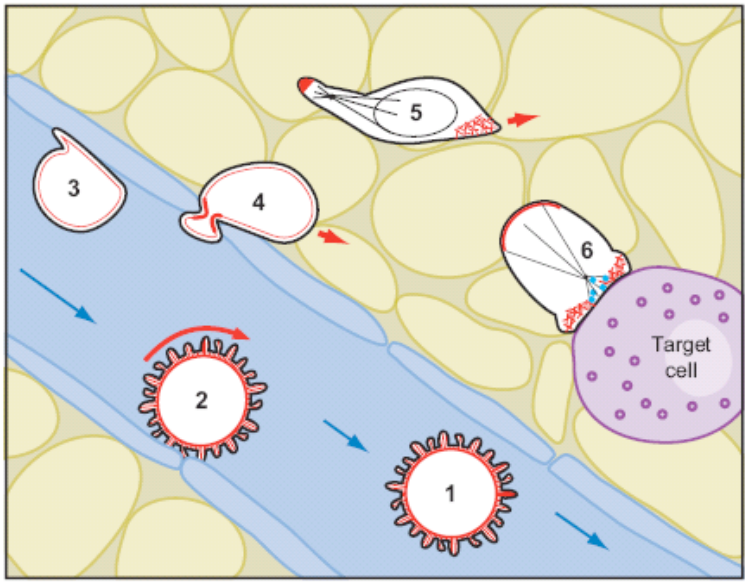

Figure 1.14 Actin remodelling in response to environmental cues. #1-#2: circulating lymphocytes are decorated with microvilli that segregate adhesion molecules during tethering/rolling on the endothelium. #3-#4: Chemokine stimulation induces microvillar collapse and lymphocyte tight adhesion before extravasation. #5-#6: Cell migration through the tissues is mediated mainly by branched actin filaments at the leading edge; #6 Upon recognition of an antigen presenting cell (APC), lymphocytes round up and form tight contact regions. Adapted from [33].

While circulating lymphocytes are covered with microvillar structures enriched in low affinity adhesion molecules (#1- #2 in **Figure 1.14**), chemokine stimulation induces rapid microvillar collapse followed by the increase in integrin avidity through a process named "inside-out" signalling that ultimately cause the cell to stop and tightly adhere to the endothelium (#3 in **Figure 1.14**). After extravasation (#4 in **Figure 1.14**) into the underlying tissues, the cell starts to migrate towards the APC. The cell moves in an ameboid fashion, through protrusion of actin-rich filopodia at the leading edge that work in concert with contractile forces at the rear of the cell (#5 in **Figure 1.14**). Upon interaction with the appropriate APC, the lymphocyte rounds up, retracts the uropod and extends large lamellipodia toward the APC, resulting in the formation of a flattened actin-rich surface at the contact zone (#6 in **Figure 1.14**). These processes allow the

spatial reorganization of adhesion molecules (e.g. LFA-1) at the interface with the APC where they bind high-affinity ligands [e.g. intercellular adhesion molecule-1 (ICAM-1)] allowing the lymphocyte to adhere effectively to the APC and organize the signalling machinery at the IS [33].
The cytoskeleton is a cellular network of structural adaptor and signaling molecules that regulates most cellular functions that are related to the immune response, including migration, extravasion, antigen reconition, activation and phagocytosis. The diverse activities of the cytoskeleton depend on the three types of protein filaments, that connect protein complexes and organelles in different region of the cell, serve as tracks for transport between them, and provide mechanical support.

The three type of filaments are:

Microtubules : are long, hollow cylinders made of the protein tubulin. They are much more rigid than actin filament, typically have one end attached to a single microtubule organizing center called centrosome. In leukocyte the microtubules system is thought to regulate the polarized secretion of effector molecules.

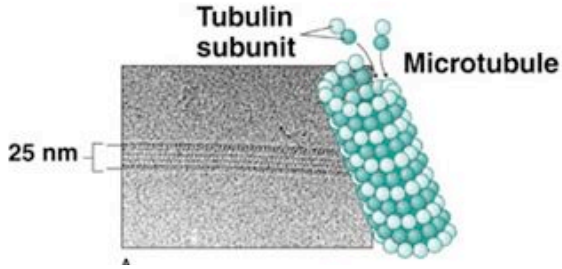

Intermediate filaments : are ropelike fibres, made of intermediate filaments proteins which constitute a large and heterogeneous family, one example of which is vimentin that maintains the overall cell shape and form a polarized network within polarized cells.

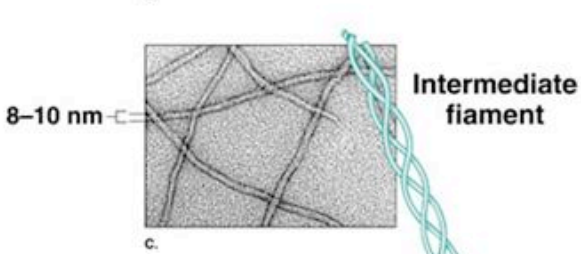

Actin filaments: also known as filamentous F-actin, are two–stranded helical polymers of the protein actin. They are organized into a variety of linear bundles, two-dimensional networks and three-dimensional gels. They are dispersed throughout the cell but they are most concentrated in the cortex just beneath the plasma membrane.

In leukocytes they control cell morphology and plasticity and provide the mechanical force necessary for motility. F-actin undergoes dynamic polymerization and depolymerization during cellular activation thanks to polymerization machinery finely regulated in a signaling-dependent mode. Among these there are proteins that promote nucleation and branching of actin, such as the ARP2/3 complex, Formin, WAWE and WASP.

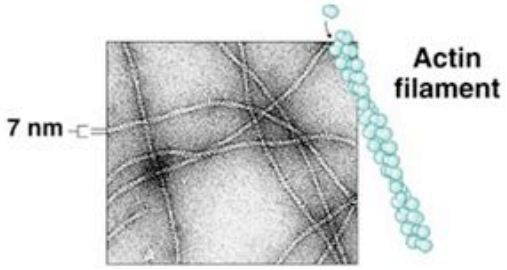

The high rates of actin polymerization or depolymerization are finely tuned by signalling activation and regulated by many capping proteins, nucleator proteins and adaptor proteins. Capping proteins bind to the growing (plus) end of microfilaments, blocking actin polymerization. Nucleator proteins (Arp2/3, Verprolin homologous protein (WAVE), Wiscott Aldrich syndrome protein (WASp), Cortactin) bind to the plus or minus ends of microfilaments and promote actin polymerization. Adaptor proteins (Ezrin-Radixin-Moesin (ERM) proteins, haematopoietic progenitor kinase 1 (HPK1)-interacting protein of 55 kDa (HIP55)) lack any known enzymatic activity, DNA binding or receptor function but mediate protein-protein or lipid-protein interactions.

Major players in the regulation of actin polymerization are two families of signalling proteins: the Vav proteins [34] and the Rho-GTPases [35].

VAV

The Vav family of Rho guanine nucleotide exchange factors (GEFs) includes three structural related proteins: Vav1 is found primarily in haematopoietic cells, while Vav2 and Vav3 expression is less restricted. Their principal function is to catalyze the activation of Rho-GTPases by promoting the exchange of guanosine diphosphate (GDP) for guanosine triphosphate (GTP). The GEF activity is modulated by the regulatory residue Y174; when unphosphorylated, Y174 interacts with a pocket within the DBL homology (DH) domain, thus inhibiting the GEF activity that is restored after tyrosine phosphorylation. The protein structure with a brief description of the functional domains is shown in **Figure1.15**.

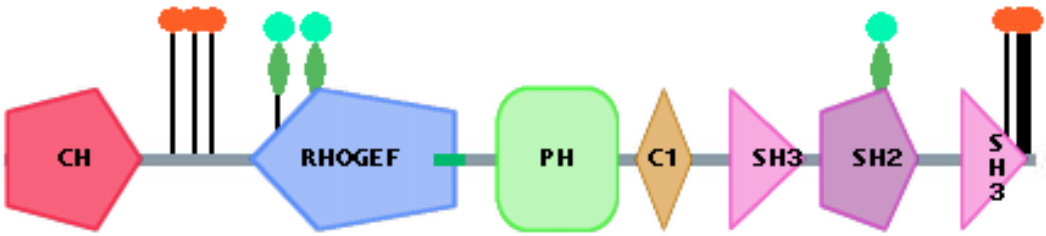

Figure 1.15. **A schematic representation of Vav structure**. Calponin homology (CH) domain: regulation of guanine exchange factor (GEF) activity, Ca^{++} mobilization; acidic (Ac) motif: autoinhibition of GEF activity; contains three regulatory tyrosines, among which Y174; DBL homology (DH) domain: GEF activity; pleckstrin homology (PH) domain: regulation of GEF activity, interaction with phosphoinositide 3-kinase (PI3K) generated lipids; zinc-finger (ZF) domain: Rho GTPases binding; proline-rich (PR) region and Src homology 3 (SH3) domain: protein-protein interaction; Src homology 2 (SH2) domain: recruitment of phosphorylated tyrosines. N, N-terminus; C, C-terminus. Adapted from human protein reference database

Vav proteins are crucial for both cytoskeletal remodelling and signalosome assembly at the IS of B [14] and T cells [36].

Vav proteins are recruited to activated receptors on lymphocytes via their SH2 domain and become phosphorylated by several tyrosine kinases such as Lyn and Syk {Deckert, 1996 #693}. The protein can also directly interact with adaptors and coreceptors, such as BLNK and CD19 and modulate the activity of several BCR proximal kinases such as Btk and PI3K [37]. Cooperation with PLCγ2 in early signalling regulation and Ca^{++} mobilization ultimately leads to

activation of nuclear factor of activated T cells (NFAT) and nuclear factor kappa B (NFκB) transcription factors [14].

Besides being essential in BCR signalling initiation, Vav proteins are also required for peripheral maturation and survival of B cells, although seem not to be relevant for B-cell development in the bone marrow [38].

Rho GTPases

The Rho-GTPase family comprises twenty-two proteins found in all eukaryotic cells that act as molecular switches cycling between an active GTP-bound state and an inactive GDP-bound state.

Their activity is finely regulated: GEFs catalyze the exchange of GDP for GTP; GTPase-activating proteins (GAPs) stimulate the intrinsic Rho-GTPase activity to inactivate the protein; guanine nucleotide dissociation inhibitors (GDIs) appear to block spontaneous activation (**Figure 1.16**).

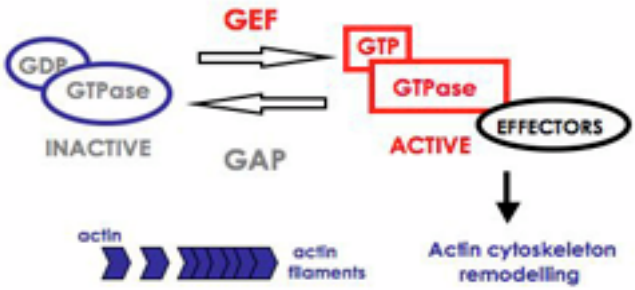

Figure 1.16. **The Rho GTPase cycle**. Rho GTPases cycle between an inactive GDP-bound form and an active GTP-bound form. Guanine exchange factors (GEFs) catalyze the exchange of GDP for GTP, thus activating the protein, while GTPase activating proteins (GAPs) stimulate the intrinsic GTPase activity to inactivate the protein. GDI, guanine nucleotide dissociation inhibitor. Adapted from [35].

The most characterized proteins are Rho, Rac and Cdc42 that, among other functions, are crucial for the regulation of actin dynamics. Rho activation leads to the assembly of acto-myosin filaments, while Rac and Cdc42 are involved in the generation of lamellipodia and filopodia at the rear of the cell, respectively [35]. In B cells, Rac and Cdc42 stimulate actin polymerization through the activation of the Arp2/3 complex via the nucleator WASP after CD40 and IL-4 stimulation [39].

Furthermore, recent evidences underlie the importance of Rac proteins in the regulation of B-cell responses. Downstream of BCR engagement, Lyn, Vav1, Vav2 and PI3K regulate the activation of Rac1 and Rac2, that are rapidly recruited to the IS, where they contribute

(especially Rac2) to integrin-mediated adhesion to APCs [40]. In addition, conditional Rac1/2 knock-out mice showed impaired B-cell development, proliferation and survival [41].

HIP55

HIP55 (haematopoietic progenitor kinase 1 (HPK1)-interacting protein of 55 kDa; also called SHP3P7 and mAbp1) is a cytoskeletal adaptor composed of an N-terminal ADF homology (ADF-H) actin-binding domain, two consensus tyrosine phosphorylation sites, and a C-terminal SH3 domain (**Figure 1.17**).

Figure 1.17. **A schematic representation of haematopoietic progenitor kinase 1 (HPK1)-interacting protein of 55 kDa (HIP55) structure**. ADF homology (ADF-H) domain: actin binding; Src homology 3 (SH3): proline-rich peptide binding. N, N-terminus; C, C-terminus. Adapted from human protein reference database

In T cells, following TCR engagement, HIP55 is phosphorylated and recruited to the IS [42], where it interacts and becomes tyrosine phosphorylated by ζ chain associated protein (ZAP) 70 , a proximal TCR kinase similar to Syk. Besides positive contribution to TCR signalling, HIP55 is also known to interact with negative regulators of TCR signalling such as HPK1 and SLP76 . Nevertheless, HIP55 recruitment requires a functional actin-binding domain and depends on Rac2 activation [43], suggesting a link between cytoskeletal remodelling and the activation of this adaptor protein.

While HIP55 involvement in T-cell proliferation and cytokine production is clear , its role in B-cell responses still needs to be established. Our group recently showed that HIP55 interacts with HS1 in normal and leukemic B lymphocytes [44], thus suggesting a potential role for HIP55 in IS formation and signalling modulation also after BCR engagement.

Nonmuscle myosin II

Members of the nonmuscle myosin II family are composed of a heavy-chain dimer and each heavy chain (MyH, myosin heavy chain) is associated with two myosin light chains (MLCs) (**Figure 1.18**). Following MLC phosphorylation by myosin light chain kinase (MLCK), myosin assembles into bipolar filaments (**Figure 1.18**) and mediates contraction after actin binding. MyH9, MyH10 and MyH14 are the three mammalian isoforms, among which MyH9 is dominant in lymphocytes. MyH9 assembles with MLCs to form the myosin IIA complex.

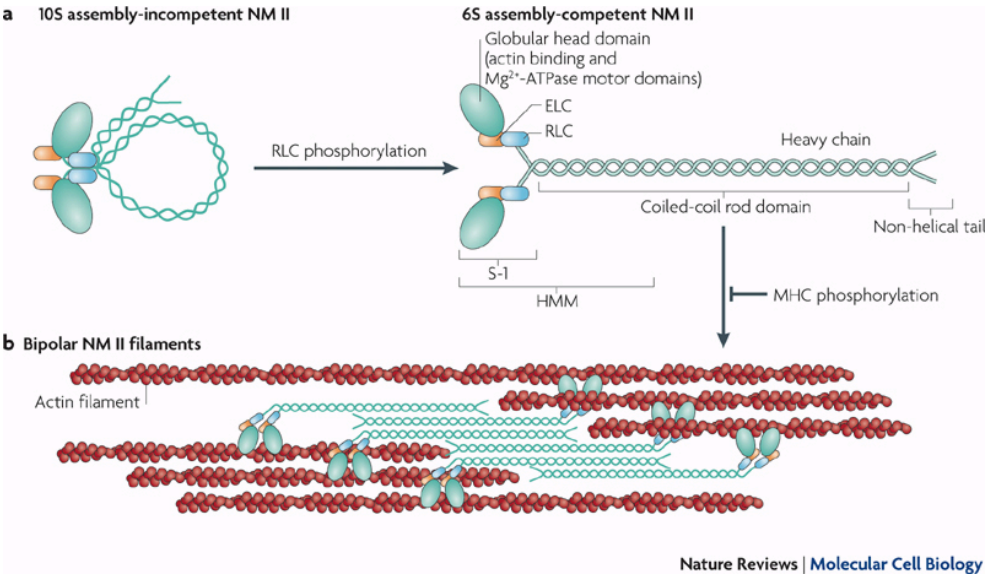

Figure 1.18. **(a) Representation of a myosin molecule** showing the globular head region, the helical coiled-coil rod and the short non-helical tail. **(b)** An example of a **bipolar filament**, which is formed by interaction among the rod domains following phosphorylation of myosin light chains (MLC). Adapted from[45]

Besides mediating several cellular functions, including cell polarization, migration, adhesion and cytokinesis through acto-myosin based contraction [46], myosin IIA is an essential molecular motor at the T-cell IS, while its role at the B-cell IS needs to be elucidated. It has been recently found that myosin IIA is essential for T-cell IS assembly and stabilization [47], whereas inhibition of myosin IIA filament formation is required for the T-cell "stop signal" after antigen encounter. After T-cell engagement, myosin IIA is activated by phosphorylation of MLCs and its activity is necessary for proper assembly of the signalosome, direct movement of the TCR microclusters to the cSMAC and downstream signalling amplification (e.g. Ca^{++} responses) [47]. Myosin IIA activity is finely modulated by several signalling components, such as Rho GTPases, and by Ca^{++} signalling, both acting directly on MLCK [48].

1.5 Haematopoietic cell-specific Lyn substrate 1 (HS1)

HS1 is a 75 kDa intracellular protein expressed in haematopoietic cells. HS1 contains an Arp2/3 complex binding domain [49] followed by a region of three and a half 37 amino acid tandem repeats and a coil-coiled (CC) region, both of which bind F-actin [16], a proline-rich (PR) domain and a C-terminal SH3 domain [50]. HS1 and cortactin, a widely expressed and structurally related gene [51], can activate Arp2/3-dependent actin polymerization and prolong the half-life of branched actin structures [49] (**Figure 1.19**).

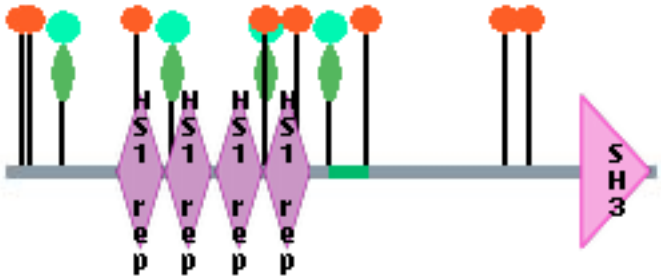

Figure 1.19. **A schematic representation of haematopoietic lineage cell-specific protein (HS1) structure**. Arp2/3 binding domain: binding to the actin nucleator Arp2/3; 37 amino acid tandem repeats: actin binding; coiled-coil (CC) domain: actin binding; proline-rich (PR) domain: protein-protein interaction via Src homology 3 (SH3) domains; SH3: protein-proten interaction via proline-rich peptide binding. N, N-terminus; C, C-terminus.
Adapted from human protein reference database

HS1 role in B cells

HS1 has been originally identified in B lymphocytes as a major substrate of BCR-induced phosphorylation after antigen stimulation [52]. Phosphorylation is first initiated by Syk [53] at Y388/Y405 in murine HS1 or Y378/Y397 in human HS1 and subsequently by Src kinases (including Lyn) at Y222 [54]. While Syk-mediated phosphorylation is crucial for HS1 recruitment to BCR signalosomes, this process is not affected by Lyn deficiency [55]. HS1 has a central role in B-cell responsiveness, as indicated by a defective antigen-induced clonal expansion and deletion in HS1$^{-/-}$ mice [56], though it also seems to be required for programmed cell death, as low levels of HS1 expression are associated with apoptosis resistance [56].

Scielzo et al. [57], using a proteomic approach, demonstrated that B-cell subpopulations differ in terms of HS1 phosphorylation status. Two-dimensional electrophoresis (2-DE) and mass spectrometry (MS) analysis showed the presence of two forms of the protein, one partially-phosphorylated (right spot) and one hyper-phosphorylated (left spot). While naïve B cells exhibit both spots, both memory and anti-IgM stimulated B cells show a shift towards the left spot (**Figure 1.20**).

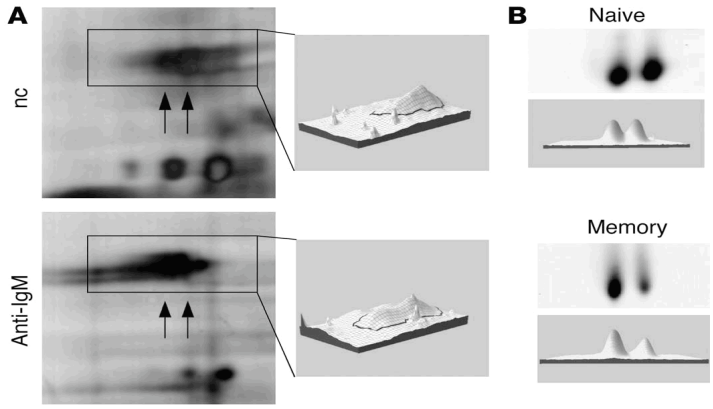

Figure 1.20. **HS1 pattern of expression in normal B lymphocytes**. **(A)** Proteins from tonsillar B cells before and after anti-IgM stimulation were resolved on two dimensional electrophoresis (2-DE) and revealed by silver staining. The arrows indicate the 2 HS1 protein spots (left panels) and densitometric analysis shows a shift from a less acidic to a more acidic form of HS1 following anti-IgM stimulation (right panels). **(B)** The same analysis is conducted on naïve and memory tonsillar B cells. 2-DE: top panels; densitometric analysis: bottom panels of each population. Adapted from [57].

These evidences suggest that HS1 hyperphosphorylation is a direct consequence of BCR stimulation. Nonetheless, the physiological role of HS1 in B cells has not yet been clarified. HS1 has been found to form a multi-protein complex with ZAP70 and several cytoskeletal molecules, such as cortactin and HIP55 [44], suggesting that HS1 might take part in the regulation of the B-cell cytoskeleton.

HS1 role in T cells

One of the first major findings concerning HS1 function in haematopoietic cells regards its role as an actin-regulatory protein at the IS of T lymphocytes. After TCR engagement by an antigen presented on the surface of an APC, HS1 is phosphorylated by TCR proximal kinases [50], such as ZAP70, and efficiently recruited to the IS [58]. Phosphorylation of both Y378 and Y397 residues

on HS1 is required for stable recruitment of Vav1,that is essential for actin polymerization. Phospho-HS1 is also able to interact with other signalosome components, such as PLCγ1, the T-cell specific isoform of PLC. HS1-mediated actin stabilization overtime is required for sustained TCR signalling; indeed, $HS1^{-/-}$ T cells show an overall reduction in Ca^{++} signalling, IL-2 promoter activity and nuclear transcription [58].

A more recent report [59] includes Abl, a non-receptor tyrosine kinase whose mutants are associated with several tumors, in the regulation of HS1 at the IS via direct interaction and enhancement of HS1 phosphorylation by ZAP70. Since Abl seems to be involved in the regulation of chemotactic migration, these findings suggest the potential involvement of HS1 in T-cell migration.

HS1 role in NK cells

HS1 has been shown to be essential in the promotion of NK-cell cytolitic responses [60]. Indeed, knock-down (KD) of HS1 results in several functional defects including impaired lysis of target cells, cell adhesion, chemotaxis and actin assembly at the lytic synapse. After adhesion to target cells through integrin-mediated binding, HS1 and the cytoskeletal proteins Vav1 and WASP are required for actin remodelling at the contact zone. In addition, HS1 is essential for integrin-mediated signalling, since KD cells show reduced Lyn and Vav1 phosphorylation and reduced Rac1 activation after ICAM-1 binding, while showing no differences in the phosphorylation status of kinases such as Syk and PI3K. To a similar extent, signalling pathways emerging from chemotactic stimuli (e.g. SDF-1 exposure) or direct activation of NK cells (e.g. through the activating killer cell lectin-like receptor NKG2D) are impaired after HS1 KD. Interestingly, phosphorylation at Y397 is required for adhesion to ICAM-1 and for cytolysis, while phosphorylation at Y378 is required for chemotaxis (**Figure 1.21)**

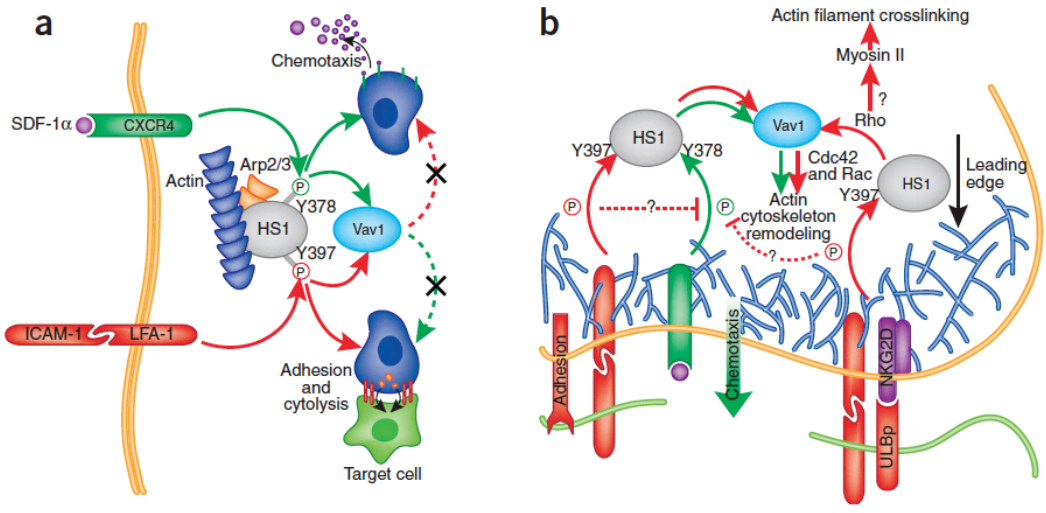

Figure 1.21: Distinct HS1-mediated signaling paths converge at Vav1 through HS1. (**a**) Adhesion receptor signals induce phosphorylation of HS1 at Tyr397, which leads to Vav activation and adhesion (red solid arrows), but not chemotaxis (red dashed arrow). Chemokine receptor signals induce phosphorylation of HS1 at Tyr378, which also induces Vav phosphorylation but triggers chemotaxis (green solid arrows), not adhesion (green dashed arrow). (**b**) Both chemotaxis and adhesion lead to the assembly of a branched actin filament network (blue). However, the two signals are not redundant. Phosphorylation of HS1 at Tyr397 may downregulate pathways mediated by HS1 phosphorylated at Tyr378 (left, dashed arrow),leading to migration arrest. Alternatively, a separate population of HS1 molecules phosphorylated exclusively at Tyr397 may induce migration arrest by initially inducing actin filament crosslinking and inhibiting Cdc42 and Rac (right, dashed arrow); subsequent reactivation of Cdc42- and Rac-mediated cytoskeleton remodeling might then facilitate adhesion. Commentay to [60]

HS1 role in Dentritic cells

It has been recently shown by Huang et al [61]that dendritic cells (DCs) from HS1(-/-) mice differentiate normally and display normal LPS-induced upregulation of surface markers and cytokines. Consistent with their normal expression of MHC and costimulatory molecules, HS1(-/-) DCs present OVA peptide efficiently to CD4(+) T cells. However, presentation of OVA protein is defective. Similarly, MHC class I-dependent presentation of VSV8 peptide to CD8(+) T cells occurs normally, but cross-presentation of GRP94/VSV8 complexes is defective. Analysis of Ag uptake pathways shows that HS1 is required for receptor-mediated endocytosis, but not for phagocytosis or macropinocytosis. HS1 interacts with dynamin 2, a protein involved in scission of endocytic vesicles. However, HS1(-/-) DCs showed decreased numbers of endocytic invaginations, whereas dynamin-inhibited cells showed accumulation of these endocytic intermediates. Taken together, these studies show that HS1 promotes an early step in the endocytic pathway that is required for efficient Ag presentation of exogenous Ag by DCs.

1.6 B cell Chronic Lymphocytic Leukemia (CLL)

Chronic Lymphocytic Leukemia (CLL) is the most frequent leukemia in the Western world, with an incidence of about 5 new cases per 100.000 individuals annually. The disease affects mainly elderly people but one third of new cases are diagnosed before the age of 55 years. CLL is characterized by the clonal expansion and accumulation of mature CD5+ B lymphocytes in peripheral blood, bone marrow and secondary lymphoid organs (lymph nodes and spleen).
CLL is not caused by any known environmental factors such as chemical compounds or ionizing radiations, but a relevant genetic and familial predisposition is evident as suggested by the fact that is a rare disease in the Far East and the low incidence is not modified in Japanese emigrants, thereby excluding other environmental factors.

The normal counterpart of leukemic B lymphocytes

CLL cells show phenotypic features resembling B lymphocytes activated after antigen encounter. In particular, they express high levels of CD (Cluster of Differentiation) molecules (like CD23, CD25, CD69 and CD71) that are up-regulated after activation, while they show low expression of markers which are typically downregulated after cellular activation like CD22, FcγRIIb, CD79b and IgD. In addition, they express the memory B cell marker CD27.
CLL cells are also characterized by the expression of CD5, initially identified as a T cell marker. It was then recognized that a proportion of B lymphocytes from peripheral blood of healthy donors may also carry this molecule [62]. CD5 positive B lymphocytes can also be found in the mouse in which they are called B1 cells. These lymphocytes produce low affinity immunoglobulins (Ig) specific for bacterial components, and thus they can represent a form of natural protection against microrganisms. In some cases the produced antibodies crossreact with auto-antigens that share homologies with bacterial antigens [63].
In humans, CD5 expressing B lymphocytes are predominant during fetal life [64], while in adults they are absent in the bone marrow but they represent 30% of B lymphocytes of peripheral lymphoid organs (where they are located in the mantle zone of the follicle), 10% of splenic B lymphocytes and most B cells located in the peritoneal cavity [65].
In contrast to the mouse where CD5 is essentially a lineage marker among B lymphocytes, in humans CD5 can be considered as an activation marker. Treatment of $CD5^-$ cells with anti IgM [66] induces its expression, thereby suggesting that its expression on CLL cells may just be considered as a sign of a previous activation (e.g. by an antigen) rather than a feature of a distinct cell lineage of origin.
Another typical phenotypic feature of CLL is the expression of low to undetectable levels of surface Ig (sIg), a feature shared by murine B cells anergized by the chronic exposure to auto-antigens (Ag) [67,68]. Nevertheless, this anergy-related feature does not necessarily indicate a

functional impairment of BCR signaling as at least half of the cases can be actually stimulated *in vitro* through their sIg, irrespective of their low level. In contrast, the remaining CLL cases are unresponsive to BCR crosslinking thereby resembling also at functional level B cells anergized *in vivo* after chronic stimulation by an antigen [69]. Still and despite extensive studies, the molecular bases for this functional difference are ill defined.

Current new hypotheses: [70]

Documenting that CLL clones use either mutated or unmutated IGHV genes (see below charter: Biological features and their influence on the clinical corse) and that this feature distinguishes patient subgroups with distinct clinical courses gave rise to the postulate that the 2 subgroups of CLL originated from distinct cell types with different differentiation and antigen encounter histories, consistent with a 2-cell origin model. Furthermore, several lines of evidence implicated B-cell receptor (BCR) signaling as a promoting factor that could lead to divergent cell biology and patient pathology. First, the IGHV repertoire in CLL is not random and differs between U-CLL and M-CLL as well as between CLL cells and normal B cells.

Second, the preponderance of polyreactive and/or autoreactive BCRs, especially among U-CLL cases, and retention of signaling through U-CLL BCRs suggest that antigen-binding specificity and BCR signaling capacity influence clonal expansion, possibly by facilitating tumor survival and growth. However, key microarray analyses of gene expression identified only a relatively small number of gene use differences between U-CLL and M-CLL, as opposed to thousands of differences between normal B lymphocytes and either U-CLL or M-CLL. These findings suggested a singular originating cell with additional, nongenetic promoting factors explaining differences in cellular features between U-CLL and M-CLL and their respective clinical outcomes.

To overcome the difficulties of reconciling a 2-cell origin model, which was more consistent with BCR findings, with a one-cell model, supported by gene expression data, a unifying parsimonious theory was proposed in which both U-CLL and M-CLL derive from marginal zone (MZ) B cells. In the spleen, the MZ is an area at the outermost portion of the white pulp; MZ-like regions exist in tonsil subepithelial areas, dome regions of Peyer patches, and subcapsular regions of lymph nodes (LNs). MZ B cells are defined as IgMhighIgDlow cells that respond to bacterial polysaccharides in a T cell-independent manner. They can express either mutated or unmutated IGVs, although the proportion of cells expressing mutated genes varies depending on anatomic site, animal species, and immunization conditions. In humans, the highest proportion of IGVH mutated MZ B cells is in the spleen. Occasionally, IGHV mutations and immunoglobulin (Ig) isotype switching occur during responses of IgMhighIgDlow B cells in MZ or MZ-like areas of humans and mice. However, B cells more often do acquire such mutations, frequently along with class switch recombination, in germinal centers (GCs), and some of these B lymphocytes migrate and take up residence in MZs. MZ B cells are often antigen-experienced as evidenced by clonal expansion of IgMhighIgDlow B cells without IGV mutations and by diversification and expansion in the MZ for those cells with mutations. In

addition, B cells expressing IgG or IgA found in MZ and MZ-like areas are often referred to as switched memory B cells, use mutated IGHV, and are predominantly of post-GC origin.

Role of the Micro-environment in CLL: cytoskeleton function and players

Several studies indicate that the microenvironment has a critical role in CLL cell survival and accumulation suggesting also its fundamental influence on clonal evolution [71].

Circulating CLL cells are largely arrested in G_0/ G_1 phase of the cell cycle but a small proportion of leukemic lymphocytes accumulate in the so-called "proliferation-centers" (PC) in the lymph nodes and the bone marrow (BM) where signals delivered from the microenvironment are likely crucial in inducing proliferation of the leukemic cells [72]. Furthermore, in the PCs, leukemic lymphocytes are in contact with numerous $CD4^+$ T cells that express CD40 ligand (CD40L) and can support the growth of CLL cells through CD40 ligation. It can also be hypothesized that antigen (in particular auto-Antigen) stimulation may be another triggering event that induces leukemic cell activation and cell cycle entry in the PCs. *In vitro* (and likely *in vivo*) CLL cell apoptosis can be rescued by the presence of stromal cells and nurse-like cells [73, 74]. It is also possible that the interaction between CD38 on the surface of CLL cells and its ligand CD31 may play a role [75]. Indeed the usage of deuterium to *in vivo* label proliferating cells have revealed that, within each clone, $CD38^+$ cells proliferate 2.5 times faster than those CD38- [76]. In the same study, a relationship between *in vivo* kinetics, levels of expression CXCR4 and clinical outcome of the patients was suggested. Cytokines such as IL-4, and chemokines such as CXCL12 (SDF-1, CXCR4 ligand) might support the expansion of the CLL clone by promoting the up-regulation of antiapoptotic proteins including Bcl-2, survivin, and Mcl-1 thus favouring the extended survival of leukemic cells [77].

The possibility that microenvironmental elements may be utilized by CLL cells to avoid apoptosis and to acquire better growing conditions in the PCs has led to the assumption that CLL B cells repeatedly migrate from the peripheral blood to the lymph node or BM to receive the proper signals for their expansion and propagation. Though the precise mechanisms are currently unknown, it is likely that lymphocyte trafficking and homing to specialized microenvironments may partially depend on the sequential engagement of adhesion molecules and activation through chemokine receptors. CLL B cells express functional CXCR3, CXCR4 and CXCR5 chemokine receptors that have been shown to direct leukemia-cell chemotaxis *in vitro* [78]. Cell movement and migration involve complex molecular mechanisms driving cytoskeletal reorganization. These processes are ill defined in leukemic B cells. Therefore, it is essential to investigate the role of cellular networks of structural adaptors and signalling molecules which regulate most cellular functions related to the immune response including migration, adhesion, transendothelial migration, antigen recognition and intracellular activation.

Different studies demonstrated that CLL cells have a high fragility and undergo severe morphologic deformities in the preparation of blood films giving rise to the so-called (and unique to CLL) "smudge" cells suggesting a cytoskeletal alteration (**Figure 1.22)**.

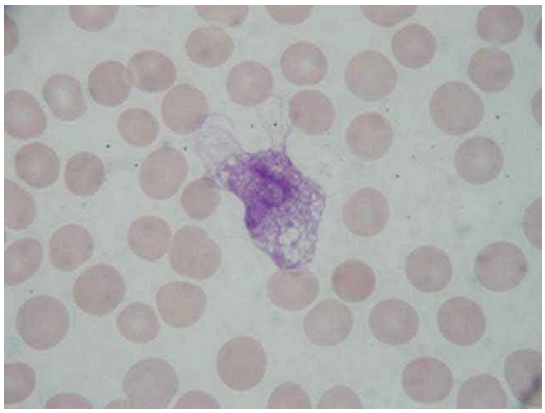

Figure 1.22 "smudge" cells

CLL cells have impaired cell motility, diminished capping by multivalent ligands, increased shedding of membrane proteins and enhanced susceptibility to microtubule-disrupting drugs [79]. The organization of actin-containing microfilaments and vimentin-containing intermediate filaments has revealed that adhesion structures are present and that the *in vitro* adhesion capacity is marked [80]. It has been recently shown that low vimentin content of CLL cells correlates with increased percentage of smudge cells and with increased survival [81].

CLL B cells ZAP-70^{+} respond *in vitro* more readily than ZAP-70^{-} CLL and normal B cells to chemokine driven migration by modulating CCR7 expression and increasing responsiveness to its ligands CCL19 and CCL21 [82]. In addition, ZAP-70^{+} CLL cells exhibit sustained ERK activation following stimulation with CXCL12 (SDF-1) as compared to ZAP-70^{-} cells [78]. Further, CD38 and ZAP70 are functionally linked and associated with CLL endowed with high migratory potential [82]. These advantageous migratory and survival responses may promote easier access to and greater proliferation within PCs and contribute to explain the progression of ZAP-70^{+} $CD38^{+}$ leukemic clone.

Furthermore, recent evidence suggest that the transmigration and adhesion capacity of CLL cells are altered. The majority of CLL cells express on average reduced levels of the two major lymphocyte integrins, LFA-1 and VLA-4 although with wide variations between patients [83]. The study suggested a critical role of these receptors by showing a reduced capacity of CLL cells with reduced LFA-1 and VLA-4 to adhere and transmigrate through multiple vascular endothelial beds and poorly home to lymphoid organs other than the spleen. Interestingly, Montresor *et al* suggest that the neoplastic progression may completely bypass Rac1 and CDC42 regulation (both GTPase family members fundamental for cytoskeleton regulation, [84,85], and show a consistent divergence in the signalling mechanics controlling integrin activation in

CLL patients as compared to normal B cells. While LFA-1 was found modulated by RhoA in all CLL patients, Rac1 and CDC42 display on the contrary a consistent variability among the cases [84]. Along this line of evidences Till *et al* show that the chemokine-induced transendothelial migration (TEM) is defective in CLL due to defective Rap1 and alphaLbeta2 integrin activation [86].

The cytoskeleton has an important role also in the BCR mediated process of Ag recognition; normal B cells exhibit a two-phase response in which they first spread over the Ag and then collect bound Ag into a central cluster of BCR/Ag complexes surrounded by a ring of adhesion molecules (LFA-1/ICAM-1) similarly to the synaptic structure originally described for T cells [87]. These processes imply the need of actin polymerization and cytoskeleton reorganization [15].

Interestingly, cytoskeletal defects are present also in T cells from CLL patients which exhibit defective immune synapse (IS) formation with B cells [88].

Together with the cytoskeletal functions numerous studies have highlighted new F-actin-regulatory molecules controlling various aspects of leukocyte biology [46]. Much attention has been drawn on proteins that regulate actin dynamics through their effects on the Arp2/3 complex (i.e. WASP and VAV family)[16]**.** Furthermore it has been recently shown that RhoH (GTPases family member) expression correlates with the expression of ZAP70 in CLL and a potential role in the progression of the disease is suggested [89]

In this scenario we recently identified HS1 (hematopoietic lineage cell-specific protein 1) as a putative prognostic marker in CLL [57]. HS1 is a 75 kD intracellular protein which is expressed mainly in haematopoietic cells [90,91]. HS1 binds actin and it contains an Arp2/3 complex binding domain [16] and a proline-rich domain [50]. HS1 has been shown to be an important actin regulator at the T-cell immunological synapse [58,92] and also to influence numerous functions of NK cells including lysis of target cells, cell adhesion, chemotaxis and actin assembly at the lytic synapse [60]. By dissecting HS1 molecular function in CLL B cells we recently demonstrated that HS1 takes part in the formation of a novel complex together with the ZAP-70 kinase and several cytoskeleton adapters (namely HIP-55 and Cortactin), and that it co-localizes with F-actin and Vimentin thereby showing a potential role in the regulation of the B-cell cytoskeleton [44].

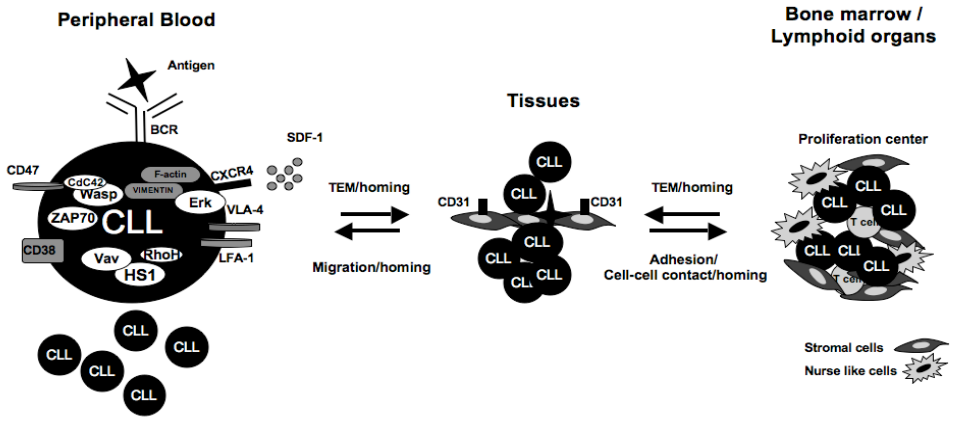

Figure 1.23. Cytoskeleton activities and key layers in CLL [93]

Biological features and their influence on the clinical course

CLL has a very heterogeneous clinical course; some patients remain free of symptoms and survive for as long as 20 years after the initial diagnosis and do not need therapy, whereas others experience an aggressive disease and die within 2 or 3 years. For this reason prognostic factors able to predict the disease course at the time of diagnosis are essential for the optimal management of CLL patients. The traditional prognostic factors are essentially based on clinical features and define disease extension at any given moment, but they are not capable of predicting the evolution of the disease at initial diagnosis:

- The **clinical stage** according to Rai or Binet: patients can be subdivided into three groups (Rai: low-intermediate-high risk; Binet: stage A-B-C) based on the clinical evaluation of several parameters including lymphoid tissue involvement;
- The **lymphocyte doubling time** (LDT): the time required for an increase in the absolute lymphocyte count in the blood to twice the baseline value in a patient not subjected to therapy (if < 6 months the disease is progressing);
- The pattern of **lymphocytic infiltration** in the marrow: diffuse infiltration correlates with poor prognosis.

In addition, several biological parameters can be used to measure the extension of the disease but not to predict its outcome:
- **Presence of prolymphocytes** in the peripheral blood (if >10% the clinical course is aggressive) [94];
- **β2 microglobulin** levels (inverse correlation with survival and response to chemotherapy) [95];
- **Thymidine kinase** (tk) serum levels (inverse correlation with survival) [96];
- **Soluble CD23** serum levels (inverse correlation with survival) [97];
- **p53** expression (direct correlation with prolymphocytic transformation) [98].

New biological markers have been identified that allow a risk-stratification of CLL patients already at the initial diagnosis, regardless the diseade burden. All carry an independent prognostic value, though there is a great overlap among them. However a significant percentage of discordance is present between each other.

(1) Somatic mutations of IGHV genes [99]. The presence or the absence of IgV_H mutations in CLL cells correlates with different clinical courses and outcomes. A ≥98% similarity of the IGHV gene with the corresponding germline sequence (unmutated-CLL) is associated with a more aggressive disease and a shorter median survival time as compared to "mutated cases" (homology <98%) (8 years versus 24 years). That notwithstanding, the technology to sequence Ig genes is technically difficult and expensive and some debates on the proper cut-off value to define significant levels of mutations exist (98% versus 97%).

(2) CD38 expression on the cell surface of CLL cells [100]. CD38 is a 45 kDa transmembrane protein that, through the engagement of its ligand CD31, induces activation and differentiation signals in T and B lymphocytes and natural killer (NK) cells. CD38 positive B-CLL cells are able to bind CD31, with consequent increase of proliferation and cell survival. This interaction is an example of the interactions occurring between leukemic cells and microenvironment that may ensure lymphocytes proliferation.

CD38 has been initially considered a surrogate marker for the IGVH mutational status. Subsequent studies confirmed the prognostic relevance of CD38 expression and its independent prognostic value. CD38 positive CLL cases has a shorter time to progression and shorter survival times. Still, there is controversy among different studies on the actual percentage value of CD38 expression which may better separate patients with good versus bad prognosis. Debate exists also on the stability of the marker during the course of the disease, especially after therapy [101].

(3) Intracellular ZAP70 expression in CLL cells [102]. ZAP70 (ζ chain associated protein), a key signaling molecule involved in signal transduction from the T Cell Receptor (TCR), was initially considered to be expressed exclusively by T and NK cells. However, gene expression profiling revealed that ZAP70 mRNA is expressed also in some CLL cases. ZAP70 is homologous to Syk and can associate with BCR complex in antigen stimulated CLL B cells, indicating that it may function to modulate BCR derived signals. In particular, after BCR triggering, ZAP70 is not phosphorylated, thus activated, but its adaptor functions appeared to be preserved . From these data is possible to suggest that this protein is able to regulate BCR signaling not through its kinase activity but through the recruitment of other signaling molecules.

Initially ZAP70 was described as a reliable surrogate for IGVH gene mutation status, as expression of ZAP70 appeared to correlate with U-CLL cases, but this correspondence is not absolute, so it has to be considered another independent prognostic marker.

In particular, ZAP70 expression in >20% of the leukemic cells carries an adverse prognostic value [103].

(4) Genetic aberrations [104].

There is a significant correlation between certain cytogenetic abnormalities and CLL patients' survival. The most frequent aberrations are 13q deletions (55%), chromosome 12 trisomy (15%), 11q (12%) and 17p (8%) deletions.

Patients with the 13q deletion have the best survival expectancy (around 12 years). The deleted region comprises two miRNAs, *mir-15-a* and *mir-16-1*, that are ubiquitously and highly expressed in normal $CD5^+$ B cells, where they may act as negative regulators of the antiapoptotic molecule Bcl-2. Therefore, it is possible that perturbation of the expression of these oncosuppressor miRNAs may favor an initial survival of the leukemic cells. Chromosome

12 trisomy does not affect survival, as compared to normal kariotype. 17p and 11q deletions, comprising the *p53* and the ataxia telangiectasia mutated (*ATM*) gene, respectively, have the worst clinical outcome. Indeed, both p53 and ATM play a crucial role in the control of cell cycle progression. Some of these abnormalities may be present at diagnosis, while others (e.g. 17p and 11q deletions) may be acquired during the course of the disease. Recently Puente et al [105] performed whole-genome sequencing of four cases of CLL and identified 46 somatic mutations that potentially affect gene function. Further analysis of these mutations in 363 patients with CLL identified four genes that are recurrently mutated: notch 1(NOTCH1), exportin 1 (XPO1), myeloid differentiation primary response gene 88 (MYD88) and kelch-like 6 (KLHL6). Mutations in MYD88 and KLHL6 are predominant in cases of CLL with mutated immunoglobulin genes, whereas NOTCH1 and XPO1 mutations are mainly detected in patients with unmutated immunoglobulins. The patterns of somatic mutation, supported by functional and clinical analyses, strongly indicate that the recurrent NOTCH1, MYD88 and XPO1 mutations are oncogenic changes that contribute to the clinical evolution of the disease. To our knowledge, this is the first comprehensive analysis of CLL combining whole-genome sequencing with clinical characteristics and clinical outcomes. It highlights the usefulness of this approach for the identification of clinically relevant mutations in cancer (**Figure 1.24).**

BCR signalling in CLL

CLL is heterogeneous in terms of functional responses following B-cell receptor ligation. Half of the cases, mainly those with unmutated *IGHV* genes and poor prognosis, can be stimulated *in vitro* through their surface Ig, with functional activation and recruitment of proximal kinases, such as Lyn (**Figure 1.24)**. On the other hand, mutated-CLL cases are unresponsive to BCR cross-linking, thus resembling B cells anergized *in vivo* after chronic antigenic stimulation [69]; [67]. These findings have been associated with the capacity of the BCR signalling machinery to translocate to lipid rafts upon receptor engagement [106]. The molecular basis of CLL-cell responsiveness needs to be established though it is known to be independent of surface IgM density [107].

Despite the clinical and biological heterogeneity of the disease, several signalling pathways appear to be constitutively activated in CLL cells. Leukemic lymphocytes show aberrant Lyn expression and localization and restore apoptosis upon Src inhibition, suggesting a role for Lyn in CLL-cell survival [108]. Constitutive activation of Syk, [69] NFAT [109], NFκB [110], and of the PI3K/Akt pathway [111] have been reported. Muzio et al., [112] recently found that a subset of patients with a good clinical prognosis show constitutively phosphorylated ERK1/2 in the absence of Akt activation and constitutive NFAT activation, while being characterized by unresponsiveness to surface Ig ligation. This biochemical profile has been associated with anergy in murine B lymphocytes and might therefore represent a molecular signature of anergy that occurs *in vivo* in a proportion of CLL patients.

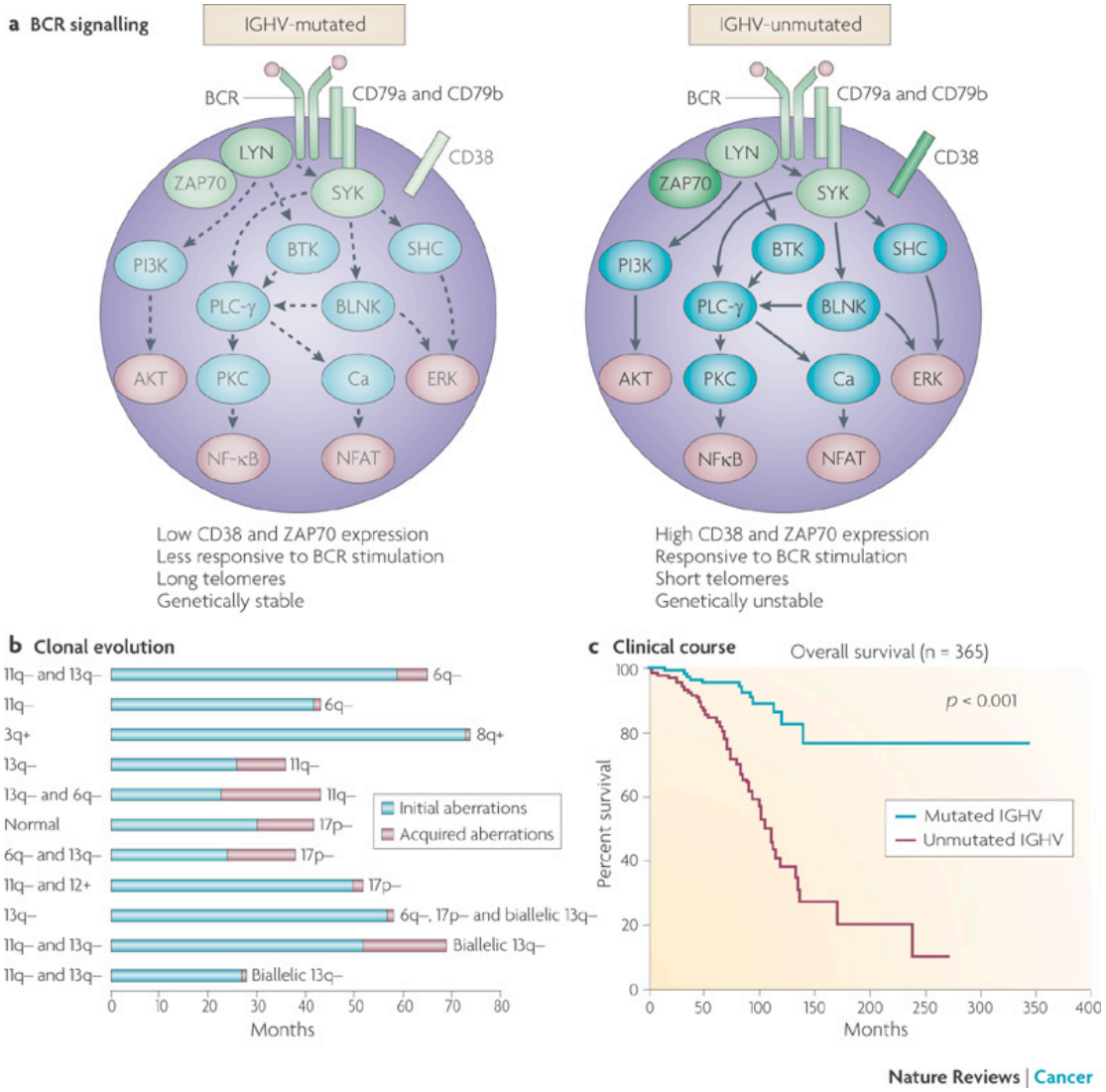

Figure 1.24 Summary of biological and clinical features in CLL. Based on the degree of somatic hypermutation, chronic lymphocytic leukaemias (CLLs) can be differentiated into those with mutated and those with unmutated immunoglobulin heavy chain variable region (IGHV) genes. **a**There are important biological differences between the two groups. IGHV-unmutated CLLs have higher levels of the protein tyrosine kinase zeta-associated protein 70 (ZAP70) and CD38 expression (shown in dark green) than IGHV-mutated CLLs (shown in light green). IGHV-unmutated CLLs activate key signal transduction pathways in response to BCR activation (for example, LYN, SYK, ERK and AKT) and show a different gene expression profile from IGHV-mutated CLL. Reduced signalling in IGHV-mutated CLLs is indicated by grey text and dotted arrows. **B** IGHV-unmutated CLLs have a greater likelihood of carrying and acquiring detrimental genetic lesions (11q23 and 17p13 deletion) than IGHV-mutated CLLs26, 30, 35, 147. The duration of the presence of the initial and the acquired aberrations are indicated in blue and red, respectively. Overall, 11 out of 64 patients showed clonal evolution, which was only observed in IGHV-unmutated cases. c | These biological differences may explain the different clinical courses associated with IGHV-unmutated and mutated CLLs. In a retrospective cohort from our centre (n = 365), the estimated median survival was not reached for the group with mutated IGHV versus 111 months for the group with unmutated IGHV ($p < 0.001$).
Adapted from [113].

HS1 identification in Chronic Lymphocytic Leukemia (CLL)

In an effort to identify novel biological prognostic markers, our group has recently studied, by using a proteomic approach, cells from 40 CLL cases characterized on the basis of their biological and clinical features. By 2-dimensional electrophoresis (2-DE) and mass spectrometry (MS) analysis we have found that the hematopoietic lineage cell-specific protein 1 (HS1) is differentially expressed and shows different distinct features in different subsets of patients (**Figure 1.25**). We demonstrated that HS1 is present in the gels as a single spot or two spots, and the difference between this spots is in term of phosphorylation. We were able to divide CLL patients in two groups based on HS1 phosphorylation pattern.

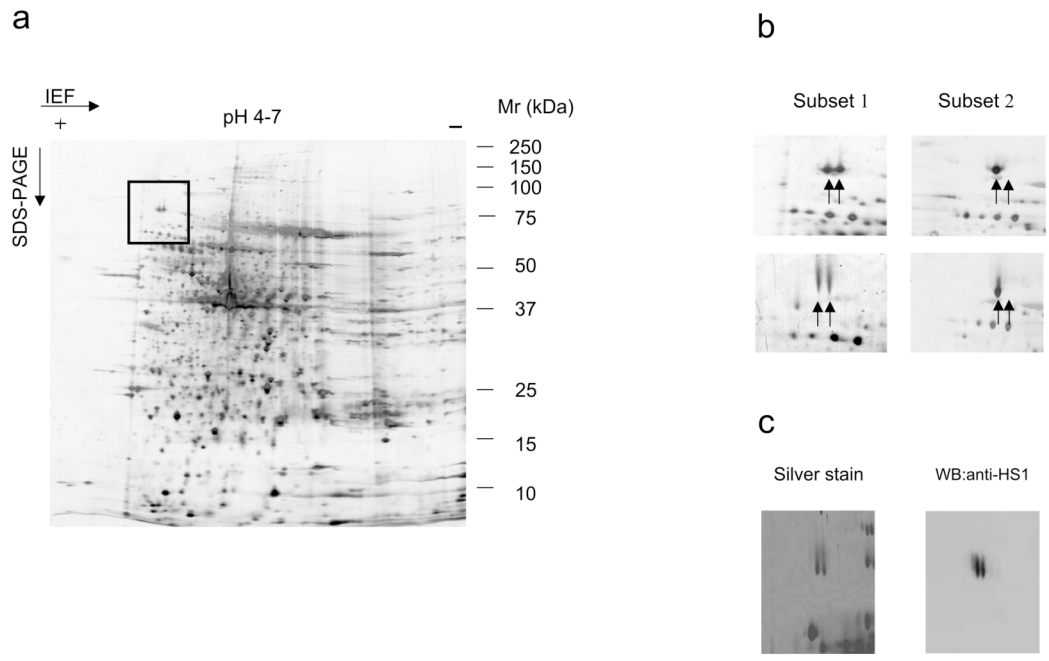

Figure 1.25. 2-DE proteomic analysis of purified CLL cells.

The square identifies two close spots with the same molecular mass (Mr) of 79 Kda and different isoeletric point (pI) of 4,83 and 4,86 respectively, which were identified by MALDI-TOF mass spectometry analysis as HS1 protein. (b) Both right and left spots are expressed in 2D-gels obtained from 2 representative good prognosis CLL patients (Subset 1) while only the more acidic one is present in 2D-gels obtained from 2 representative bad prognosis CLL patients (Subset 2). (c) Proteins obtained from 5 representative CLL patients were resolved on 2-DE that were either silver stained (left panel) or transferred onto nitrocellulose and incubated with an anti-HS1 antibody (right panel). One representative case is shown. The antibody hybridizes in an area corresponding to the spots of interest.

HS1 expression as a prognostic factors in CLL

In a series of 40 CLL patients the differential pattern of HS1 expression was found to correlate with both the expression of CD38 (p=0.022) and IGVH mutations (p=0.008). Rather unexpectedly no significant correlation was found with the expression of Zap-70 (p=0.505). When the 40 patients were grouped according to the HS1 profile it appeared that those presenting 1 single HS1 spot had a median survival time (184 months) significantly shorter than those with two spots,(median survival not reached; p=0.024)(**Figure1.26**).

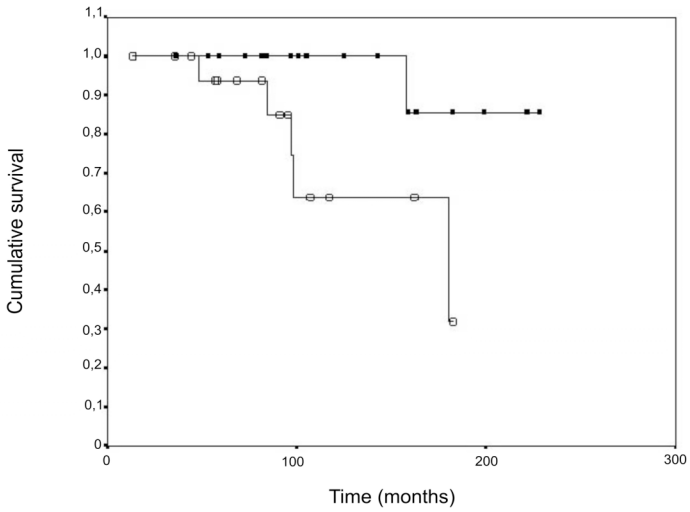

Figure 1.26. Kaplan-Meier curves show cumulative survival of CLL patients grouped according to HS1 expression pattern (1 single spot vs 2 spots). Patients with 2 spots (black dots) have a significantly longer survival (median survival not reached) than those with only one (white dots) (median survival 184 months) (p=0.024).

1.7 Mouse models of CLL: TCL-1 tg mouse

TCL-1 gene identification was due to its position in the break point of chromosome 14, that is involved in abnormal rearrangements associated with mature T cell leukemias and lymphomas [114]. This 350-kb gene is located within the 14q32.1 region and encodes a 1,3 kb-transcript composed of 4 exons (**Figure 1.27**). cDNA sequence studies have revealed that the mature transcript consists in a 342-nucleotides open reading frame encoding a protein of 114 aa and 14 kDa.

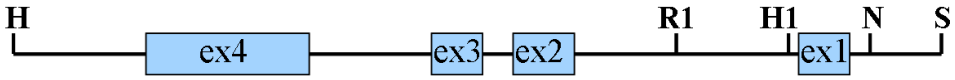

Figure 1.27. **Genomic organization of the human TCL-1 gene [115].**

The gene is normally expressed in restricted subsets of cells within the lymphoid lineage, preferentially in the early stages of differentiation. Looking at the B lymphoid compartment it is detectable in early pre-B cells, sIgM-expressing virgin B cells, mantle cells and, at weak levels, in $CD34^+$ $CD19^+$ pro-B cells and GC B lymphocytes but not in the mature population, like plasma cells. Concerning the T lymphoid compartment, it appears only in $CD3^-CD4^-CD8^-$ thymic progenitors [115].

Eμ-TCL-1 tg mouse model

Clear evidences of TCL-1 involvement in CLL have emerged from the Eμ-TCL-1 tg mouse model. This model has been obtained in the C3HBL/6 strain by inserting the hTCL-1 gene under the control of the IGHV promoter and IGH enhancer (Eμ), together with the 3' end and untranslated region of the human β-globin gene [116]

The construct has driven expression of the human gene in immature and mature B cells, while it was not expressed in the mature B cell compartment in physiological conditions. hTCL-1 expression has been confirmed in the spleen and bone marrow of adult tg mice by western blot analysis. Homozygous mice developed an increasing expansion of $CD19^+CD5^+Ig\kappa^+IgM^+$ B cells [116], [117], that was detected by flow cytometry at 2 months in the peritoneal cavity, at 3-5 months in the spleen, at 6 months in the peripheral blood and at 8 months in the bone marrow. This population was mostly composed of not-dividing B lymphocytes, arrested in the G_0/G_1 phase of the cell cycle, that resemble human CLL cells. The progressive accumulation of $CD19^+CD5^+$ B cells led to splenomegaly, with MZ enlargement, although the expanded cells expressed low levels of CD21, the typical marker of MZ B cells. Between 13 and 18 months of age, Eμ-TCL-1 tg mice developed a disease resembling the aggressive form of CLL, characterized by elevated

WBC counts and massive infiltrations of a monoclonal $CD5^+Ig\kappa^+$ B cell pool in the spleen, lymph nodes and liver [116]. Variable macroscopical and/or microscopical alterations have been also observed in the lungs, kidneys, heart, salivary glands, esophagus, thymus, trachea and thoracic cavity [118].

To investigate the origin of the $CD5^+$ enlarged B cell population, Yan et al. analysed IG gene rearrangements in Eμ-TCL-1 tg mice. They found that $CD5^+$ expanded B cells expressed IGV genes very similar to the germline genes (less than 2% of difference), meaning that they were not significantly altered by SHM. The frequency of the single IGHV, IGHD, IGHJ and IGKV family genes differed from that occurring in the normal B cell repertoire and the HCDR3 regions were usually longer than their normal counterpart, because of the addition of supplementary nucleotides or joining of long IGHJ segments. Finally HCDR3s from sets of leukemic clones often revealed more than 80% of similarity in the amino acidic sequence, suggesting the presence of stereotypic H and L chain rearrangements [119]. All these molecular aspects reproduced the features of human U-CLL and pointed out that leukemic cells may originate from a subset of $CD5^+$ B cells with restricted BCR structure, selected by autoantigens or microbial antigens and forced to clonal expansion. Taken together, Eμ-TCL-1 tg specificities have lead to suggest peritoneal B-1a cells as potential original cells for murine leukemia.

To evaluate the role for TCL-1 overexpression in Akt-dependent immune receptor signalling, the activation status of some Akt downstream molecules has been studied. One known Akt effector is mTOR (mammalian target of rapamycin), a serine/threonine kinase that normally regulates translation by phosphorylating key components of the protein synthesis machinery, including the ribosomal protein S6 kinase [120]. Hoyer et al. previously demonstrated that in the pEμ-B29-hTCL-1 tg mouse model, TCL-1 increased the phosphorylation level of the S6 ribosomal protein, confirming that hyperactivation of the PI3K pathway was at least part of the mechanism for initiating lymphoid transformation [121]. To prove that enhanced Akt activity was also involved in CLL pathogenesis, Zanesi et al. investigated rapamycin effect in the Eμ-TCL-1 tg mouse model. Rapamycin is a potent mmunosuppressant agent that disrupts Akt signalling through mTOR inhibition. S6 ribosomal protein phosphorylation was detected in the lymph nodes of untreated B-CLL-translanted leukemic mice, but not in the lymphoid tissues of rapamycin-treated mice. In addition mice treated before the appearance of disease symptoms showed a 2 weeks-delay in disease onset and a prolonged life expectancy compared to untreated mice [118].

Eμ-TCL-1 tg mice not only developed a CLL-like disease, but were also prone to secondary malignancies, that frequently affect CLL patients and are the most common cause of death. Even if patients often develop secondary lymphoid malignancies, several cases of solid tumours are reported, especially of skin cancer. Pathologic analysis of leukemic mice have revealed some cases of intestinal histiocytic sarcoma, spindle cell sarcoma of the gallbladder, malignant pilomatricoma of the skin, all unrelated to CLL and to the abnormal TCL-1 gene expression [118]. Patients predisposition to secondary tumours may be due to genetic features, carcinogen

exposure, side effects of therapeutic treatment and immune deficiency. Indeed profound B and T cell defects also affected Eμ-TCL-1 tg mice, favouring infectious morbidity [122].

Taken together, these observations make Eμ-TCL-1 tg mouse a valuable model for the aggressive form of human CLL, which could help to investigate further mechanisms and to test new therapies. Nevertheless, this model shows some limitations due in particular to the long time required to develop leukemia and the variable age of onset. Such limits still encourage the research of new and more convenient mouse models, where it could be useful to take into account the role played by the biological prognostic factors involved in CLL development and progression.

Aim of the Thesis

The aim of my project is to define the biological function of Hematopoietic-cell-specific Lyn-substrate-1 (HS1) protein in normal and malignant B-cells since it is poorly defined.

These aspects will help defining the role of HS1 in the pathogenesis of the disease and in particular whether it may become a potential target for the development of novel therapeutic treatments.

We demostrated that the lack of expression of HS1 in B-cells results in diminished formation of actomyosin microclusters (signalosome), impaired cell migration, abnormal cell adhesion and aggregation. Both xenograft and genetically modified animal models of CLL lacking HS1 show a different pattern of tissue infiltration with a preferential localization in the bone marrow: the leukemia also has an earlier onset and a faster growth similarly to patients with aggressive disease. We propose that HS1 is a central regulator between the B-cell-receptor signaling and the cytoskeleton remodeling that affects B lymphocyte trafficking and homing and influences tissue invasion in CLL.

2. Materials & methods

2.1 Antibodies and reagents

Mouse Anti-Lyn (BD-Bioscience). Mouse anti-Syk, Rabbit anti-SHP-1/2, Mouse anti-Phospotyrosine (Upstate Biotech). Rabbit anti-Blnk, Rabbit anti- Plc-γ2, Rabbit anti-VAV1 (Cell Signaling). Rabbit ant-HIP-55 (BD-Bioscience). Anti-GFP, Phalloidin alexa fluor 633, secondary antibody goat anti-Mouse and Rabbit Alexafluor 488, Human and mouse Goat F(ab)2Anti-IgM(μ) used at the concentration of 20μg/ml (Invitrogen). Anti-Mouse IgG HRP-linked and Anti-Rabbit IgG HRP-linked (GE Healthcare). TrueBlot Anti-Mouse IgG and TrueBlot Anti-Rabbit IgG (EBioscience). Rac1/Cdc42 activation assay Kit (Millipore). Recombinant SDF-1a human and mouse (Preprotech Inc.). ICAM-1/Fc (R&D). PMA, PP2 used 1μg/μl (Calbiochem).

2.2 Cell cultures

MEC1 cell line was obtained from Deutsche Sammlung von Mikroorganismen und Zellkulturen GmbH (DMSZ) and cultured in RPMI 1640 medium supplemented with 10% Fetal Calf Serum (FCS) and 15 mg/ml gentamicin (complete RPMI; Invitrogen). MEC1 cell lines after tranfection were cultured with the addition of 5 mg/ml Blasticidin (Invitrogen) and cell-sorted after 1 month for GFP expression (BD FACSVantage™ SE Cell Sorter). HS-5 human bone marrow, stroma (ATTC) were grown in DMEM (GIBCO) 10% FCS, 15 mg/ml gentamicin at 10% CO2.

2.3 Human tissue samples and cell purification

Leukemic lymphocytes were obtained from the PB of CLL patients, diagnosed according to Mulligan et al [123]. All tissue samples were obtained with approval of the institutional review board of San Raffaele University Hospital (Milano, Italy). Purity of all preparations was always above 99%, and the cells coexpressed CD19 and CD5 on their cell surfaces as checked by flow cytometry (FC500; Beckman Coulter); preparations were virtually devoid of NK, T lymphocytes and monocytes using a human B cell enrichment cocktail (RosetteSep; StemCell Technologies) or column separated (Miltenyi Biotech).

2.4 Generation of stable cell lines expressing GFP

We used a BLOCK-iT Pol II miR-RNAi Expression Vector Kit (Invitrogen) for vector based expression of miRNA according to the manufacturer's instructions.

We generated 4 different double stranded oligo duplex encoding a miRNA target sequence for HS1. Cell were transfected taking advantage of Nucleofactor technology (AMAXA) using program X-001, solution V. A pcDNA 6.2-GW/ EmGFP-miR negative control was used to perform a parallel control transfection (CNTR). We generated two stable cell lines transfected with two different miRNA-containing plasmids, resulting in HS1 KD1 and HS1 KD2.

Single-stranded DNA oligos used for HS1 silencing

HS1 1 TOP

TGCTGATGTCATTCACAAAGTCAGGAGTTTTGGCCACTGACTGACTCCTGACTGTGAATGACAT

HS1 1 BOT

CCTGATGTCATTCACAGTCAGGAGTCAGTCAGTGGCCAAAACTCCTGACTTTGTGAATGACAT

HS1 2 TOP

TGCTGCATTGAAGCCGACAGCGCTCTGTTTTGGCCACTGACTGACAGAGCGCTCGGCTTCAATG

HS1 2 BOT

CCTGCATTGAAGCCGAGCGCTCTGTCAGTCAGTGGCCAAAACAGAGCGCTGTCGGCTTCAATGC

HS1 3 TOP

TGCTGACTAGAAGCGGCTTCTATGGGGTTTTGGCCACTGACTGACCCCATAGACCGCTTCTAGT

HS1 3 BOT

CCTGACTAGAAGCGGTCTATGGGGTCAGTCAGTGGCCAAAACCCCATAGAAGCCGCTTCTAGTC

HS1 4 TOP

TGCTGTCAAATTTCGCCTTCAGCCCAGTTTTGGCCACTGACTGACTGGGCTGAGCGAAATTTGA

HS1 4 BOT

CCTGTCAAATTTCGCTCAGCCCAGTCAGTCAGTGGCCAAAACTGGGCTGAAGGCGAAATTTGAC

2.5 Human cells flow cytometry

$1x10^6$ from CNTR and HS1 KD cells were stained for the following CD antigen:
CD5, CD19, CD20, CD23, CD25, CD38, CD54, CD62L, CD83, CD80, CD86, CD150 CD200 and IgM from BD Biosciences Pharmingen. The surface expression levels were analysed using Cytomics FC500 (Beckman Coulter).

2.6 RNA extraction and Real time PCR

After Trizol (Invitrogen) extraction, 1 μg of total RNA were reverse transcribed into cDNA using random primers oligonucleotides and ThermoScript II (Invitrogen). Real time PCR was performed using a 10 fold dilution of cDNA sample in each reaction. The Applied Biosystems "real time" version of the assay on the ABI Prism 7900 thermal-cycler and TaqMan Universal PCR MasterMix (Applied Biosystems) was used.
Primers and Probes for HS1 were included in the HS00232048 from Applied Biosystem, and evaluation of the housekeeping gene was done with HPRT TaqMan Pre-developed Assay reagent (Applied Biosystem). All PCR experiments were performed in triplicate. The analysis of Real time PCR output data was performed with the SDS2 software following the manufacturer-suggested absolute quantification method, with a calibration curve generated from 2 fold dilution of Hek293T cDNA samples; mRNA levels were normalized on the expression of HPRT housekeeping gene.

2.7 Cell lysis and Western blot (WB) analysis

Cells were lysed with ice cold Lysis Buffer (NaCl 0.15M; 1% NP40; 1mM EDTA pH=8; 50mM Tris-HCl pH=7, pepstatin, leupeptin, PMSF, sodium orthovanadate and NAF). For SDS-PAGE, polyacrylamide gels were made with different percentages of acrylamide (7,5%, 10%, or 12%), depending on the molecular weight of the protein to be resolved. Immunoreactivity was revealed by incubation with secondary antibodies conjugated with Horseradish peroxidase (HRP).

2.8 Immunoprecipitation (IP)

Total cell lysates (≅500 μg of proteins) were incubated with the indicated antibody and immobilized on protein G microbeads (Miltenyi Biotech); immunoprecipitated proteins were purified using specific columns according to the manufacturer's instructions (Miltenyi Biotech). Proteins were eluted in Laemmli buffer (50mM TrisHCl pH=6.8, 1% SDS, 0.005% Bromophenol Blue, 10% Glycerol, 50mM fresh DTT) and resolved by SDS-PAGE. TrueBlot secondary antibodies were used for the detection.

2.9 Rac1 and Cdc42 activation assay

We utilized the "Rac1 and Cdc42 pull-down activation assay" kit (Millipore), following the manufacturer instructions. In details, 10x106 cells per sample were lysed with MLB Buffer provided with the kit and lysates were pre-cleared with Glutathione Agarose Beads (Sigma Aldrich) for 10 minutes at 4°C. For positive and negative controls, 100X GTPgS and 100X GDP were added to the cell extracts, respectively, and incubated for 15 minutes at 30°C. GTPgS is a non-hydrolyzable form of GTP that, through binding to Rac1 and Cdc42, blocks it in the active GTP-bound state. On the other hand, increasing the cellular concentration of GDP leads to the accumulation of inactive GDP-bound proteins. Lysates were incubated for 60 minutes at 4°C (30 minutes for GTPgS and GDP loaded lysates) with Rac1/Cdc42 Assay Reagent (PAK-1 PBD, agarose beads), which binds selectively to either Rac1-GTP or Cdc42-GTP, thus leading to their enrichment. The beads were then pelletted by 1 minute centrifugation at 14.000 rpm at 4°C, washed, resuspended in Laemmli Buffer and resolved by SDS-PAGE.

2.10 Densitometric analysis

Densitometric analysis was performed with Personal Densitometer SI (Molecular Dynamics). HS1 expression levels were evaluated as optical density (OD) ratio with β-actin.

2.11 Peptide and Protein identification by nanoLC-MS/MS

Selected bands were excised from the gel previously stained with blue-comassie, rinsed with distilled water, and then treated for the trypsinization. Briefly, after shrinking with acetonitrile (ACN), 10 mM DTT was added, followed by incubation at 56°C for 40 minutes. Alkylation with iodoacetamide 55 mM was performed at room temperature in the dark for 25 minutes, thereafter trypsin was added and left overnight. 10 ml of the supernatant containing the peptide mixtures were cleaned on a StageTip C18 (Proxeon Biosystems) and then resuspended in 10 ml of 10% formic acid prior to MS/MS analysis. 5 μL of tryptic digest for each sample were injected in a capillary chromatographic system (EasyLC, Proxeon Biosystem). Peptide separations occurred on a homemade 12-cm reverse phase spraying fused silica capillary column (75 μm i.d. x 10 cm), packed with 3-μm ReproSil 100C18 (Dr. Maisch GmbH, Germany). A gradient of eluents A (H2O, 2% v/v ACN, 0.1% v/v formic acid) and B (ACN, 2% v/v H2O, 0.1% v/v formic acid) was used to achieve separation, from: 4% B (at 0 min 0.2 mL/min flow rate) to 45% B (at 55 min, 0.2 mL/min flow rate). The LC system was connected to an LTQ-Orbitrap mass spectrometer (ThermoScientific) equipped with a nanoelectrospray ion source (Proxeon Biosystems). Full scan mass spectra were acquired in the LTQ Orbitrap

mass spectrometer with the resolution set to 60,000 (after accumulation to a "target value" of 400,000). For accurate mass measurements the lock-mass option was used [124]. The acquisition mass range for each sample was from m/z 350 to 1650 and the analysis were made in duplicate. The four most intense doubly and triply charged ions were automatically selected and fragmented in the ion trap (after accumulation to a "target value" of 10000). Target ions already selected for the MS/MS were dynamically excluded for 180 seconds.

2.12 NanoLC-MS/MS data analysis

Tandem mass spectra were extracted by Raw2MSM, version 1.5_2007.02.22 [124]. All MS/MS samples were analyzed using Mascot (version 2.2, Matrix Science) and X! Tandem (www.thegpm.org; version 2007.01.01.1). Both Mascot and X! Tandem were set up to search the human International Protein Index (IPI) database [125] assuming as digestion enzyme trypsin. Mascot and X! Tandem were searched with a fragment ion mass tolerance of 0.60 Da and a parent ion tolerance of 5.0 PPM. Iodoacetamide derivative of cysteine was specified as fixed modification. Oxidation of methionine, acetylation of the N-terminus and phosphorylation of serine, threonine and tyrosine were specified as variable modifications. Scaffold (version Scaffold_2_01_01, Proteome Software Inc.) was used to validate MS/MS based peptide and protein identifications. Peptide identifications were accepted if they could be established at more than 95.0% probability as specified by the Peptide Prophet algorithm [126]. Protein identifications were accepted if they could be established at more than 99.0% probability and contained at least 2 identified peptides. Protein probabilities were assigned by the Protein Prophet algorithm [127]. Proteins that contained similar peptides and could not be differentiated based on MS/MS analysis alone were grouped to satisfy the principles of parsimony.

2.13 In vitro migration on transwell

1x106 purified B cells from mice (Wild type (WT), HS1-/-) and CNTR/HS1 KD cells were seeded on a transwell chamber 6.5 mm diameter and 5.0 μm pore size (Cornig Incorporated); after 4 hours the cells migrated in the lower part of the chamber were counted at the cytometer (FC500). Spontaneous migration was evaluated as number of cells collected in the lower chamber and counted by flow cytometer for 1 minute.

2.14 Adhesion assay

CNTR, HS1 KD, purified B cells from mice (WT, HS1-/-) were labeled with 1 mM CMFDA cell tracker green (Invitrogen) and added at 5x105 cells/well (triplicate) in precoated flat-bottom 96-well plates with 2% BSA-PBS (as background) or with 4 mg/ml of ICAM-1/Fc in PBS. Adhesion was quantified using VICTOR3 (Perkin Elmer) plate reader.

Adhesion was quantified after 1 hour incubation using VICTOR3 (Perkin Elmer) plate reader. For CLL cells we calculated the mean fluorescence obtained by the subtraction of the background (mean reading for wells coated with PBS only). For murine cells, able to adhere on ICAM-1 coating, we calculated the specific adhesion, by subtracting background adhesion from the reading for each well. This specific adhesion was expressed as a percentage of the total emission before the washing, that is the total cell input.

2.15 Polymerization assay

$1x10^6$ purified B cells from mice (WT, $HS1^{-/-}$) were pre-warmed at 37°C in RPMI w/o serum. After a 10-minute incubation with anti-IgM the reaction was stopped with 4% paraformaldehyde and cells were permeabilized with saponine 0,2% on ice. We added Phalloidin Alexafluor 633 (1:1000) and we analyzed the percentage of F-actin by flow cytometry (FC500). We finally quantified by flow the F-actin increase as the result of: (mean fluorescence intensity after anti-IgM stimulation)/mean fluorescence time zero.

2.16 Total Internal Reflection Fluorescence (TIRF) microscopy

CNTR and HS1 KD cells were incubated on poli-L-Ornithine coated glass bottom dishes (WillCO-dish) for 2h at 37°C and 5% CO_2. Cells were fixed with 4% paraformaldheyde, permeabilized with 0.1% Triton-X100 (SIGMA), stained for phalloidin alexa fluor 633 (1:500), and acquired at a Leica AM TIRF MC microscope.

2.17 Confocal microscopy

Sterile glass slides were placed in a 24-well plate and coated with 400ml poly-L-ornithine (Sigma Aldrich) overnight at 4°C. CNTR and HS1 KD cells were disseminated on the slides. After 4 h incubation, cells were washed and fixed with 4% v/v paraformaldeyde (PAF- Sigma Aldrich). After blocking (Blocking buffer: 0,1% w/v BSA, 10% v/v FBS in PBS), cells were permeabilized in Blocking buffer containing 0.3% v/v Triton-X100 (Sigma Aldrich). Cells were incubated for 4 h with primary antibodies (diluted in Blocking buffer) and stained with secondary antibodies (diluted in Blocking buffer). Slides were then mounted using FluorSave (Calbiochem) as mounting media. Slides containing cells alone or secondary antibodies alone were used as controls. Images were acquired using Laser Scanning Confocal Microscope (LEICA) with an inverted 60x objective.

Slides of different organs from Rag2-/-γc-/- mice injected with GFP-expressing MEC1 cells (CNTR, HS1 KD) were fixed with 4% paraformaldheyde and permeabilized with Triton-X100 0.1% (Sigma). The slides were incubated with primary antibody rabbit anti-GFP followed by a secondary alexafluor 488-conjugated anti-rabbit antibody, as the GFP fluorescence loses intensity after organ fixation. We used TO-PRO3 (Invitrogen) for the nuclear staining. Cells were acquired using Confocal microscopy (Radiance 2100; BioRad) dual-laser (excitation wavelengths: 488, 633 nm) with an inverted x40 objective. Fluorescent signals from single optical sections were sequentially acquired and analyzed by Paint Shop Pro 7.02 (JascSoftware).

2.18 In vivo *migration assay*

$HS1^{-/-}$ mice and age-matched WT C57BL/6 mice were used as donors and recipients for *in vivo* migration experiments. Purified B cells from spleen were labeled with 2 different concentrations (0,125 μM for WT cell population and 1,25 μM for $HS1^{-/-}$ cell population) of 5-(6-) carboxyfluorescein succinimidyl ester (CFSE) according to the manufacturer's instructions (Molecular Probes). A 1:1 mixture of CFSE-high and CFSE-low labeled B cells was prepared and resuspended in PBS. Each recipient mouse, WT or $HS1^{-/-}$, was injected intravenously (i.v.) with a 1:1 mixture of CFSE-high and CFSE-low labeled B lymphocytes $20x10^6$ mixed cells in a

total volume of 300 µl. The ratio of CFSE-high and CFSE-low labeled donor cells before injection was confirmed by flow cytometry. Twenty hours later, recipient mice were killed and lymphoid organs and blood were recovered and analyzed by flow cytometry. The same experimental procedure was used for *in vivo* migration assay with human B cells from CLL patients.

2.19 Xenograft studies

Eight week old $Rag2^{-/-}\gamma_c^{-/-}$ male mice were challenged subcutaneuosly (s.c.) in the left flank with 10x 10^6 MEC1 cells expressing GFP (CNTR or HS1 KD) in 0.1 ml saline through a 27-gauge needle. Animals were monitored twice a week for weight and tumor growth (measuring three perpendicular diameters), and sacrificed when the mean tumor volume reached a dimension of ≥1000 mm^3. Subcutaneous tumors and organs (spleen, lymph nodes, kidneys, liver, lungs and femoral BM) were extracted and tissue sections were prepared for confocal microscopy as described before.

2.20 Mice

Mice were housed and bred in a specific pathogen free animal facility, treated in accordance with the European Union guidelines and approval of the Institutional Ethical Committee.

$HS1^{-/-}$ mice (background strain C57BL/6) and Eµ-TCL1 tg mice (background strain C3HBL/6) were expanded in our mouse colony. WT C57BL/6 and C3HBL/6 mice were supplied by Charles River Laboratories. Homozygous Eµ-TCL1 tg ($T^{tg/tg}$) were crossed with $HS1^{-/-}$ ($H^{-/-}$) to obtain age-matched $H^{-/-}/T^{wt}$, H^{wt}/T^{tg}, $H^{-/-}/T^{wt}$, $H^{-/-}/T^{tg}$, H^{wt}/T^{wt} mice (F2 progeny).

Genotyping was performed on tail DNAs by PCR and real-time PCR using primers described in Primers were: (5'-GAGAGGAAAGGTAGACACCAG-3' and 5'-GGCATGGATGGCTGCTGGAC- 3') at an annealing temperature of 62°C for HS1 wt allele; (5'-GAGAGGAAAGGTAGACACCAG-3' and 5'-CATGCTTGGAACAACGAGCGC-3') at an annealing temperature of 59°C for HS1 mutated allele; (5'-GCCGAGTGCCCGACACTC-3' and 5'-CATCTGGCAGCAGCTCGA-3') at an annealing temperature of 55°C for the hTCL-1 gene. Heterozygosity for the hTCL-1 gene was confirmed by Sybr Green real-time PCR using hTCL-1-specific primers (hTCL-1 fwd, 5'-GCCTGGCTGCCCTTAACC-3' and hTCL-1 rev, 5'-GACGCAAGAGCACCCGTAAC-3') and murine β-actin-specific primers (Actin fwd, 5'-AAGAGAAGGGTTACCCGGGATA-3' and Actin rev, 5'-CCTAAGGCCAACCGTGAAAA-3') at an annealing temperature of 59°C.

2.21 Mice genotyping

Primers were: (5'-GAGAGGAAAGGTAGACACCAG-3' and 5'-GGCATGGATGGCTGCTGGAC- 3') at an annealing temperature of 62°C for HS1 wt allele; (5'-GAGAGGAAAGGTAGACACCAG-3' and 5'-CATGCTTGGAACAACGAGCGC-3') at an annealing temperature of 59°C for HS1 mutated allele; (5'-GCCGAGTGCCCGACACTC-3' and 5'-CATCTGGCAGCAGCTCGA-3') at an annealing temperature of 55°C for the hTCL-1 gene. Heterozygosity for the hTCL-1 gene was confirmed by Sybr Green real-time PCR using hTCL-1-specific primers (hTCL-1 fwd, 5'-GCCTGGCTGCCCTTAACC-3' and hTCL-1 rev, 5'-

GACGCAAGAGCACCCGTAAC-3') and murine β-actin-specific primers (Actin fwd, 5'-AAGAGAAGGGTTACCCGGGATA-3' and Actin rev, 5'-CCTAAGGCCAACCGTGAAAA-3') at an annealing temperature of 59°C.

2.22 Murine cell preparations

H^{wt}/T^{tg} mice and $H^{-/-}/T^{tg}$ mice were bled once a month starting from two months of age in order to monitor leukemic lymphocytes appearance in PB by flow cytometry. H^{wt}/T^{tg} and $H^{-/-}/T^{tg}$ mice were sacrificed around 7-13 months of age when they developed ≥30% expansion of $CD5^+$ B cells in PB, together with age-matched WT littermates and organs (PB, spleen, mesenteric, axillary and inguinal lymph nodes, kidneys, liver, lungs and femur) were extracted. For WB, IG gene rearrangement analysis and migration studies, $CD19^+$ cells from the spleen were enriched by depletion of non-B cells through the EasySep Negative selection Mouse B Cell Enrichment Cocktail on EasySep Magnet (StemCell Technologies), following manufacturer's indications. Full counts of WBC in each lymphoid compartment were made "on a cell counter" (Coulter). Cells from spleen and BM and cells isolated from the peritoneal exudates (PE) and PB (35μl) were stained to be analyzed by flow cytometry (see below) both surface antigen expression and clonality.

2.23 Murine cells flow cytometry

Peripheral blood and/or tissue single cell suspensions were first incubated in an ammonium chloride solution (ACK) lysis buffer (NH_4Cl 0,15 M, $KHCO_3$ 10 mM, Na_2EDTA 0,1 mM, pH 7,2-7,4) to lyse red cells and then stained after blocking fragment crystallizable (Fc) receptors. The following antibodies were used: allophycocyanin (APC) anti-mouse CD5 (53-7.3), phycoerythrine-cyanine 7 (PE-Cy7) rat anti-mouse CD19 (1D3), from BD Biosciences Pharmingen; rat anti-mouse Lambda-PE (JC5-1), rat anti-mouse IgD-PE (11-26), rat anti-mouse Kappa-FITC (187.1) from Beckman Coulter and goat anti-mouse IgM-FITC (μ chain) from Cappel. All antibodies were used at 1:200 dilution except for goat anti-mouse IgM-FITC, that was diluted 1:10000. Finally the samples were analysed using Cytomics FC500 (Beckman Coulter).

2.24 Histopathology and Immunohistochemistry

Tissues were fixed in 4% formalin for 12 hours, then embedded and included in paraffin wax. Five-mm thick sections were cut and stained with hematoxylin and eosin (H&E) according to standard protocols. Microscopic specimens were evaluated by a pathologist in a blind fashion and mice were defined leukemic when spleen structure was subverted and the white pulp was greatly expanded.

Mice sections were de-paraffinized in xylene, rehydrated in ethanol, immersed in 0,1 M citric acid pH 6.0, heated in microwave and cooled at room temperature. Endogenous peroxidases were quenched with 3% H_2O_2. Slides were incubated with 3% BSA and with primary monoclonal antibody to B220 (RA3-6B2, Serotec) at a 1:750 dilution or to Ki67 (SP6,Neo Markers) at a 1:100 dilution for 30 min, followed by incubation with biotinylated goat anti-rat IgG diluted 1:200. Slides were incubated with streptavidin 1:500 for 30 min. Slides were then

incubated with 3,3'-diaminobenizidine tetrahydrochloride (DAB) for 5 min and the counterstain was done with Mayer-Hematoxylin. After dehydratation in ethanol and xylene, slides were permanently mounted in Eukitt (Bio-Optica).

2.25 IGHV-D-J gene rearrangement analysis

Genomic DNA was extracted from BM and $CD19^+$ purified spleen cells according to QUIAmp® DNA mini kit (QIAGEN) protocol and from whole blood samples using Maxwell® 16 DNA Purification Kit and Maxwell® Instrument (Promega Corporation).

DNA was subjected to PCR using IGHV1a,14 and IGHJintron gene primers and products were run on a 7,5% PAGE (PROTOCOL 1). This protocol amplifies 4 distinct IG heavy chain derived products of different molecular weight (reflecting IGHV-D-J1, IGHV-D-J2, IGHV-D-J3, and IGHV-D-J4 rearrangements) in polyclonal B cell populations with loss of these bands in oligoclonal or monoclonal populations.

When a monoclonal band was evident using the previous approach, we amplified the IGHV-D-J rearrangements with a nested PCR approach, using 4 different FR1 primers combined with either a mix of 4 IGHJ primers or a mix of 4 VLJH primers (first and second round, respectively) (PROTOCOL 2). Low melting point agarose gel-purified monoclonal PCR products were subjected to sequencing and sequence data were analyzed using the IMGT database.

PCR amplification of IGHV-D-J rearrangements

The primers used in PROTOCOL 1 were:

- IGHV1a,14: 5'-CAGGTGCAGCTGCAGCAGTCTGG-3'
- IGHJintron: 5'- TGAGGCTCTGAGATCCCTAGACAG-3',

for 29 cycles at an annealing temperature of 60°C;

The primers used in PROTOCOL 2 were:

FR1 primers (first and second round):

- IGHV1a,14, (same as above)
- IGHV1b: 5'-CAGGTCCAACTGCAGCAGCCTGG-3',
- IGHV2,3,12: 5'-CAGGTGCAGCTGCAGGAGTCAGG-3'
- IGHV4,5: 5'-CAGGTGCAGCTGCAGGAGTCGGG-3'

IGHJ primers (first round):

- IGHJ1-2: 5'-TGAGGAGACGGTGACCAGGGTGCC-3'
- IGHJ3: 5'-TGAAGAGACGGTGACCATTGTCCC-3'
- IGHJ4-5: 5'-TGAGGAGACGGTGACCAGGGTTCC-3'
- IGHJ6: 5'-TGAGGAGACGGTGACCGTGGTCCC-3'

VLJH primers (second round):

- VLJH 5'-GTGACCAGGGT(A/T/G/C)CCTTGGCCCCAG-3'

40 cycles at an annealing temperature of 59°C).

Using this approach, almost 90% of all possible rearrangements for the C57BL/6 mouse strain and 70% of all the strains were detectable. All primer sets were provided by Primm srl.

2.26 Statistical analysis

Statistical analyses were performed using Student's T test. Data were expressed as the mean value ± standard deviation and comparison of growth curves was considered statistically significant for $p<0.05$. Comparison of survival curves was performed using the Log-Rank test.

3. Results

3.1 Establishment of HS1 knock-down stable CLL cell lines

We knocked down HS1 protein in the CLL cell line MEC1 [128] and we generated three stable cell lines by using miRNA-expressing vectors (**Figure 3.1**).

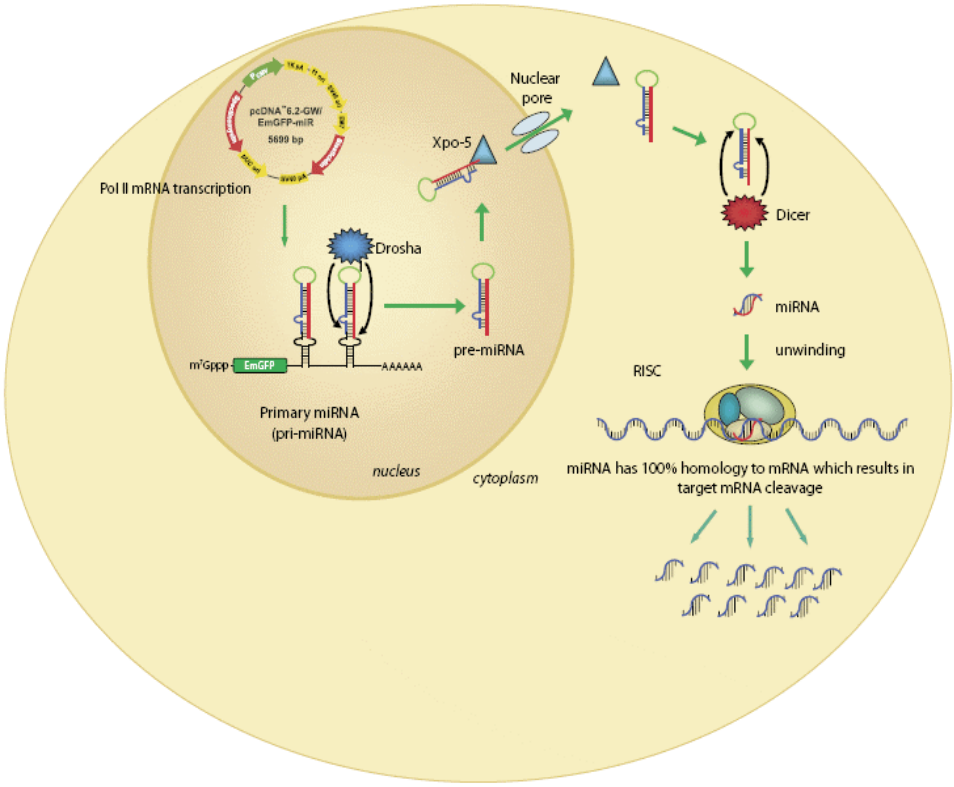

Figure 3.1. **miRNA expression vector system**. The pcDNA 6.2-GW/EmGFP mir plasmids code for the emerald green fluorescent protein (EmGFP) and for specific HS1-targeting primary (pri)-miRNAs. Drosha, a nuclear RNase II, cleaves the stem-loop structure of the pri-miRNAs to generate small hairpin precursor (pre)-miRNAs that are exported from the nucleus to the cytoplasm by exportin 5. Following the nuclear export, the pre-miRNAs are processed by Dicer to generate mature miRNAs. The RNA-induced silencing complex (RISC) then incorporates the miRNAs and targets complementary cellular transcripts [129]. Additional elements: P_{CMV}, human cytomegalovirus promoter; attB1 and attB2, recombination sites; TK pA, herpes simplex virus thymidine kinase polyadenylation signal; spectinomycin and blasticidin resistance genes; pUC origin for high-copy maintenance.

The first expressed a control plasmid (CNTR), the other two were transfected with two different miRNA-containing plasmids, resulting in HS1 KD1 and HS1 KD2 which respectively expressed 10% and 80% of HS1 mRNA. The transfected cells had proportionally reduced HS1 protein levels (**Figure 3.2 a,b**); as the silencing was more effective in HS1 KD1 cells in further experiments we used only this cell line which is from now on defined HS1 KD.

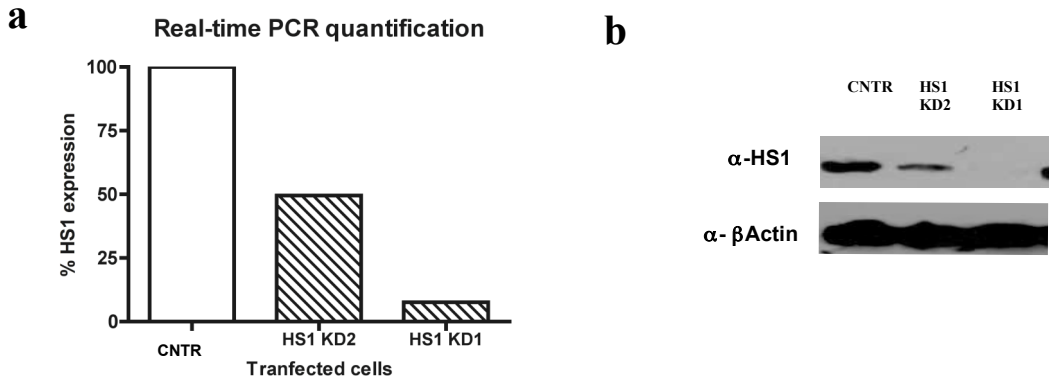

Figure 3.2 HS1 silencing in MEC1 cells and spontaneous migration analysis.
(a) Relative expression of HS1 evaluated by real-time PCR in 3 stable cell lines obtained from MEC1 cell line, either expressing GFP only (CNTR) or after silencing HS1 (HS1 KD1 and KD2) (b) WB analysis for HS1 on silenced cell lines (CNTR, KD1 and KD2). β-actin is utilized as control.

3.2 Surface markers screening

We analyzed several surface molecules on CNTR and HS1 KD cell lines in order to evaluate potential phenotypic changes following the transfection procedure in comparison with the wild type cells. In particular we studied the expression of the following markers: CD5, a CLL characteristic feature [130]; CD19 and CD20, B-cell lineage markers; CD23 and CD25, activation markers, the former being a requisite to make CLL diagnosis; CD38 [100], another activation marker whose expression has a negative prognostic value in CLL; CD54 (also termed ICAM-1), an adhesion molecule that is usually downmodulated on the surface of CLL cells [131]; CD62L, the L-selectin that enables lymphocytes to efficiently recirculate within lymphoid organs, and is usually expressed at low levels on CLL cells possibly accounting for their impairment in transendothelial migration [132]; CD200 [133] and CD83 [134], immunosuppressive molecules, whose soluble isoforms are often shed from CLL-cell membranes and found at high concentrations in the blood of patients with a worse clinical outcome.
We did not observe any significant changes in these markers and in surface IgM levels, while we found differences in the expression of other activation markers, namely CD80 and CD86 (increased in HS1

KD cells) and CD150 (also termed SLAM; decreased in HS1 KD cells), the latter playing also a role in cellular adhesion and lymphocyte interactions [135]. All these molecules are known to be induced following CD40 engagement, beside other stimuli [136].

3.3 Actin and myosin are less represented in HS1 knock-down immunoprecipitates

A total anti-phosphotyrosine immunoprecipitation showed that the total amount of immunoprecipitated phospho-proteins was lower in HS1 KD cells as compared to CNTR (**Figure 3.3**).

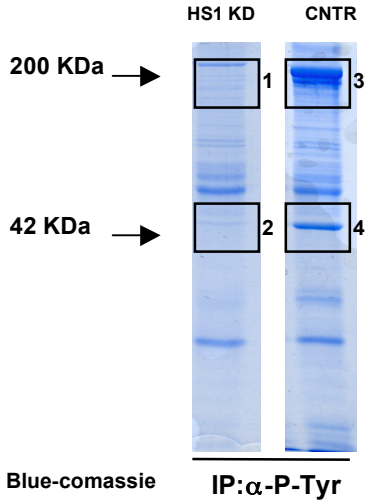

Figure 3.3. Immunoprecipitation (IP) experiments showing total phosphotyrosine (PTyr) content in protein lysates from control (CNTR) and HS1 knock-down (KD) cells; the gel was stained with blue-comassie and band 1,2,3,4 were trypsin digested and analyzed by high resolution mass spectrometry. The molecular weights of the selected bands are shown.

By NanoLC-MS/MS we sequenced in the CNTR sample the two bands that were less (if at all) represented in the HS1 KD immunoprecipitation and found actin in the lower band and myosin heavy chains 9 and 10 in the higher band (**Table 1 and Figure 3.3**).

Table 1. **NanoLC- MS/MS data analysis**. Analysis of Band 1-4 excised from the blue-comassie stained gel from the total phosphotyrosine immunoprecipitation on control (CNTR) and HS1 knock-down (HS1 KD) cell protein lysates.

#	Identified Proteins (18)	Accession Number	Molecular Weight	BAND1 (F005632)		BAND2 (F005633)		BAND3 (F005634)		BAND4 (F005631)	
				Unique peptides	Protein probability	Unique peptides	Protein probability	Unique peptides	Protein probability	Unique peptides	Protein probability
1	MYH9 Isoform 1 of Myosin-9	IPI00019502	227 kDa	52	100%			117	100%	3	100%
2	ACTB Actin, cytoplasmic 1	IPI00021439 (+1)	42 kDa			15	100%			26	100%
3	APOA1 Apolipoprotein A-I	IPI00021841	31 kDa	5	100%	4	100%			6	100%
4	MYH10 Isoform 1 of Myosin-10	IPI00397526 (+2)	229 kDa	3	100%			19	100%		
5	VTN Vitronectin	IPI00298971	54 kDa	2	100%	4	100%			4	100%
6	CLU Clusterin	IPI00291262 (+2)	52 kDa	3	100%	3	100%			4	100%
7	APOA4 Apolipoprotein A-IV	IPI00304273 (+1)	45 kDa	3	100%	3	100%			3	100%
8	F2 Prothrombin (Fragment)	IPI00019568	70 kDa	2	100%	3	100%			4	100%
9	APOC3 Apolipoprotein C-III	IPI00021857 (+1)	11 kDa	2	100%	2	100%			2	100%
10	C3 Complement C3 (Fragment)	IPI00783987	187 kDa	3	100%	4	100%			3	100%
11	KNG1 Isoform HMW of Kininogen-1	IPI00032328 (+2)	72 kDa	2	100%	5	100%				
12	UQCRC2 Cytochrome b-c1 complex subunit 2, mitochondrial	IPI00305383	48 kDa			3	100%			3	100%
13	KRT1 Keratin, type II cytoskeletal 1	IPI00220327	66 kDa	2	100%	3	100%				
14	HP HP protein	IPI00431645 (+4)	31 kDa			2	100%				
15	APOC2 Apolipoprotein C-II	IPI00021856	11 kDa			2	100%				
16	TMOD1 Tropomodulin-1	IPI00002375 (+2)	41 kDa							2	100%
17	APOE Apolipoprotein E	IPI00021842	36 kDa			2	100%				
18	PUF60 Isoform 1 of Poly(U)-binding-splicing factor PUF60	IPI00069750 (+5)	60 kDa			2	100%				

Scaffold Version: Scaffold_2_01_01
Peptide Thresholds: 95.0% minimum
Protein Thresholds: 99.0% minimum and 2 peptides minimum

It is known that acto-myosin complexes formation, together with tyrosine phosphorylation, is crucial for TCR microcluster formation and signalling initiation after TCR engagement in T cells [137]; [138]; [47]. In addition, it has been suggested that HS1 is relevant for proper assembly of these structures in fibroblasts [139].

For these reasons and based on our results, we hypothesized that CLL B lymphocytes may also require HS1 for acto-myosin assembly and phosphorylation to initiate the signalling pathways downstream the BCR. Therefore, we studied in details the signalosome components [14] involved in proximal BCR signalling events.

3.4 Signalosome components activation involved in proximal BCR signalling events.

HS1 knock-down impairs Lyn phosphorylation but not Syk

Syk and Lyn are among the first kinases [20] to be phosphorylated and activated after BCR engagement, and are crucial for signal initiation and phosphorylation of downstream adaptors (such as BLNK) [21] and effector molecules, including HS1 [52].

We performed immunoprecipitation with anti-Lyn antibody and WB analysis for phosphotyrosines on whole cell lysates from CNTR and HS1 KD cells, either left untreated or stimulated with anti-IgM antibodies. In the absence of HS1, Lyn fails to undergo phosphorylation even after anti-IgM stimulation. In contrast, CNTR cells show constitutive phosphorylation of Lyn that increases after anti-IgM stimulation (**Figure 3.4**).

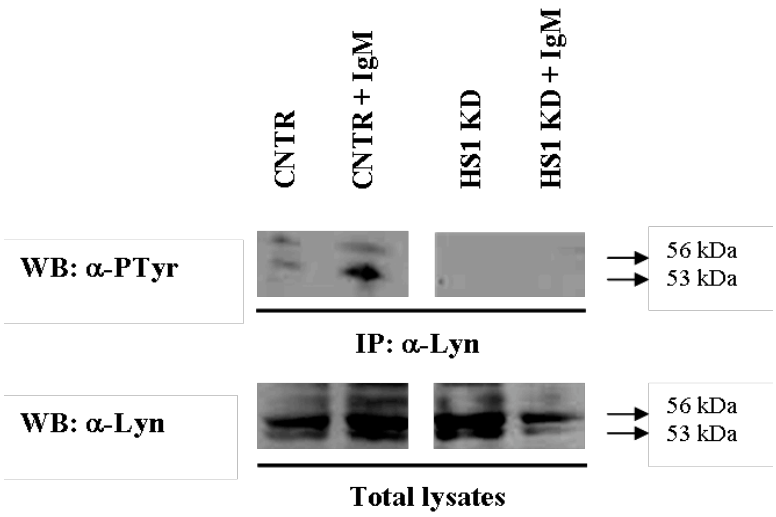

Figure 3.4. Immunoprecipitation (IP) experiments using anti-Lyn on control (CNTR) and HS1 knock-down (KD) cells before and after anti-IgM stimulation and Western Blot (WB) analysis for total phosphotyrosines (PTyr) (upper panels). WB analysis for Lyn on total lysates is shown as control (bottom panels). The results are representative of two independent experiments. Syk phosphorylation

was detected by immunoprecipitation for total phosphotyrosines on CNTR and HS1 KD cell lysates, before and after anti-IgM stimulation, and WB analysis for Syk.

Syk phosphorylation is constitutive in both CNTR and HS1 KD cells and does not further increase after anti-IgM stimulation (**Figure 3.5**), indicating that HS1 deficiency does not affect Syk tyrosine phosphorylation.

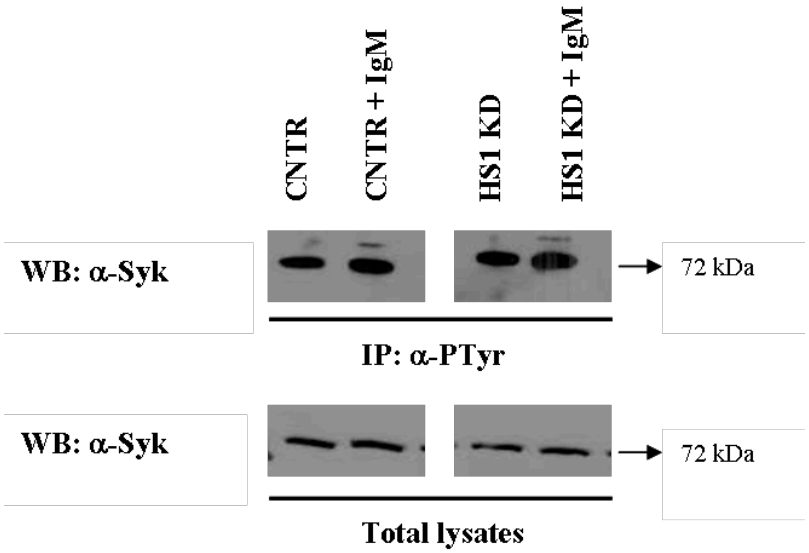

Figure 3.5. Immunoprecipitation (IP) experiments using anti-phosphotyrosine (PTyr) on control (CNTR) and HS1 knock-down (KD) cells before and after anti-IgM stimulation and Western Blot (WB) analysis for Syk (upper panels). WB analysis for Syk on total lysates is shown as control (bottom panels). The results are representative of two independent experiments.

HS1 knock-down does not affect BLNK and PLCγ2 phosphorylation

The adaptor molecule BLNK is phosphorylated by Syk and early recruited to the signalosomes [25]. Tyrosine phosphorylation is essential for binding and activation of PLCγ2, an important mediator of Ca^{++} signalling [26].

BLNK and PLCγ2 phosphorylation was detected by immunoprecipitation for total phosphotyrosines on CNTR and HS1 KD cell lysates, before and after anti-IgM stimulation, and WB analysis with specific antibodies. HS1 is dispensable for BLNK (**Figure 3.6**) and PLCγ2 (**Figure 3.7**) tyrosine phosphorylation, as no differences in the total level of phosphorylation of both proteins was detected,

and a similar increase in BLNK phosphorylation could be observed after anti-IgM stimulation in both CNTR and HS1 KD cells.

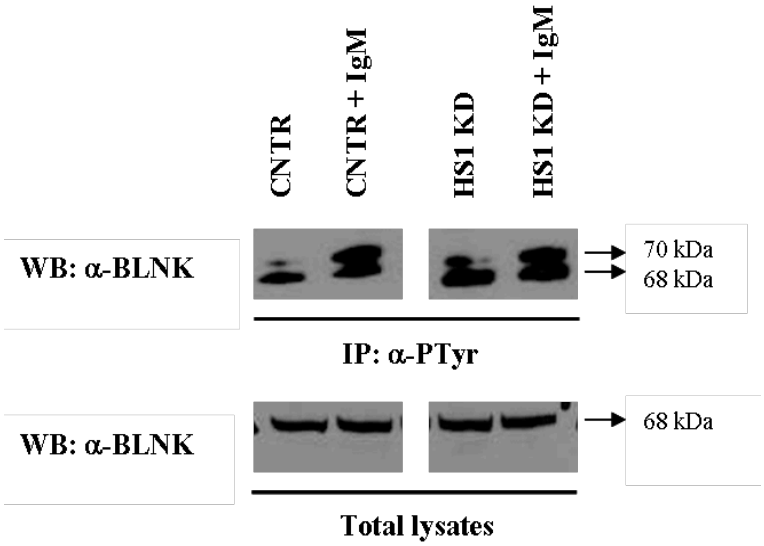

Figure 3.6. Immunoprecipitation (IP) experiments using anti-phosphotyrosine (PTyr) on control (CNTR) and HS1 knock-down (KD) cells before and after anti-IgM stimulation and Western Blot (WB) analysis for BLNK.

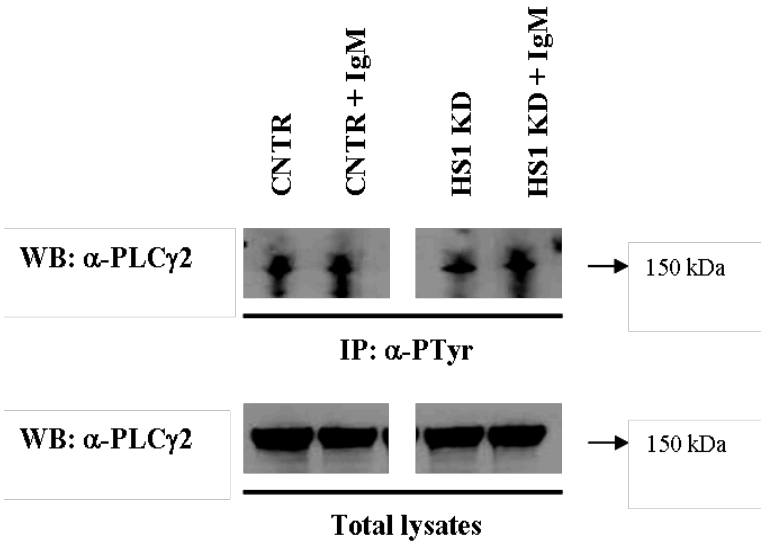

Figure 3.7 Immunoprecipitation (IP) experiments using anti-phosphotyrosine (PTyr) on control (CNTR) and HS1 knock-down (KD) cells before and after anti-IgM stimulation and Western Blot (WB) analysis for PLCγ2 on total lysates is shown as control. The results are representative of two independent experiments.

HS1 knock-down impairs SHP phosphorylation

The phosphatases SHP1 and SHP2 are activated early after BCR engagement and are essential for the regulation of the signalling pathway. In addition, SHP1 is thought to be a negative regulator, while SHP2 seems to be a positive regulator [32]. Lyn has been shown to be essential for SHP1 recruitment [22] leading to the subsequent dephosphorylation of several targets, including Syk [24] and BLNK [31].

SHP1/2 phosphorylation was detected by immunoprecipitation for total phosphotyrosines on CNTR and HS1 KD cell lysates, before and after anti-IgM stimulation, and WB analysis with a specific antibody (**Figure 3.8**). Constitutive SHP1/2 phosphorylation was observed in CNTR cells, and was not modified after anti-IgM treatment. On the contrary, SHP1/2 phosphorylation was not detected in unstimulated HS1 KD cells, and was partially restored after anti-IgM stimulation, suggesting that HS1 might be involved in the regulation of SHP1/2 phosphorylation.

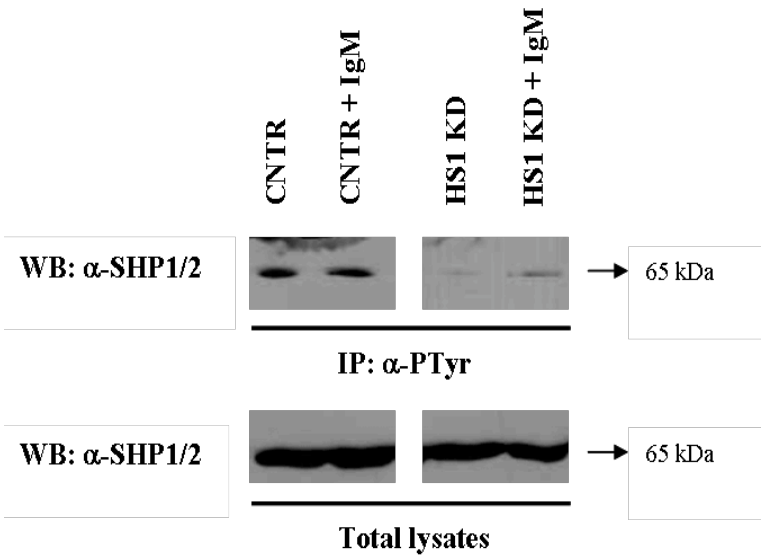

Figure 3.8. Immunoprecipitation (IP) experiments using anti-phosphotyrosine (PTyr) on control (CNTR) and HS1 knock-down (KD) cells before and after anti-IgM stimulation and Western Blot (WB) analysis for SHP1/2 (upper panels). WB analysis for SHP1/2 on total lysates is shown as control (bottom panels). The results are representative of two independent experiments.

3.5 Lyn phosphorylation studies on CLL patients

HS1 hyperphosphorylation correlates with the loss of Lyn phosphorylation in CLL patients

The results obtained with the cell lines prompted us to investigate the status of the signalling pathway in 10 different samples **(Table 2)** of primary CLL cells with different HS1 phosphorylation patterns, either hyper-phosphorylated ($HS1^{hyperp}$) (5/10) or partially-phosphorylated ($HS1^{p}$) (5/10) [57]. Lyn was tyrosine un-phosphorylated in the cells from 3/5 samples presenting $HS1^{hyperp}$ while it was phosphorylated in the cells from 5/5 patients with the $HS1^{p}$ version of HS1 (**Figure 3.9**). Comparing this pattern with the one observed in CNTR (constitutively phosphorylated Lyn) and HS1 KD cells (unphosphorylated Lyn) we can conclude that HS1 KD CLL cells resemble $HS1^{hyperp}$ B lymphocytes, thus suggesting that HS1 phosphorylation might be inactivatory.

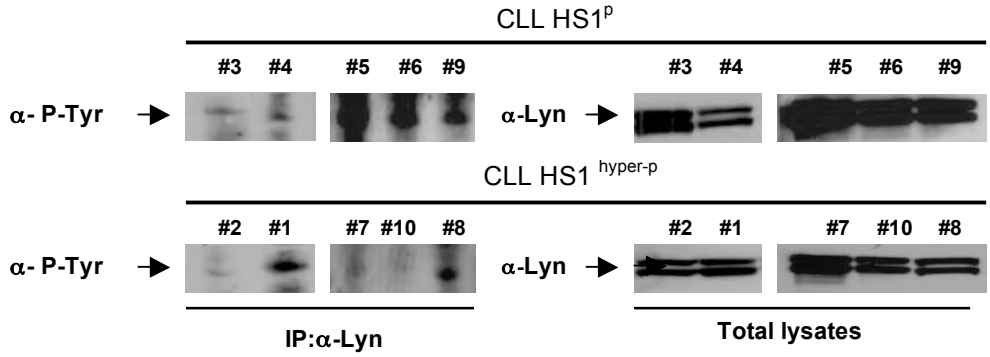

Figure 3.9. Immunoprecipitation (IP) experiments for Lyn and Western Blot (WB) analysis for total phosphotyrosines (PTyr) on leukemic B lymphocytes purified from the peripheral blood of 5 CLL patients (#1-#5 in **Table 2**) expressing the partially-phosphorylated form of HS1 (CLL $HS1^{p}$) and of 5 other patients (#6-#10 in **Table 2**) expressing the hyper-phosphorylated form of the protein (CLL $HS1^{hyperp}$). Top panels show representative two dimensional electrophoresis (2-DE) proteomic analysis of CLL cells [adapted from [57]]. WB analysis for Lyn on total lysates from all CLL cases is shown as control.

We are confirmed this results in a larger series of patients (n=60), this indicates a potential correlation between the phosphorylation status of the two molecules in CLL cells. Given that differential HS1 phosphorylation correlates with clinical prognosis [57], determination of the phosphorylation status of Lyn might become in a future important during the diagnostic work-up of patients.

Table 2: Clinical and biological features of the CLL patients studied

CLL Patient	RAI Stage*	BINET Stage*	CLINICAL COURSE	FOLLOW UP (month)	HC▲	LC▲	CD38 %▲	ZAP70 %▲♦	IGHV %	HS1 hyper-phospho Ψ	Lyn phosp■
#1	2	A	progress	123 (alive)	D	λ	3,68	Pos	100	yes	+
#2	0	A	progress	196 (dead)	MD	neg	0,70	Pos	91,67	yes	-
#3	0	A	stable	56 (alive)	MD	κ	1,81	Neg	100	no	+
#4	0	A	progress	120 (lost)	MD	neg	1,2	Pos	100	no	+
#5	0	A	stable	101 (lost)	MD	κ	0,4	Neg	89,5	no	+
#6	1	B	stable	159 (lost)	MD	κ	0,1	Neg	96,2	no	+
#7	0	A	progress	180 (dead)	MD	λ	88,5	Neg	100	yes	-
#8	0	A	progress	117 (lost)	MD	κ	78	Neg	100	yes	+
#9	0	A	stable	182 (lost)	MD	λ	1,0	Pos	89,5	no	+
#10	0	A	progress	97 (dead)	MD	κ	41	Pos	100	yes	-

***Determined at diagnosis ▲Heavy chain (HC), Light chain (LC), CD38 and ZAP70 were determined by flow cytometry, ♦ positive (pos) or negative (neg) determined with a cut-off of 20%, Ψ number of spots revealed on silver stained 2D gels, ■ WB analysis**
ND: not determined

.

3.6 Cytoskeletal proteins activation studies in HS1 KD cells

We first analyzed the phosphorylation status of several molecules known to be major players in the cytoskeletal remodelling after antigen-receptor engagement. We focused our attention on those proteins that are known to be associated with HS1 function, at least in T [58] and NK cells [60].
Then, we investigated how cytoskeletal reorganization in terms of actin and myosin distribution and functionality might be affected by the absence of HS1 expression.

HS1 knock-down up-regulates HIP55 phosphorylation

HIP55 is an adaptor molecule that modulates TCR signalling after recruitment to the IS [42]. Although its role in BCR signalling needs to be clarified, HIP55 is known to directly interact with HS1 in normal and leukemic B cells [44].
We analyzed HIP55 with the same approach used for BCR proximal molecules: IP with anti-PTyr on CNTR and HS1 KD cells before and after anti-IgM stimulation and WB analysis with a specific antibody. HIP55 undergoes phosphorylation in the absence of HS1 in clear contrast with CNTR cells regardless anti-IgM stimulation (**Figure 3.10**), implying that the presence of HS1 may interfere with its phosphorylation.

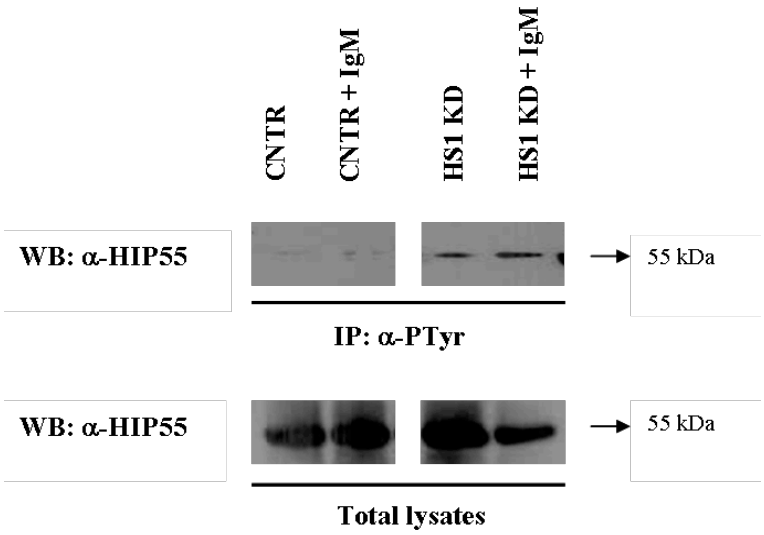

Figure 3.10. Immunoprecipitation (IP) experiments using anti-phosphotyrosine (PTyr) on control (CNTR) and HS1 knock-down (KD) cells before and after anti-IgM stimulation and Western Blot (WB) analysis for HIP55 (upper panels). WB analysis for HIP55 on total lysates is shown as control (bottom panels). The results are representative of two independent experiments.

HS1 knock-down impairs Vav1 phosphorylation

Vav proteins are Rho GEFs responsible for the activation of Rho GTPases and actin polymerization [37]. Moreover, Vav proteins are involved in signalosome assembly and IS formation in B [14] and T cells [36]. Vav activity has multiple layers of regulation, among which tyrosine phosphorylation.

Vav1 (the haematopoietic-restricted Vav protein) phosphorylation was detected by immunoprecipitation for total phosphotyrosines on CNTR and HS1 KD cell lysates, before and after anti-IgM stimulation, and WB analysis with a specific antibody. Vav1 tyrosine phosphorylation is lost in the absence of HS1 and partially restored after anti-IgM stimulation of HS1 KD cells (**Figure 3.11**), indicating a crucial role for HS1 in the regulation of this process, thereby closely resembling what previously shown in T cells [58].

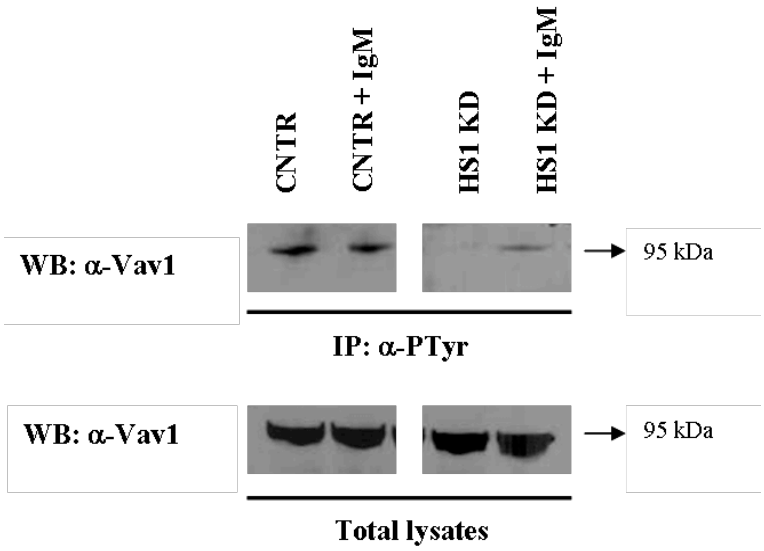

Figure 3.11. Immunoprecipitation (IP) experiments using anti-phosphotyrosine (PTyr) on control (CNTR) and HS1 knock-down (KD) cells before and after anti-IgM stimulation and Western Blot (WB) analysis for Vav1 (upper panels). WB analysis for Vav1 on total lysates is shown as control (bottom panels). The results are representative of two independent experiments.

HS1 knock-down cells show diminished Rac activation

Rac1/2 and Cdc42 are Rho GTPases directly involved in B-cell actin polymerization [35]. In addition, Rac activity is essential for B-cell adhesion to APCs [40] at the IS and is modulated both by Vav and upstream molecules such as Lyn.

We performed a Rac/Cdc42 pull-down assay in order to evaluate Rac/Cdc42 activation status. Briefly, untreated CNTR and HS1KD total cell lysates were incubated with PAK-1 PBD agarose beads that

bind selectively the GTP-bound (i.e. activated) form of Rac and Cdc42. Detection was performed with anti-Rac1 and anti-Cdc42 antibodies. Anti-Rac1 is able to detect also Rac2.

Rac is inactive in HS1 KD cells while constitutively active in CNTR cells (**Figure 3.12**), suggesting that HS1 KD signalling impairment might ultimately affect the regulation of this process. No Cdc42 constitutive activation was detected in both CNTR and HS1 KD cells (data not shown).

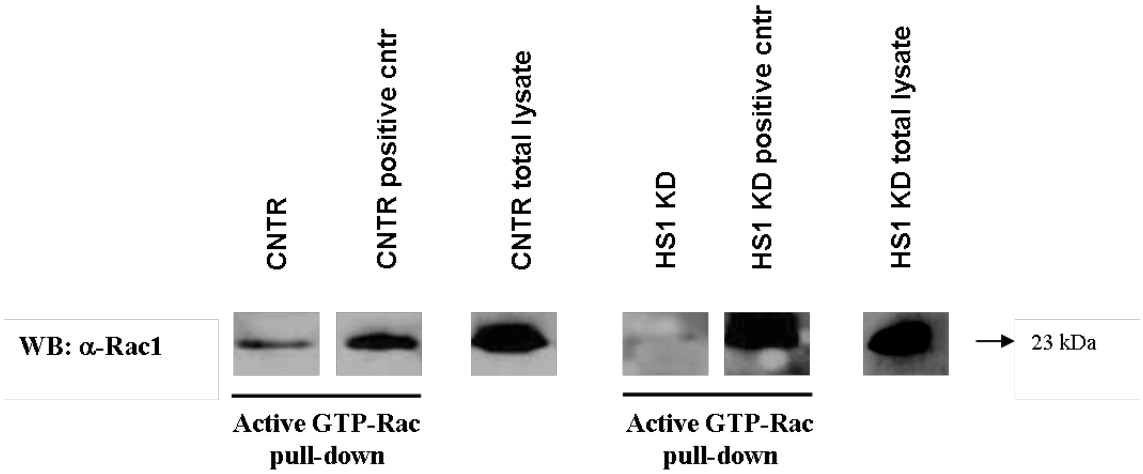

Figure 3.12. Rac activation assay was performed as pull-down on control (CNTR) and HS1 knock-down (KD) cells (for the positive controls, GTPγS, a non-hydrolysable form of GTP, was incubated with the lysates). Total lysates were also used to detect Rac expression. WB, Western Blot. The results are representative of two independent experiments.

3.7 Cytoskeletal remodelling and functional studies in HS1 knock-down cells in vitro

We reasoned that modifications of molecules involved in intracellular signalling pathways crucial for actin dynamics and cytoskeletal remodeling should be paralleled by functional consequences of HS1 impairment. To strengthen the evidence that actin is affected by HS1 downmodulation and to evaluate the functional relevance of the observed differences, we studied in parallel human HS1 KD cells and splenic B cells from HS1$^{-/-}$ mice [56] investigating some of the most important cytoskeletal related functions.

HS1 knock-down cells show altered actin distribution and polymerization

Based on these results showing major changes in the activation status of molecules known to be relevant players in the cytoskeletal reorganization after antigen-receptor engagement, we studied how the HS1 KD-cell signalling impairment would affect cytoskeletal remodelling in terms of actin and myosin distribution around the cell.

We performed an immunofluorescence staining on untreated CNTR and HS1 KD cells and, by confocal analysis, we studied actin and myosin. Both CNTR and HS1 KD cells show diffuse myosin distribution; actin, on the other hand, assembles in regular branched protrusions at the cell edge of CNTR cells, while it accumulates in small aggregates in HS1 KD cells (**Figure 3.13**). These evidences suggest that HS1 is needed for proper actin microfilaments assembly.

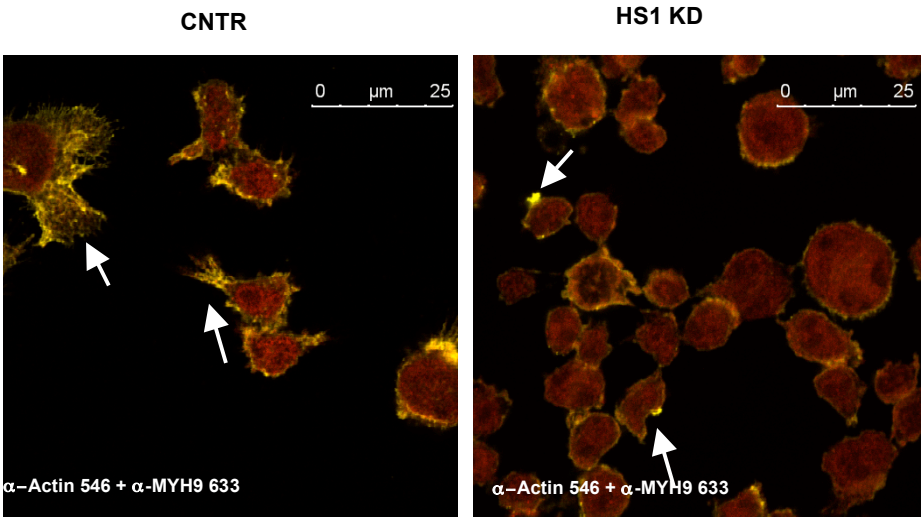

Figure 3.13. Confocal analysis of control (CNTR) and HS1 knock-down (KD) cells with anti-actin and anti-myosin heavy chain 9 (MyH9) primary antibodies detected with Alexafluor 546 (yellow) and 633 (red) conjugated secondary antibodies. White arrows indicate characteristic CNTR cell protrusions HS1 KD actin aggregates.

A disregulated F-actin distribution during HS1 KD cell adhesion (**Figure 3.13**) was also confirmed by TIRF microscopy (**Figure 3.14**).

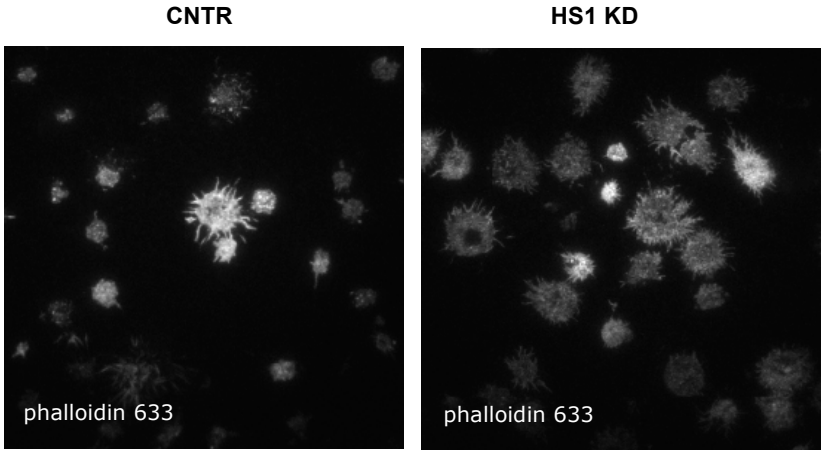

Figure 3.14. TIRF acquisition after Phalloidin Alexafluor 633 staining on CNTR cells and HS1 KD adhered on poli-L-Ornithine coating, arrows indicate the different F-actin distribution.

In addition, we observed a trend to impaired actin polymerization activity upon anti-IgM stimulation (**Figure 3.15**) that likely explains the failure of filopodia formation as described in different cellular systems [140].

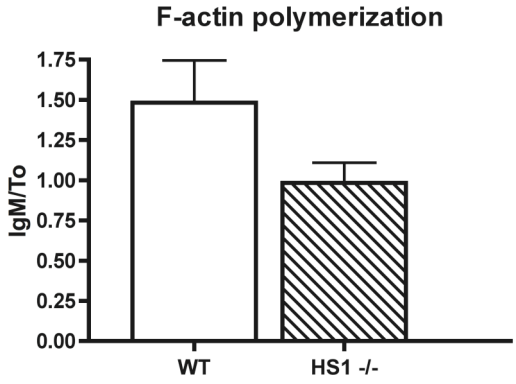

Figure 3.15 F-actin polymerization is represented as the ratio of the flow-cytometric mean fluorescence intensity (MFI) values after and before IgM stimulation in WT and HS1-/- mice B splenocytes (6 animals/group)

In vitro the absence of HS1 results into impaired cell migration, cell adhesion, and increased homotypic aggregation

First, we tested the spontaneous migratory capacity of both human HS1 KD and mouse HS1$^{-/-}$ cells. The *in vitro* spontaneous migration of human HS1 KD cells was significantly decreased (**Figure 3.16 a**). Similarly the migratory capacity of purified splenic B cells from 2 month old HS1 $^{-/-}$ mice was more than 8 fold lower as compared to WT mice (**Figure 3.16 b)**.

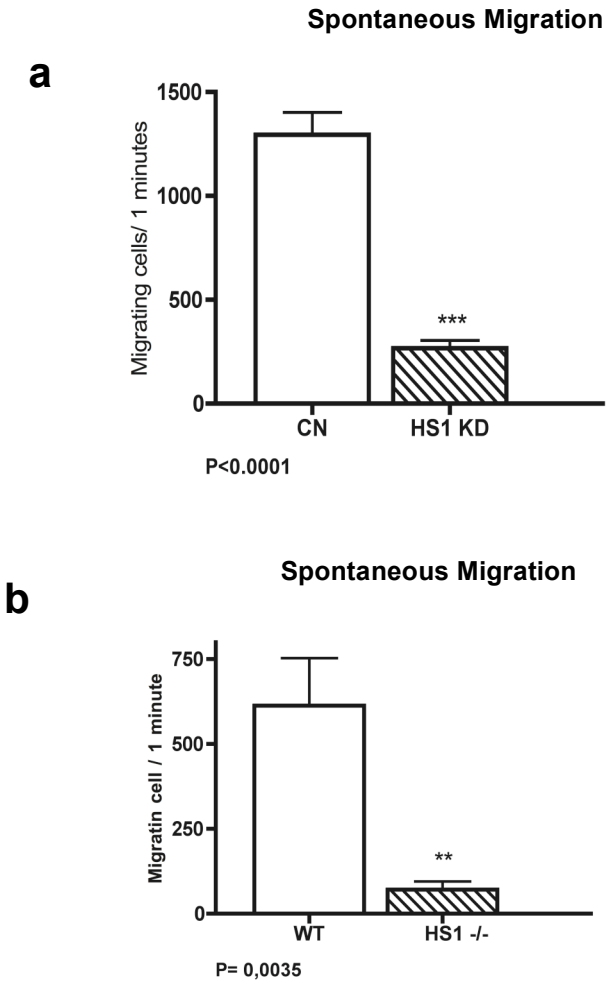

Figure 3.16 HS1 absence affects migration.
(a) Spontaneous migration after 4 hours on transwell (pore size 5.0 μm) of CNTR and HS1 KD cell and (b) WT and HS1-/- mice purified B splenocytes (6 animals/group) is shown (*p≤0,05; **p≤0,01; ***p<0,001).

No differences of CXCR4 receptor expression and no significant variation in SDF-1 chemokine-mediated migration of HS1 KD and HS1$^{-/-}$ cells was observed,suggesting that HS1 is involved in spontaneous rather than in chemokine-mediated migration.

The adhesion of cells lacking HS1 to basal (BSA) and to ICAM-1 matrices was significantly impaired (**Figure 3.17**).

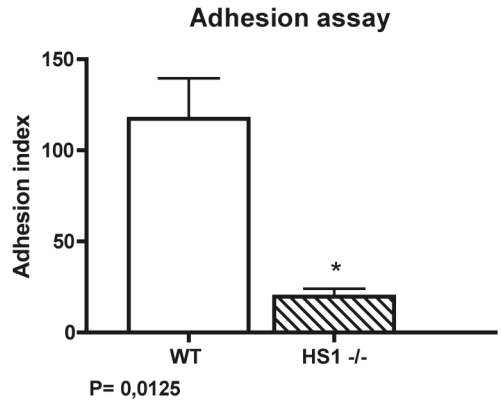

Figure 3.17 HS1 absence affects adhesion
Adhesion was quantified as adhesion index for WT and HS1-/- mice B cells (*p≤0,05; **p≤0,01; ***p<0,001

Based on the observed adhesion impairment in plastic plates, we aimed at testing the adhesion capacity of both CNTR and HS1 KD cells to a human bone marrow stroma layer (HS-5 cell line), that mimics the physiological microenvironment where CLL B lymphocytes reside in vivo.

HS1 KD cells failed to individually adhere to a BM stroma layer, the cells tended to clump and increased homotypic aggregation forming clusters **(Figure 3.18).**

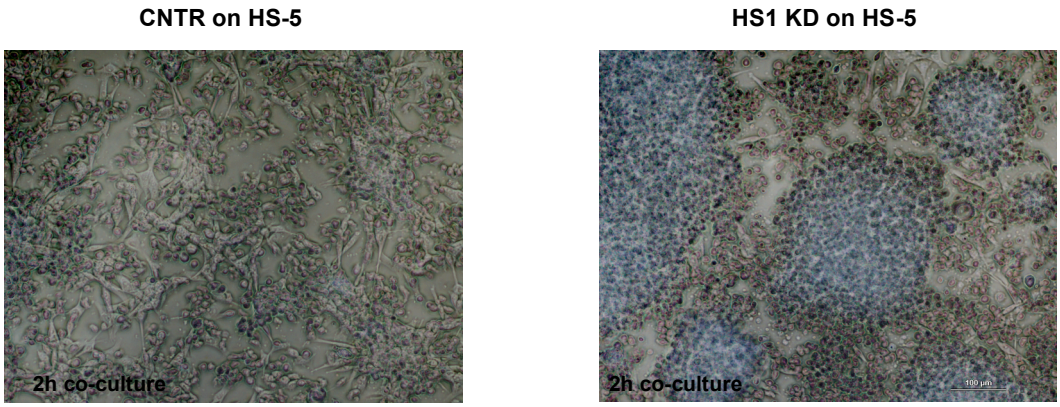

Figure 3.18 HS1 absence affects aggregation. CNTR and HS1 KD cells adhesion on a HS-5 stroma cell layer after 2 hours co-culture acquired with Nikon TS100 microscope.

3.8 Functional studies in HS1 KD cells in vivo

In vivo the absence of HS1 leads to a distinct pattern of CLL development and tissue localization

To evaluate the *in vivo* migration capacity of HS1 KD as compared to CNTR cells, we took advantage of a new CLL xenograft model developed in the lab[141]by injection of $10x10^6$ cells subcutaneously into the left flank of adult $RAG2^{-/-}\gamma_c^{-/-}$ mice (4 animals/group). The deep immunesuppression of $RAG2^{-/-}\gamma_c^{-/-}$ mice lacking B, T and NK cells, favors the growth and systemic spreading of CLL cells compared to previously reported NOD/SCID mice [83], that retain NK cells and do not allow engraftment of leukemic cells.

All transplanted animals developed tumors resembling CLL one week after injection, but HS1 KD tumors reached a volume of approximately 1000 mm^3 10 days earlier than CNTR cells (HS1 KD vs CNTR cells: p=0,01; day 35) (**Figure 3.19**).

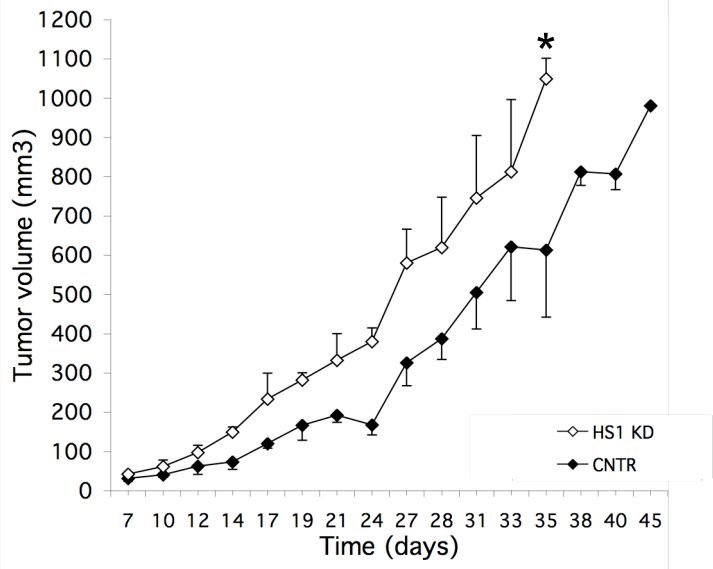

Figure 3.19 HS1 KD cells show a distinct in vivo pattern of growth and localization. Tumor volume was evaluated by measuring perpendicular diameters by a caliper. Animals were killed when the tumor volume reached 1000 mm3 (*p≤0,05; day 35)

The tissue localization also differed depending on the presence or the absence of HS1, As in CNTR cells, HS1 KD cells accumulated in the axillary and inguinal lymph nodes draining the site of injection and in the BM as well as in the site of injection. In contrast, HS1 KD cells were virtually absent in the spleen, liver, lungs and kidneys (**Figure 3.20 a,b and Figure 3.21**). The presence of large cellular aggregates closely resembled the clustering adhesion behaviour shown *in vitro* by HS1 KD cells cultured on human BM stroma (**Figure 3.18**). These results suggest a relationship between the

expression of HS1 and the capacity to localize in the BM as well as in the lymph nodes (**Figure 3.21**).[142].

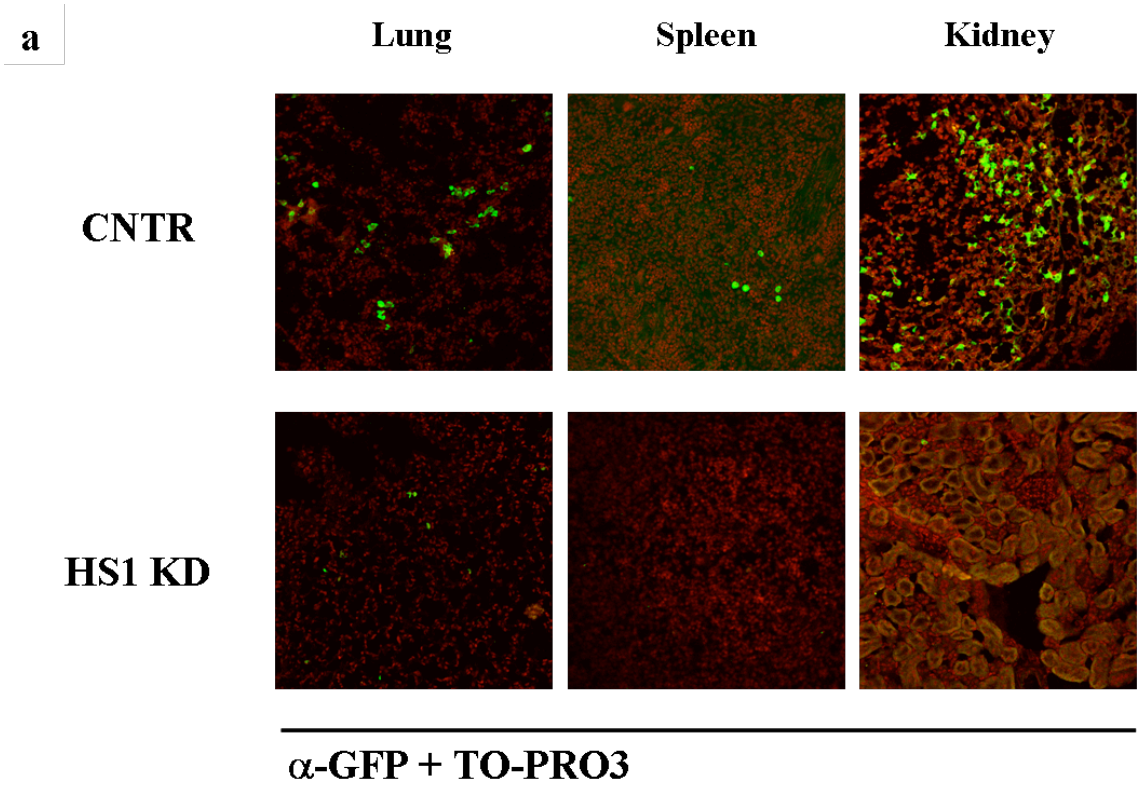

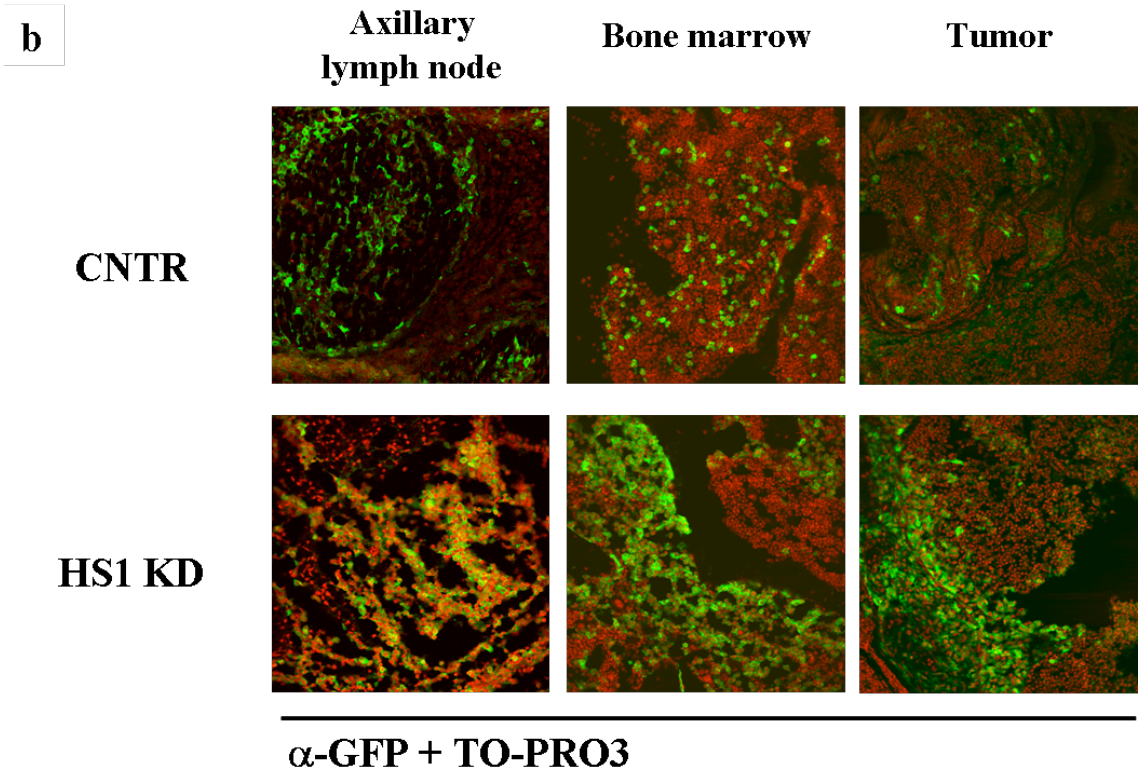

Figure 3.20 HS1 KD cells show a distinct in vivo pattern of growth and localization Lung, spleen, liver, kidney, axillary tumor draining lymph node, bone marrow and site of injection were collected. The slides were stained with anti-GFP Alexafluor 488 (green) and TO-PRO3 (red) for the nuclear staining (overlap yellow). Slides were analyzed by confocal microscope using an inverted 20x objective. The extent and pattern of invasion is demonstrated by the presence of green GFP^+ leukemic cells.

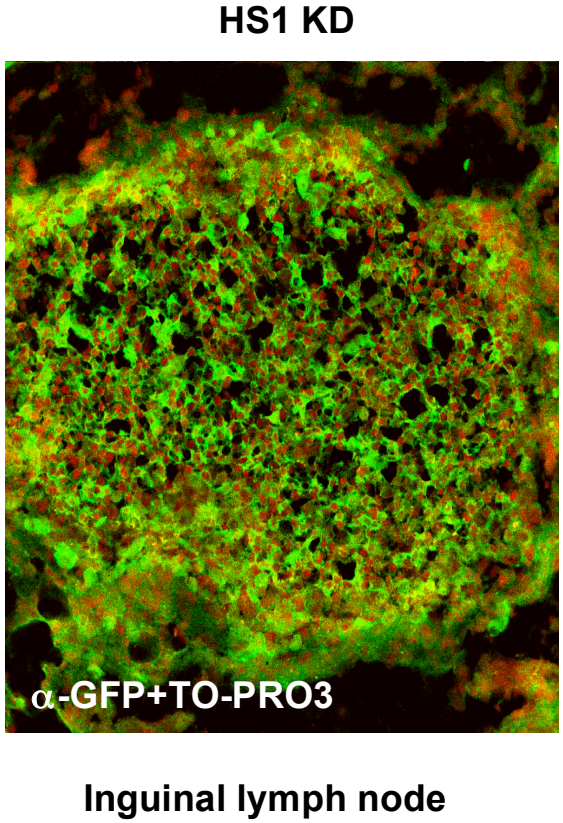

Figure 3.21 HS1 KD MEC1 localization in the inguinal draining lymph node.
Inguinal draining lymph node was extracted from $Rag2^{-/-}\gamma_c^{-/-}$ male mice transplanted s.c. in the left flank with HS1 KD expressing GFP and analyzed by confocal microscopy. The slide was stained for anti-GFP Alexafluor 488 and TO-PRO3 for nuclear staining. The slide was analyzed at a confocal microscopy with an inverted 20x objective. The extent and pattern of invasion is demonstrated by the presence of green GFP^+ leukemic cells.

In vivo migration of B splenocytes from HS1$^{-/-}$ mice

To further substantiate our observations, CD19^{+} cells were purified from the spleen of 5-6 month old HS1$^{-/-}$ and WT mice, labeled with different concentrations of CFSE, admixed (**Figure 3.22**) and injected intravenously (i.v.) into 5 month old HS1$^{-/-}$ and WT recipients.

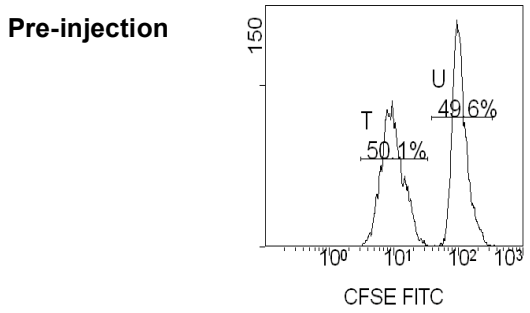

Figure 3.22 *In vivo* migration of B splenocytes from HS1$^{-/-}$ mice.
Flow cytometric analysis of CD19^{+}CD5^{+} cells in the pre-injection mixture. The histogram plot is gated on 7-AAD^{-}CFSE^{+} cells and on physical parameters. Percentages of cells are indicated

The expression of CFSE fluorescence on 7AAD^{-}-gated lymphocytes confirmed the presence of two populations, CFSE-low (WT) and CFSE-high (HS1$^{-/-}$) labeled cells. No differences were observed in the spleen, mesenteric lymph nodes, PB of both recipient mice and in the BM of WT recipient mice (**Figure 3.23 a**). On the contrary, HS1$^{-/-}$ B lymphocytes preferentially accumulated in the BM of HS1$^{-/-}$ recipient mice, where they represented almost 75% of CFSE^{+} cells (**Figure 3.23 b**).

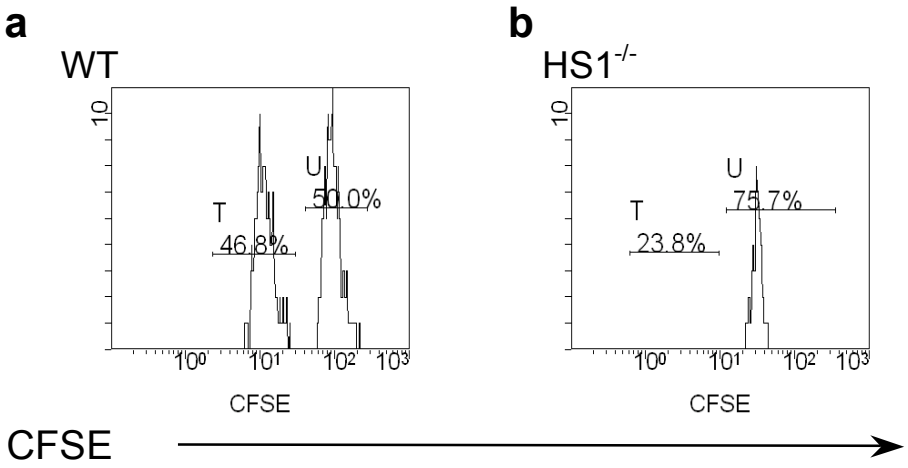

Figure 3.23 *In vivo* migration of B splenocytes from HS1$^{-/-}$ mice.
HS1$^{-/-}$ mice (n=3, repeated twice) and age-matched WT mice (n=3, repeated twice) were given i.v. injections of a mixture of CFSE-low and CFSE-high labeled CD19^{+} purified splenocytes from WT and HS1$^{-/-}$ mice, respectively. Hystogram plots represent flow cytometric analysis of 7-AAD^{-} CFSE-low (WT cells, peak T) and CFSE-high (HS1$^{-/-}$cells, peak U) splenocytes obtained from BM of representative WT (**a**) and HS1$^{-/-}$(**b**) recipient mice sacrificed 20 hours after cell injection. Cells represented in each plot were gated on physical parameters. Numbers show percentages of cells falling in peaks T and U.

These data suggest a preferential homing to the BM that cannot simply be due to the absence of HS1 in leukemic cells but also to the lack of HS1 in still undefined cellular components of the microenvironment.

The in vivo propensity of human CLL cells to migrate to the bone marrow correlates with HS1 phosphorylation and expression

We investigated the homing ability of fresh CLL cells from patients showing different HS1 phosphorylation patterns (**Table 2 and chapter 3.5**). CD19^{+} cells purified from 8 patients were paired into 4 couples according to their different HS1 phosphorylation status [57]. Each couple included a case with HS1^{p} (phosphorylated HS1) and a case with HS1$^{hyper\text{-}p}$ (hyper-phosphorylated HS1) CLL cells. Cells were labeled with different concentrations of CFSE, admixed (**Figure 3.24 A,D**) and injected i.v. into Rag2$^{-/-}\gamma_c^{-/-}$ mice recipients. The expression of CFSE fluorescence on 7AAD^{-}-gated lymphocytes allowed to discriminate two distinct populations, phosphorylated (CFSE-low labeled) and hyper-phosphorylated (CFSE-high labeled) HS1 cells. In 3/4 couples of differentially phosphorylated paired patients HS1^{p} CLL cells had a consistent homing rate to the spleen (**Figure 3.24 B**), while HS1$^{hyper\text{-}p}$ CLL cells had a preferential homing to the BM (**Figure 3.24 C**). The preferential BM homing of HS1$^{hyper\text{-}p}$ CLL was also reproduced when these cells were labeled with low concentrations of CSFE (CFSE-low), indicating that *in vivo* cell viability and migratory capacity were unaffected by different CFSE levels (**Figure 3.24 E,F**).

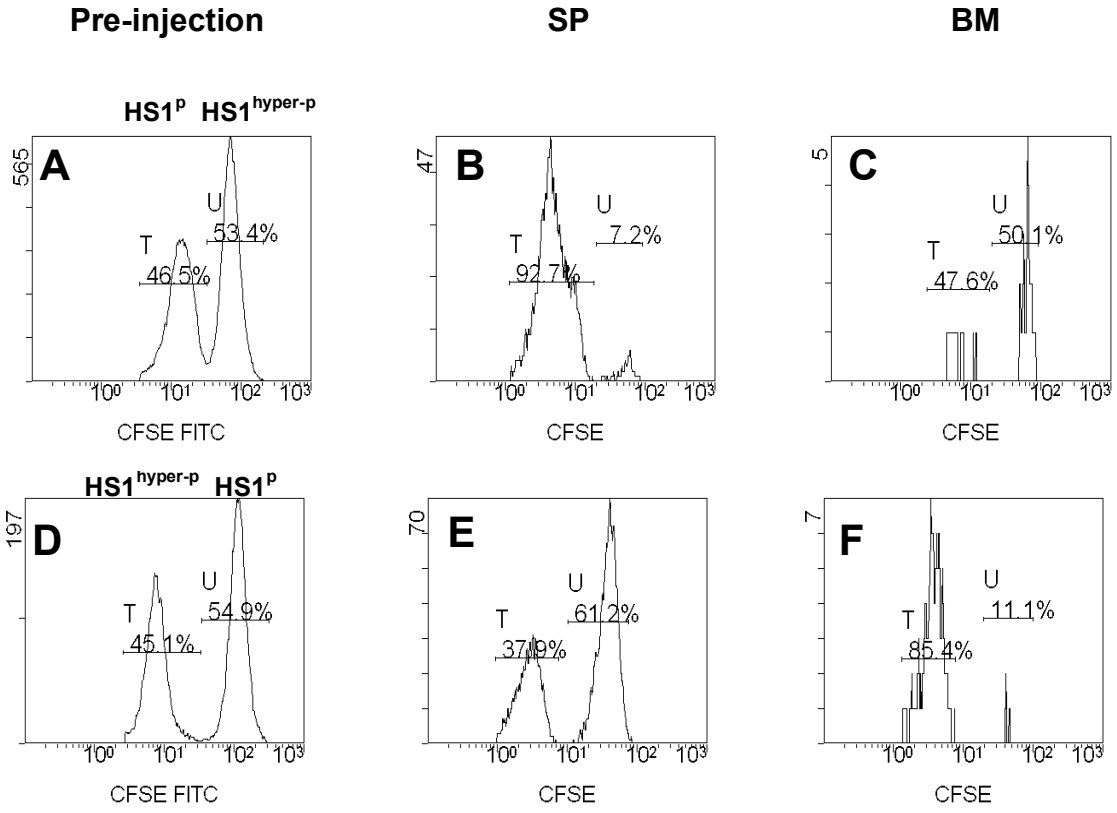

Figure 3.24 : *In vivo* migration of primary leukemic cells obtained from CLL patients.
$Rag2^{-/-}\gamma_c^{-/-}$ mice were injected i.v. with a mixture of $CD19^+$ CFSE-high and CFSE-low labeled leukemic B cells from the PB of 8 CLL patients with a different pattern of HS1 phosphorylation ($HS1^{hyper\text{-}p}$ and $HS1^{p}$). (**A,D**) Flow cytometric analysis of pre-injection samples: percentages of CFSE-low (peak T) and CFSE-high (peak U) cells are indicated. The plots are gated on 7-AAD^- $CFSE^+$ cells. (**B**,**C**) Flow cytometric plots show 7-AAD^- CFSE-low (peak T, $HS1^{p}$; patient #6 in **Table 2**) and CFSE-high (peak U, $HS1^{hyper\text{-}p}$; patient #7 in **Table 2**) cells obtained from spleen (SP) and BM of a representative $Rag2^{-/-}\gamma_c^{-/-}$ recipient mouse sacrificed 20 hours after cell injection. Percentages of cells falling in fractions T and U are indicated. (**E,F**) Flow cytometric plots show 7-AAD^- CFSE-low (peak T, $HS1^{hyper\text{-}p}$; patient #1 in **Table 2**) and CFSE-high (peak U, $HS1^{p}$; patient #4 in **Table 2**) cells obtained from SP and BM of the $Rag2^{-/-}\gamma_c^{-/-}$ recipient mouse sacrificed 20 hours after cell injection. The preferential accumulation of $HS1^{hyper\text{-}p}$ cells versus $HS1^{p}$ cells in the BM of mice is not affected by CFSE concentration.

Since HS1 hyperphosphorylated and knocked down cells show striking phenotypic similarities, we asked whether not only the phosphorylation but also the expression of HS1 might be modulated in CLL cells. To this end we investigated by immunohistochemistry the expression pattern of HS1 protein in the BM and peripheral blood (PB) of CLL patients (10 cases) either lacking or carrying the hyperphosphorylated form of the molecule. Preliminary observations revealed that in the same patient HS1 is differently expressed in the BM as compared to the peripheral blood (PB); more specifically that BM CLL cells lack the expression of HS1 when the protein is hyperphosphorylated in PB cells (**Figure 3.25**).

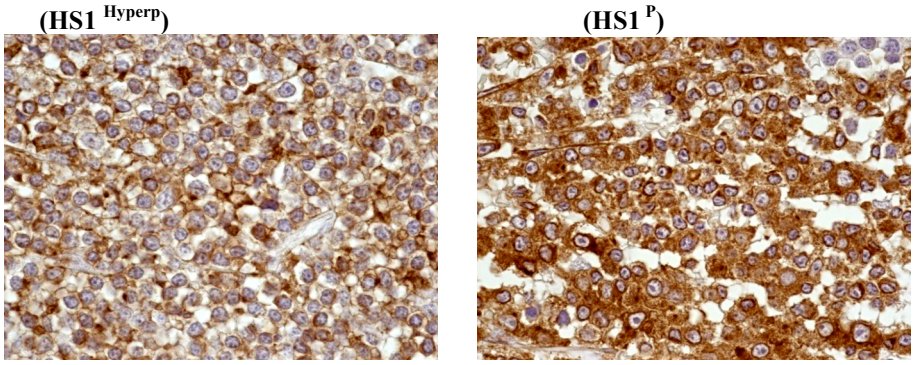

Figure 3.25 : Immunoistochemistry analysis of HS1 on CLL BM biopsies in the two subsets of patiens

3.9 HS1 influences the development and progression of CLL in the Eμ-TCL1 transgenic mouse model

To further investigate the *in vivo* role of HS1 in CLL onset and progression, we crossed $HS1^{-/-}$ ($H^{-/-}$) mice with Eμ-TCL1 tg ($T^{tg/tg}$) mice and analyzed TCL1 heterozigous $H^{-/-}/T^{tg}$ mice. $H^{-/-}/T^{tg}$ and age-matched H^{wt}/T^{tg}, $H^{-/-}/T^{wt}$ and H^{wt}/T^{wt} littermates obtained in the F2 progeny were monitored for development of CLL-like disease. $H^{-/-}/T^{tg}$ mice had a more precocious development of leukemia (7-13 months vs 13-18 months) (**Figure 3.26**) as indicated by an earlier accumulation of $CD19^{+}CD5^{+}$leukemic B cells in lymphoid organs (spleen, BM and PB) when compared to the H^{wt}/T^{tg} mice. As in H^{wt}/T^{tg} mice [116,117] $CD19^{+}CD5^{+}$ splenic B-cells from $H^{-/-}/T^{tg}$ mice showed restricted Igκ (**Figure 3.27**) and IgM expression (**Figure 3.27**) indicating monoclonality. The same IgM and Igκ restriction was observed in $CD19^{+}CD5^{+}$ cells obtained from the PB, peritoneal cavity and BM.

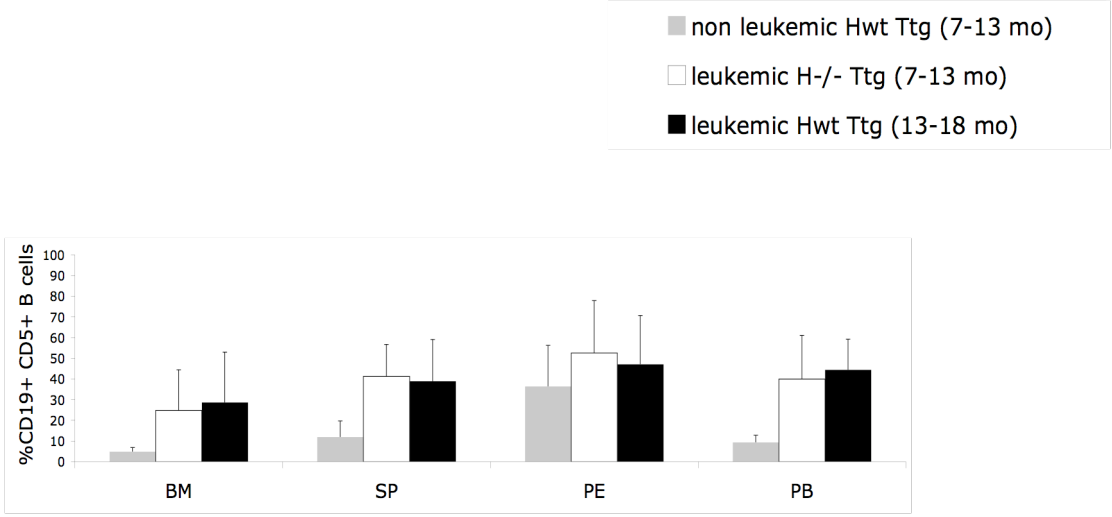

Figure 3.26 : $H^{-/-}/T^{tg/wt}$ mice show a premature accumulation of $CD19^{+}CD5^{+}$ cells.
Mice were grouped based on the presence of ≥30% $CD19^{+}CD5^{+}$ cells in PB (leukemic mice) as compared to <30% (non-leukemic mice).
Non-leukemic $H^{wt/wt}/T^{tg/wt}$ mice (7-13 month old, n=8), age-matched leukemic $H^{-/-}/T^{tg/wt}$ (n=6) and leukemic $H^{wt/wt}/T^{tg/wt}$ (13-18 month old, n=5) mice were analyzed by flow cytometry. The mean value ± standard deviation of the relative contribution of $CD19^{+}CD5^{+}$ cells to the whole B cell pool in the bone marrow (BM), spleen (SP), peritoneal cavity (PE) and peripheral blood (PB), is shown in the graph. Statistical significance was analyzed by T-test. *p≤0,05; **p≤0,01; ***p<0,001

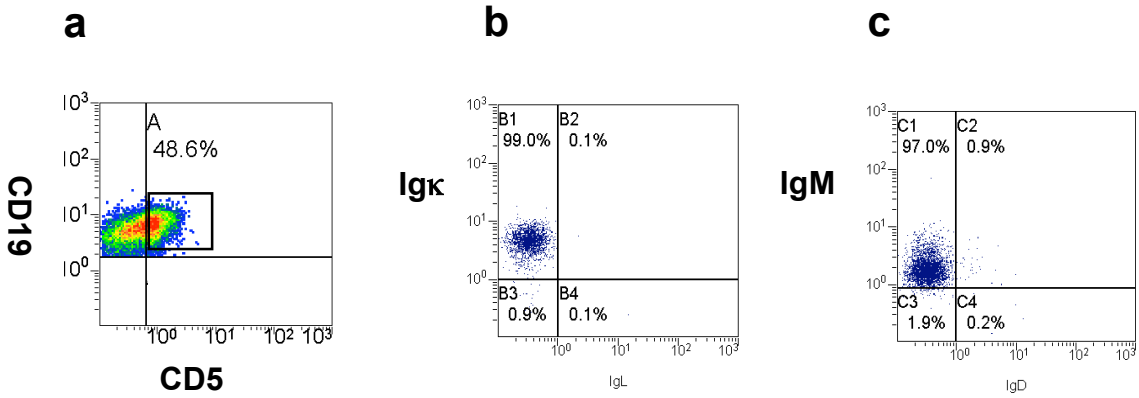

Figure 3.27 : $H^{-/-}/T^{tg/wt}$ mice show a premature accumulation of $CD19^{+}CD5^{+}$ cells.
Flow cytometric plot from a representative leukemic $H^{-/-}/T^{tg}$ mouse (9-month old) show $CD19^{+}CD5^{+}$ cells in the spleen. The cells were first gated on physical parameters and then on side scatter (SSC) and CD19. Percentage of leukemic $CD19^{+}CD5^{+}$ cells is indicated. Flow cytometric plots from a representative leukemic $H^{-/-}/T^{tg}$ animal (9-month old) showing (**a**) Igκ and (**b**) IgM expression on $CD19^{+}CD5^{+}$ cells from the spleen **(c)**.

The monoclonal origin of the $CD5^{+}Ig\kappa^{+}IgM^{+}$ B-cell expansion detected in $H^{-/-}/T^{tg}$ mice, was also confirmed by IGH gene rearrangements using nested PCR (**Table 3**). The analysis of the IGH gene rearrangement nucleotide sequence showed that all clones expressed unmutated IGHV genes.

Table 3. Features of IGH gene rearrangements in $H^{-/-}/T^{tg/wt}$ (HT) and $H^{wt/wt}/T^{tg/wt}$ (T) mice clones.

Animal no.	Tissue *	IGHV	HCDR3	Age (mo)
HT225	pb,sp,bm	IGHV2-4-1	CARFYYSYYSYYAMDYW	7
HT25	pb[1]	IGHV2-9	CAKRLLRYYAMDYW	8
HT142	pb,sp,bm	IGHV11-1	CMRYGDYWYFDVW	9
HT109	pb,sp,bm	IGHV1-82	CARGGYPFVYW	13
HT119	pb,sp	IGHV1S61	CATGAWFAYW	13
T172	pb	IGHV12-3	CAGDGS#DYW	9
T214	pb	IGHV2-9-1	CARDDDYYYAMDYW	9
T87	sp	IGHV1-55	CAIGFDYW	13
T278	pb,sp,bm	IGHV2-2	CARNGYDYAMDYW	15
T348	pb,sp,bm	IGHV1-55	CARFYYYGSSYAMDYW	15
T382	sp	IGHV1-47	CAVYYVNFDYW	15

Only tissues analyzed and positive for the presence of a IG rearrangement are listed:pb= peripheral blood; sp= spleen, bm= bone marrow
[1]sp and bm not analized.
 # indicates a stop codon, making the sequence unproductive

Histopathological examination revealed earlier accumulation of leukemic B cells in different organs (**Figure 3.28 a**) of $H^{-/-}/T^{tg}$ mice similarly to older H^{wt}/T^{tg} mice with foci of $B220^{+}$ cells (**Figure 3.28 b**), confirming the earlier onset of leukemia in $H^{-/-}/T^{tg}$ mice.

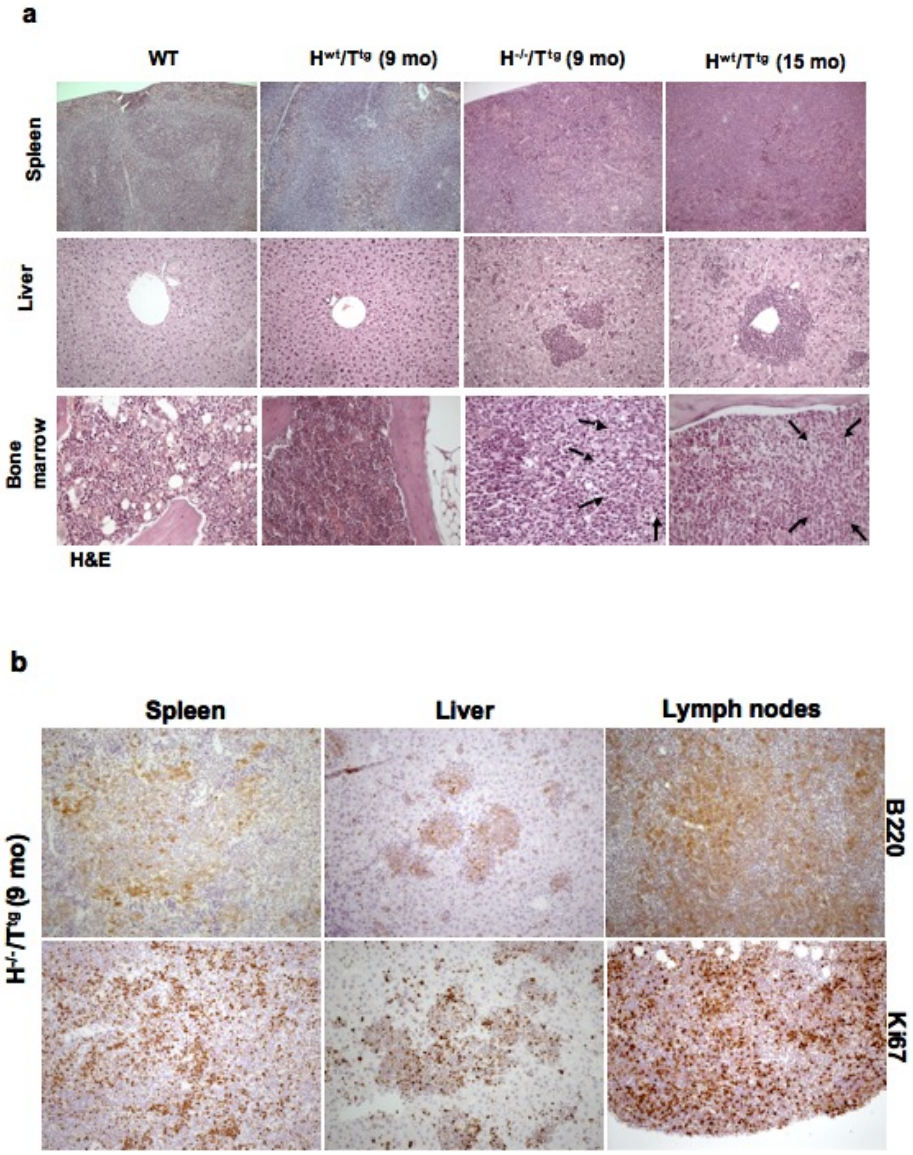

Figure 3.28 Histological analysis of wild type (WT), non leukemic $H^{wt/wt}/T^{tg/wt}$ (9 mo), leukemic $H^{-/-}/T^{tg/wt}$ mice (9 mo), leukemic $H^{wt/wt}/T^{tg/wt}$ (15 mo).(**a**) Histopathological examination of lymphoid tissues: in comparison with WT $H^{wt/wt}/T^{tg/wt}$ (9-month old) mice showed an early, interfollicular effacement of splenic architecture by medium-sized lymphoid cells, that almost completely replaced splenic tissue in $H^{wt/wt}/T^{tg/wt}$ (15-month old) and $H^{-/-}/T^{tg/wt}$ (9-month old) mice. Liver involvement with roughly similar degree of infiltration was noted only in $H^{wt/wt}/T^{tg/wt}$ (15-month old) and $H^{-/-}/T^{tg/wt}$ (9-month old) mice. Areas of BM infiltration by neoplastic lymphocytes, shown by arrows, were restricted to leukemic $H^{-/-}/T^{tg/wt}$ (9- month old) and $H^{wt/wt}/T^{tg/wt}$ (15-month old) mice (Haematoxylin-Eosin stained sections, 100x magnification for spleen, 200x for liver and 400x for bone marrow).(**b**) Immunohistochemical stains revealed that in $H^{-/-}/T^{tg/wt}$ (9-month old) mice the majority of leukemic infiltrates in spleen, liver and mesentheric lymph nodes was $B220^{+}$ (upper panel). The lower panel highlights the different replicative fraction in the evaluated organs, according to Ki-67 immunostaining (200x).

The absence of HS1 had also a significant impact on Eμ-TCL1 mice survival as some mice died already at the age of 3-5 months ($H^{-/-}/T^{tg}$ vs H^{wt}/T^{tg} : $p<0.0001$) (**Figure 3.29**). $H^{-/-}/T^{wt}$ and H^{wt}/T^{wt} littermates showed normal survival (data not shown).

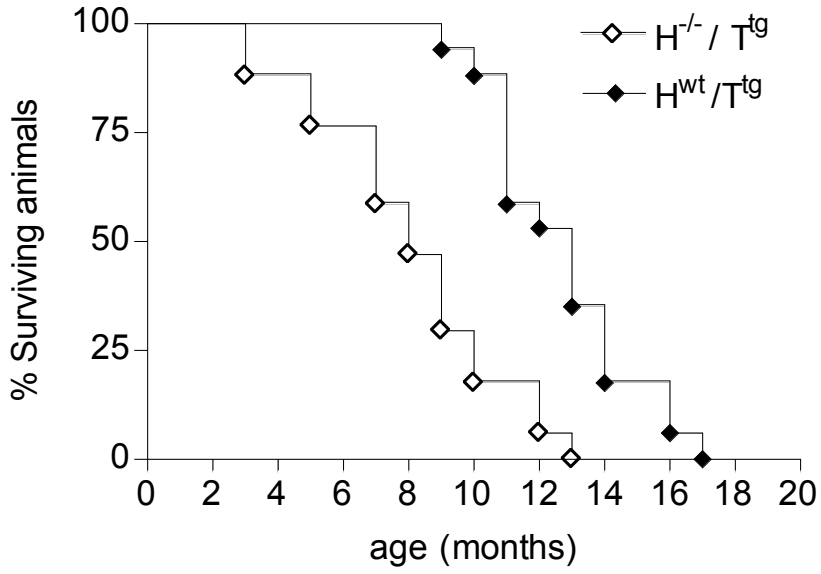

Figure 3.29 $H^{-/-}/T^{tg/wt}$ mice show a premature accumulation of $CD19^+CD5^+$ cells Kaplan-Meier survival curves of $H^{-/-}/T^{tg/wt}$ (n=18) and $H^{wt/wt}/T^{tg/wt}$ (n=17) mice are shown. Mice were included in the analysis after spontaneous death or when sacrificed because of frank leukemia development (presence of ≥30% $CD19^+CD5^+$ expansion at least in the PB, monoclonal IGH gene rearrangements, tissue infiltration). Statistical analysis between groups was performed using the log-rank test ($H^{-/-}/T^{tg/wt}$ vs $H^{wt/wt}/T^{tg/wt}$, $p<0,0001$).

4. Discussion

Chronic Lymphocytic Leukemia (CLL) has several distinct features making it an interesting topic of research. In contrast to other cancers where genetic events are the leading forces in the neoplastic transformation, CLL is still responsive to external stimuli originating from the microenvironment that plays a key role in the natural history of the disease [143]. In particular, as the disease is characterized by the accumulation of small, resting B lymphocytes expressing a monoclonal immunoglobulin (or BCR) on the cell surface, there are several evidences indicating that stimulation through the BCR is a central event in its pathogenesis [144]. In addition, though being quite homogeneous in terms of cellular phenotype, CLL is a rather heterogeneous disease at the clinical level. Some patients experience a long disease course while others suffer from a progressive form with a poor clinical outcome. In the recent past, several biological features of the disease have been proposed as prognostic factors since their expression is able to discriminate subtypes of the disease with a different clinical outcome [145]. A putative novel prognostic factor, HS1, was previously identified by our group, using a proteomic approach [57]. HS1 is a protein involved in the signal cascade triggered by the BCR and its hyper-phosphorylated status correlates with a dismal clinical prognosis.

We have investigated the function of HS1 in normal and leukemic B lymphocytes. We demonstrate that HS1 controls the trafficking and homing of B-cells and significantly influences the tissue invasion and especially the BM infiltration that typically occurs in CLL.

The rationale for this study is fourfold. First, HS1 is an actin regulator of the immune synapse in T-cells [58] and regulates adhesion, lytic synapse formation, cytolytic activity and chemotaxis in NK cells [60] while its function in B-cells is poorly defined. Second, HS1 is involved in the signal cascade triggered by the stimulation of BCR [146]: CLL leukemic B-cells are responsive to microenvironment stimuli including those originating from the BCR [147]. Third, the phosphorylation level of HS1 relates to the clinical course of CLL patients, the hyperphosporylated form of HS1 being associated with a more aggressive disease [57]. Fourth, in both normal and leukemic B-cells, HS1 interacts with cytoskeleton adapters involved in cytoskeleton reorganization [148]. Taken together, these facts indicate that CLL is an attractive model to evaluate the function of HS1 in B-cells and to elucidate how it might relate to the leukemia natural history.

To address the issue, we analyzed in parallel B-cells from $HS1^{-/-}$ mice, an HS1-silenced human CLL cell line and primary leukemic B-cells from CLL patients showing different levels of HS1 phosphorylation. All our *in vitro* results converge to the conclusion that HS1 affects migration, F-actin polymerization, cell adhesion and aggregation of B-cells, demonstrating that HS1 is involved in the regulation of B-cell cytoskeleton. HS1 KD cells maintain their ability to respond to BCR stimulation but fail to form actomyosin complexes. This likely leads to an instability of the cell signaling complex, especially of the signalosome complex proximal to the BCR, and confirms that HS1 is closely linked to actin [148,149]. Lyn, VAV1, HIP-55, SHP-1/2 and Rac1/2 are directly affected by the absence of HS1

while Syk, PLC-γ2 and Blnk appear to be unaffected. All this data suggest that HS1 localizes at the interface between proximal BCR signaling and the cytoskeleton and has a role in transferring information from the stimulated BCR to the cytoskeleton inducing the reorganization that allows cellular movements and migration.

To evaluate how HS1 influences the behavior of CLL cells *in vivo* we took advantage of several mouse models. The *in vivo* migration analysis of $CD19^{+}$ splenocytes from $HS1^{-/-}$ mice reveals a preferential accumulation of $HS1^{-/-}$ cells in the BM of $HS1^{-/-}$ recipient mice. Further and consistent with *in vitro* data, CLL cells carrying HS1 in the hyper-phosphorylated form have a lower degree of organ migration when injected into $Rag2^{-/-}\gamma^{-/-}$ mice, but accumulate in the BM indicating that $HS1^{hyperp}$ leukemic cells have a preferential BM homing.

These findings are further strengthened by the more severe BM involvement found in $HS1^{-/-}$/Eμ-TCL1 tg mice that properly reproduces the pattern of disease dissemination observed in patients with aggressive disease. Our analysis of the $HS1^{-/-}$/Eμ-TCL1 tg mice revealed, beside the great extent of BM involvement, the precocious presence of large amounts of monoclonal $CD19^{+}CD5^{+}$ cells in all the lymphoid organs. Therefore, the absence of HS1 has profound effects on the development and progression of leukemia in the original Eμ-TCL1 tg mice. The latter are characterized by a limited BM involvement [116] and have a rather delayed onset of the disease. In contrast, $H^{-/-}/T^{tg}$ animals present a large leukemia load already at 7 months of age. Leukemic cells express ZAP70, unmutated IGHV genes and infiltrate all lymphoid tissues, especially the BM, thereby closely recapitulating the aggressive form of human CLL. The early onset and the fast increase of the leukemic cell population in all the lymphoid compartments make $H^{-/-}/T^{tg}$ mice a significant model for investigating the biology of CLL.

Our results on the migration and homing of differentially phosphorylated leukemic B-cells together with *in vitro* and *in vivo* evidence gathered from $HS1^{-/-}$ cells strongly suggest that hyper-phosphorylation accounts for HS1 inactivation. This is not surprising as similar mechanisms have been reported for other cytoskeleton-related molecules [150,33]. Inactivation by hyper-phosphorylation explains the correlation between the hyper-phosphorylated form of HS1 and a more aggressive course of the disease [57],when massive BM infiltration is invariably present. Our data are also in keeping with recent observations showing that B-cells from CLL patients in the early and intermediate stage of their disease have reduced migration to lymph nodes and BM [83].

In conclusion, HS1 emerges as a key molecule that controls B-cell migration and specific organ homing and regulates the leukemic peripheral tissue invasion and dissemination especially to the BM. The regulatory role exerted by HS1 in this context can result in different cell dynamics *in vivo*. $HS1^{-/-}$ cells or leukemic cells with impaired HS1 activity may preferentially home to the BM in response to local microenvironment cross-talk that might be enhanced in the absence of HS1. Alternatively, cells with defective HS1 activity may be unable to exit the BM once they have entered and continue to accumulate locally. In either case, these cells find the BM a preferential environment for survival and/or a preferential soil for proliferation and expansion. These mechanisms are not mutually exclusive, rather they all underscore the critical effects of tissue microenvironment cross-talk in the progression of leukemia and assign a central significance to HS1.

HS1 is a key molecule between BCR signalling and cytoskeletal remodelling in CLL

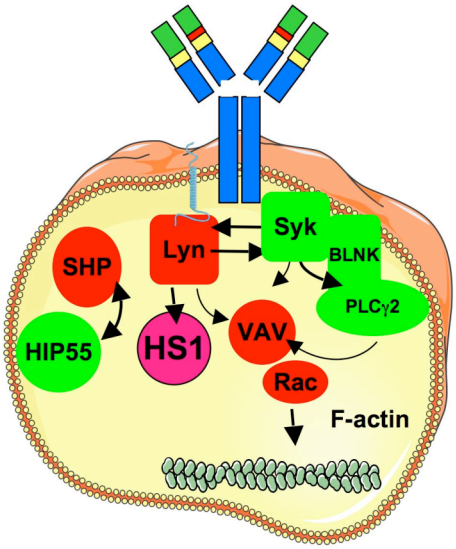

Adhesion
Migration
Aggregation
Actin-polymerization
Trafficking
Tissue homing
and BM Infiltration

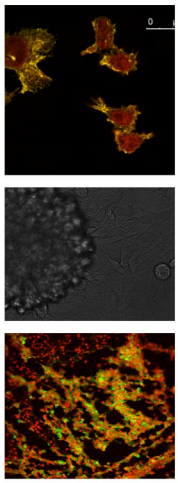

References

1 C. Nunez, N. Nishimoto, G. L. Gartland et al., *J Immunol* **156** (2), 866 (1996).
2 P. D. Burrows and M. D. Cooper, *Current opinion in immunology* **9** (2), 239 (1997).
3 I. Krop, A. L. Shaffer, D. T. Fearon et al., *J Immunol* **157** (1), 48 (1996).
4 P. Ghia, E. ten Boekel, E. Sanz et al., *The Journal of experimental medicine* **184** (6), 2217 (1996).
5 P. Ghia, E. ten Boekel, A. G. Rolink et al., *Immunol Today* **19** (10), 480 (1998).
6 L. Galibert, N. Burdin, C. Barthelemy et al., *The Journal of experimental medicine* **183** (5), 2075 (1996).
7 R. Kuppers, *Nat Rev Cancer* **5** (4), 251 (2005).
8 S. Ruiz, Y. Krupnik, M. Keating et al., *Molecular cancer therapeutics* **5** (7), 1836 (2006).
9 M. Reth, *Nature* **338** (6214), 383 (1989).
10 D. A. Fruman, A. B. Satterthwaite, and O. N. Witte, *Immunity* **13** (1), 1 (2000).
11 N. E. Harwood and F. D. Batista, *Immunity* **28** (5), 609 (2008).
12 A. Lanzavecchia, *Nature* **314** (6011), 537 (1985).
13 D. Depoil, S. Fleire, B. L. Treanor et al., *Nature immunology* **9** (1), 63 (2008).
14 M. Weber, B. Treanor, D. Depoil et al., *J Exp Med* **205** (4), 853 (2008).
15 S. J. Fleire, J. P. Goldman, Y. R. Carrasco et al., *Science (New York, N.Y* **312** (5774), 738 (2006).
16 J. J. Hao, J. Zhu, K. Zhou et al., *The Journal of biological chemistry* **280** (45), 37988 (2005).
17 D. L. Williams, C. Li, T. Ha et al., *J Immunol* **172** (1), 449 (2004).
18 M. Fujimoto, J. C. Poe, P. J. Jansen et al., *J Immunol* **162** (12), 7088 (1999).
19 J. A. Cooper and B. Howell, *Cell* **73** (6), 1051 (1993).
20 S. J. Saouaf, S. Mahajan, R. B. Rowley et al., *Proc Natl Acad Sci U S A* **91** (20), 9524 (1994).
21 T. Kurosaki and M. Hikida, *Immunol Rev* **228** (1), 132 (2009).
22 R. J. Cornall, J. G. Cyster, M. L. Hibbs et al., *Immunity* **8** (4), 497 (1998).
23 R. B. Rowley, A. L. Burkhardt, H. G. Chao et al., *The Journal of biological chemistry* **270** (19), 11590 (1995).
24 L. B. Dustin, D. R. Plas, J. Wong et al., *J Immunol* **162** (5), 2717 (1999).
25 C. Fu, C. W. Turck, T. Kurosaki et al., *Immunity* **9** (1), 93 (1998).
26 M. Ishiai, M. Kurosaki, R. Pappu et al., *Immunity* **10** (1), 117 (1999).
27 M. Takata and T. Kurosaki, *J Exp Med* **184** (1), 31 (1996).
28 S. G. Rhee, *Annual review of biochemistry* **70**, 281 (2001).
29 A. M. Scharenberg, L. A. Humphries, and D. J. Rawlings, *Nat Rev Immunol* **7** (10), 778 (2007).
30 M. Hikida, S. Casola, N. Takahashi et al., *J Exp Med* **206** (3), 681 (2009).
31 B. A. Binstadt, D. D. Billadeau, D. Jevremovic et al., *J Biol Chem* **273** (42), 27518 (1998).
32 I. Tamir, J. M. Dal Porto, and J. C. Cambier, *Curr Opin Immunol* **12** (3), 307 (2000).
33 J. K. Burkhardt, E. Carrizosa, and M. H. Shaffer, *Annu Rev Immunol* **26**, 233 (2008).
34 D. D. Billadeau, J. C. Nolz, and T. S. Gomez, *Nature reviews* **7** (2), 131 (2007).
35 A. B. Jaffe and A. Hall, *Annual review of cell and developmental biology* **21**, 247 (2005).
36 C. Wulfing, A. Bauch, G. R. Crabtree et al., *Proc Natl Acad Sci U S A* **97** (18), 10150 (2000).
37 M. Turner and D. D. Billadeau, *Nat Rev Immunol* **2** (7), 476 (2002).
38 K. Tedford, L. Nitschke, I. Girkontaite et al., *Nature immunology* **2** (6), 548 (2001).
39 L. Westerberg, G. Greicius, S. B. Snapper et al., *Blood* **98** (4), 1086 (2001).
40 E. Arana, A. Vehlow, N. E. Harwood et al., *Immunity* **28** (1), 88 (2008).
41 M. J. Walmsley, S. K. Ooi, L. F. Reynolds et al., *Science (New York, N.Y* **302** (5644), 459 (2003).
42 S. Le Bras, I. Foucault, A. Foussat et al., *J Biol Chem* **279** (15), 15550 (2004).
43 M. M. Kessels, A. E. Engqvist-Goldstein, and D. G. Drubin, *Mol Biol Cell* **11** (1), 393 (2000).
44 M. Muzio, C. Scielzo, M. Frenquelli et al., *Leukemia* (2007).
45 M. Vicente-Manzanares, X. Ma, R. S. Adelstein et al., *Nat Rev Mol Cell Biol* **10** (11), 778 (2009).
46 M. Vicente-Manzanares and F. Sanchez-Madrid, *Nature reviews* **4** (2), 110 (2004).

47 T. Ilani, G. Vasiliver-Shamis, S. Vardhana et al., *Nat Immunol* **10** (5), 531 (2009).
48 M. A. Conti and R. S. Adelstein, *Journal of cell science* **121** (Pt 1), 11 (2008).
49 T. Uruno, J. Liu, Y. Li et al., *The Journal of biological chemistry* **278** (28), 26086 (2003).
50 Y. Takemoto, M. Sato, M. Furuta et al., *Int Immunol* **8** (11), 1699 (1996).
51 A. G. van Rossum, E. Schuuring-Scholtes, V. van Buuren-van Seggelen et al., *BMC Genomics* **6** (1), 15 (2005).
52 Y. Yamanashi, M. Okada, T. Semba et al., *Proceedings of the National Academy of Sciences of the United States of America* **90** (8), 3631 (1993).
53 M. Ruzzene, A. M. Brunati, O. Marin et al., *Biochemistry* **35** (16), 5327 (1996).
54 A. M. Brunati, A. Donella-Deana, P. James et al., *The Journal of biological chemistry* **274** (11), 7557 (1999).
55 J. J. Hao, G. B. Carey, and X. Zhan, *The Journal of biological chemistry* **279** (32), 33413 (2004).
56 I. Taniuchi, D. Kitamura, Y. Maekawa et al., *The EMBO journal* **14** (15), 3664 (1995).
57 C. Scielzo, P. Ghia, A. Conti et al., *J Clin Invest* **115** (6), 1644 (2005).
58 T. S. Gomez, S. D. McCarney, E. Carrizosa et al., *Immunity* **24** (6), 741 (2006).
59 Y. Huang, E. O. Comiskey, R. S. Dupree et al., *Blood* **112** (1), 111 (2008).
60 B. Butler, D. H. Kastendieck, and J. A. Cooper, *Nat Immunol* **9** (8), 887 (2008).
61 Y. Huang, C. Biswas, D. A. Klos Dehring et al., *J Immunol* **187** (11), 5952.
62 F. Caligaris-Cappio, M. Gobbi, M. Bofill et al., *The Journal of experimental medicine* **155** (2), 623 (1982).
63 M. Murakami and T. Honjo, *Immunol Today* **16** (11), 534 (1995).
64 A. Kantor, *Immunol Today* **12** (11), 388 (1991).
65 P. Youinou, C. Jamin, and P. M. Lydyard, *Immunol Today* **20** (7), 312 (1999).
66 H. H. Wortis, M. Teutsch, M. Higer et al., *Proceedings of the National Academy of Sciences of the United States of America* **92** (8), 3348 (1995).
67 F. K. Stevenson and F. Caligaris-Cappio, *Blood* **103** (12), 4389 (2004).
68 N. Chiorazzi and M. Ferrarini, *Annu Rev Immunol* **21**, 841 (2003).
69 S. Lanham, T. Hamblin, D. Oscier et al., *Blood* **101** (3), 1087 (2003).
70 N. Chiorazzi and M. Ferrarini, *Blood* **117** (6), 1781.
71 J. A. Burger and V. Gandhi, *Blood* **114** (12), 2560 (2009).
72 F. Caligaris-Cappio, *British journal of haematology* **123** (3), 380 (2003); B. T. Messmer, E. Albesiano, D. G. Efremov et al., *The Journal of experimental medicine* **200** (4), 519 (2004).
73 J. A. Burger, N. Tsukada, M. Burger et al., *Blood* **96** (8), 2655 (2000).
74 A. V. Kurtova, K. Balakrishnan, R. Chen et al., *Blood* **114** (20), 4441 (2009).
75 S. Deaglio, A. Capobianco, L. Bergui et al., *Blood* **102** (6), 2146 (2003).
76 C. Calissano, R. N. Damle, G. Hayes et al., *Blood* **114** (23), 4832 (2009).
77 N. Chiorazzi, K. Hatzi, and E. Albesiano, *Ann N Y Acad Sci* **1062**, 1 (2005).
78 S. J. Richardson, C. Matthews, M. A. Catherwood et al., *Blood* **107** (9), 3584 (2006).
79 R. S. Stark, L. F. Liebes, M. L. Shelanski et al., *Blood* **63** (2), 415 (1984).
80 F. Caligaris-Cappio, L. Bergui, L. Tesio et al., *Blood* **67** (1), 233 (1986).
81 G. S. Nowakowski, J. D. Hoyer, T. D. Shanafelt et al., *J Clin Oncol* **27** (11), 1844 (2009).
82 S. Deaglio, T. Vaisitti, S. Aydin et al., *Blood* **110** (12), 4012 (2007).
83 T. N. Hartmann, V. Grabovsky, W. Wang et al., *Cancer research* **69** (7), 3121 (2009).
84 A. Montresor, M. Bolomini-Vittori, S. I. Simon et al., *Cancer research* **69** (24), 9281 (2009).
85 V. L. Tybulewicz and R. B. Henderson, *Nature reviews* **9** (9), 630 (2009).
86 K. J. Till, R. J. Harris, A. Linford et al., *Cancer research* **68** (20), 8429 (2008).
87 Y. R. Carrasco, S. J. Fleire, T. Cameron et al., *Immunity* **20** (5), 589 (2004).
88 A. G. Ramsay, A. J. Johnson, A. M. Lee et al., *The Journal of clinical investigation* **118** (7), 2427 (2008).
89 A. Sanchez-Aguilera, I. Rattmann, D. Z. Drew et al., *Leukemia* **24** (1), 97.
90 D. Kitamura, H. Kaneko, Y. Miyagoe et al., *Nucleic Acids Res* **17** (22), 9367 (1989).
91 U. Fischer, A. Michel, and E. U. Meese, *Int J Mol Med* **15** (4), 611 (2005).
92 E. Carrizosa, T. S. Gomez, C. M. Labno et al., *J Immunol* **183** (11), 7352 (2009).
93 C. Scielzo, E. Ten Hacken, M. T. Bertilaccio et al., *Leukemia & lymphoma* **51** (8), 1371.
94 J. V. Melo, J. Wardle, M. Chetty et al., *Br J Haematol* **64** (3), 469 (1986).
95 M. J. Keating, *Semin Oncol* **26** (5 Suppl 14), 107 (1999).
96 M. Hallek, I. Langenmayer, C. Nerl et al., *Blood* **93** (5), 1732 (1999).
97 M. Sarfati, S. Chevret, C. Chastang et al., *Blood* **88** (11), 4259 (1996).
98 G. Gaidano, P. Ballerini, J. Z. Gong et al., *Proc Natl Acad Sci U S A* **88** (12), 5413 (1991).

[99] T. J. Hamblin, Z. Davis, A. Gardiner et al., *Blood* **94** (6), 1848 (1999).
[100] R. N. Damle, T. Wasil, F. Fais et al., *Blood* **94** (6), 1840 (1999).
[101] P. Ghia, G. Guida, C. Scielzo et al., *Leukemia* **18** (10), 1733 (2004).
[102] A. Wiestner, A. Rosenwald, T. S. Barry et al., *Blood* **101** (12), 4944 (2003).
[103] M. Crespo, F. Bosch, N. Villamor et al., *The New England journal of medicine* **348** (18), 1764 (2003).
[104] S. Stilgenbauer, P. Lichter, and H. Dohner, *Rev Clin Exp Hematol* **4** (1), 48 (2000).
[105] X. S. Puente, M. Pinyol, V. Quesada et al., *Nature* **475** (7354), 101.
[106] D. J. Allsup, A. S. Kamiguti, K. Lin et al., *Cancer Res* **65** (16), 7328 (2005).
[107] C. H. Geisler, J. K. Larsen, N. E. Hansen et al., *Blood* **78** (7), 1795 (1991).
[108] A. Contri, A. M. Brunati, L. Trentin et al., *J Clin Invest* **115** (2), 369 (2005).
[109] K. Schuh, A. Avots, H. P. Tony et al., *Leuk Lymphoma* **23** (5-6), 583 (1996).
[110] R. R. Furman, Z. Asgary, J. O. Mascarenhas et al., *J Immunol* **164** (4), 2200 (2000).
[111] I. Ringshausen, F. Schneller, C. Bogner et al., *Blood* **100** (10), 3741 (2002).
[112] M. Muzio, B. Apollonio, C. Scielzo et al., *Blood* **112** (1), 188 (2008).
[113] T. Zenz, D. Mertens, R. Kuppers et al., *Nat Rev Cancer* **10** (1), 37.
[114] F. Hecht, R. Morgan, B. K. Hecht et al., *Science (New York, N.Y* **226** (4681), 1445 (1984).
[115] T. B. Fu, L. Virgilio, M. G. Narducci et al., *Cancer research* **54** (24), 6297 (1994).
[116] R. Bichi, S. A. Shinton, E. S. Martin et al., *Proceedings of the National Academy of Sciences of the United States of America* **99** (10), 6955 (2002).
[117] A. J. Johnson, D. M. Lucas, N. Muthusamy et al., *Blood* **108** (4), 1334 (2006).
[118] N. Zanesi, R. Aqeilan, A. Drusco et al., *Cancer research* **66** (2), 915 (2006).
[119] J. W. Tung, M. D. Mrazek, Y. Yang et al., *Proceedings of the National Academy of Sciences of the United States of America* **103** (16), 6293 (2006).
[120] H. G. Wendel, E. De Stanchina, J. S. Fridman et al., *Nature* **428** (6980), 332 (2004).
[121] K. K. Hoyer, S. W. French, D. E. Turner et al., *Proceedings of the National Academy of Sciences of the United States of America* **99** (22), 14392 (2002).
[122] G. Gorgun, T. A. Holderried, D. Zahrieh et al., *The Journal of clinical investigation* **115** (7), 1797 (2005).
[123] C. S. Mulligan, M. E. Thomas, and S. P. Mulligan, *Blood* **113** (25), 6496 (2009).
[124] J. V. Olsen, L. M. de Godoy, G. Li et al., *Mol Cell Proteomics* **4** (12), 2010 (2005).
[125] P. J. Kersey, J. Duarte, A. Williams et al., *Proteomics* **4** (7), 1985 (2004).
[126] A. Keller, A. I. Nesvizhskii, E. Kolker et al., *Anal Chem* **74** (20), 5383 (2002).
[127] A. I. Nesvizhskii, A. Keller, E. Kolker et al., *Anal Chem* **75** (17), 4646 (2003).
[128] A. Stacchini, M. Aragno, A. Vallario et al., *Leukemia research* **23** (2), 127 (1999).
[129] H. F. Lodish, B. Zhou, G. Liu et al., *Nat Rev Immunol* **8** (2), 120 (2008).
[130] A. S. Freedman, A. W. Boyd, F. R. Bieber et al., *Blood* **70** (2), 418 (1987).
[131] M. Maio, A. Pinto, A. Carbone et al., *Blood* **76** (4), 783 (1990).
[132] B. Gu, L. P. Dao, and J. Wiley, *Leuk Lymphoma* **42** (1-2), 5 (2001).
[133] A. Kretz-Rommel, F. Qin, N. Dakappagari et al., *J Immunol* **178** (9), 5595 (2007).
[134] B. D. Hock, L. J. Fernyhough, S. M. Gough et al., *Leuk Res* **33** (8), 1089 (2009).
[135] P. L. Schwartzberg, K. L. Mueller, H. Qi et al., *Nat Rev Immunol* **9** (1), 39 (2009).
[136] G. Runarsson, A. Liu, Y. Mahshid et al., *Blood* **105** (3), 1274 (2005).
[137] A. Trautmann, *Nat Immunol* **6** (12), 1213 (2005).
[138] T. Yokosuka, K. Sakata-Sogawa, W. Kobayashi et al., *Nat Immunol* **6** (12), 1253 (2005); M. C. Seminario and S. C. Bunnell, *Immunol Rev* **221**, 90 (2008).
[139] H. He, T. Watanabe, X. Zhan et al., *Mol Cell Biol* **18** (7), 3829 (1998).
[140] P. K. Mattila and P. Lappalainen, *Nat Rev Mol Cell Biol* **9** (6), 446 (2008).
[141] M. T. Bertilaccio, C. Scielzo, G. Simonetti et al., *Blood* **115** (8), 1605.
[142] R. N. Kaplan, R. D. Riba, S. Zacharoulis et al., *Nature* **438** (7069), 820 (2005); T. Lwin, L. A. Crespo, A. Wu et al., *Leukemia* **23** (1), 170 (2009).
[143] J. A. Burger, P. Ghia, A. Rosenwald et al., *Blood* (2009).
[144] F. Caligaris-Cappio and P. Ghia, *J Clin Oncol* **26** (27), 4497 (2008).
[145] T. D. Shanafelt, S. M. Geyer, and N. E. Kay, *Blood* **103** (4), 1202 (2004).
[146] Y. Yamanashi, T. Fukuda, H. Nishizumi et al., *The Journal of experimental medicine* **185** (7), 1387 (1997).
[147] P. Ghia, P. Circosta, C. Scielzo et al., *Curr Top Microbiol Immunol* **294**, 135 (2005).
[148] M. Muzio, C. Scielzo, M. Frenquelli et al., *Leukemia* **21** (9), 2067 (2007).
[149] Y. Huang and J. K. Burkhardt, *Journal of cell science* **120** (Pt 5), 723 (2007).
[150] W. M. Yokoyama, *Immunity* **29** (4), 515 (2008).

Published Papers 2009-2011

1) Bertilaccio MT, **Scielzo C**, Simonetti G, Ponzoni M, Apollonio B, Fazi C, Scarfò L, Rocchi M, Muzio M, Caligaris-Cappio F, Ghia P. A novel Rag2-/-gammac-/--xenograft model of human CLL. Blood. 2010 Feb 25;115(8):1605-9.

2) Frenquelli M, Muzio M, **Scielzo C**, Fazi C, Scarfò L, Rossi C, Ferrari G, Ghia P, Caligaris-Cappio F. MicroRNA and proliferation control in chronic lymphocytic leukemia: functional relationship between miR-221/222 cluster and p27. Blood. 2010 Mar 4

3) **Scielzo C**, Bertilaccio MT, Simonetti G, Dagklis A, ten Hacken E, Fazi C, Muzio M, Caiolfa V, Kitamura D, Restuccia U, Bachi A, Rocchi M, Ponzoni M, Ghia P, Caligaris-Cappio F.
HS1 has a central role in the trafficking and homing of leukemic B cells
Blood. 2010 Nov 4;116(18):3537-46.

4) Bertilaccio MT, **Scielzo C**, Muzio M, Caligaris-Cappio F. An overview of chronic lymphocytic leukaemia biology. Best Pract Res Clin Haematol. 2010 Mar;23(1):21-32. Review

5) **Scielzo C**, Ten Hacken E, Bertilaccio MT, Muzio M, Calissano C, Ghia P, Caligaris-Cappio F.
How the microenvironment shapes chronic lymphocytic leukemia: the cytoskeleton connection.
Leuk Lymphoma. 2010 Aug; 51(8):1371-4.

6) Scarfò L, Dagklis A, **Scielzo C**, Fazi C, Ghia P. CLL-like monoclonal B-cell lymphocytosis: are we all bound to have it? Semin Cancer Biol. 2010 Dec;20(6):384-90.

7) **Scielzo C**, Apollonio B, Scarfò L, Janus A, Muzio M, ten Hacken E, Ghia P and Caligaris Cappio F. The functional in vitro response to CD40 ligation reflects a different clinical outcome in patients with Chronic Lymphocytic Leukemia. Leukemia. 2011 Nov;25(11):1760-7. d

Appendix